FINAL PROJECT

HEC-RAS 6.6 DAM BREAK ANALYSIS WITH InaSAFE DISASTER IMPACT ASSESSMENT APPROACH OF BILI BILI DAM

Proposed to the University of Islam Indonesia Yogyakarta to Fulfill the Requirements for Obtaining a Bachelor's Degree in Civil Engineering

Teuku Dimaz Rahmatna
21511274

CIVIL ENGINEERING
INTERNATIONAL UNDERGRADUATE PROGRAM
FACULTY OF CIVIL ENGINEERING AND PLANNING
UNIVERSITY OF ISLAM INDONESIA

2026

FINAL PROJECT

HEC-RAS 6.6 DAM BREAK ANALYSIS WITH InaSAFE DISASTER IMPACT ASSESSMENT APPROACH OF BILI BILI DAM

Arranged by

Teuku Dimaz Rahmatna
21511274

Has been accepted as the requirement for obtaining
a Bachelor's degree in Civil Engineering

Has been evaluated and reviewed on February 13th, 2026
By The Board of Examiners:

Lecturer Supervisor	Examiner I	Examiner II
adipta **Nandi W., S.T., M.Eng.**	**Shofwatul Fadilah, S.T.P., M.Eng**	**Dinia Anggraheni, S.T., M.Eng.**
135111102	NIK: 215111101	NIK: 165110105

Authorized,
Head of the Civil Engineering Undergraduate Study Program

3/3 2026

Ir. Yunalia Muntafi S.T., M.T., Ph.D. (Eng)., IPM.
NIK: 095110101

PLAGIARISM-FREE STATEMENT

Hereby, I declare that this final project that I have arranged as one of the requirements for obtaining a Bachelor's Degree in the International Undergraduate Study Program of the Civil Engineering Department, Faculty of Civil Engineering and Planning, Universitas Islam Indonesia, is my original work. As for the parts in the writing of the final project that I cited from other people's creations, the sources have been mentioned clearly in accordance with the norms, rules, and ethics of scientific writing. Suppose in the future it is found that all or part of this final project is not my work, or there is plagiarism in certain parts. In that case, I am willing to accept sanctions, including revocation of my student status under applicable laws.

Yogyakarta, May 2025

The Declarant,

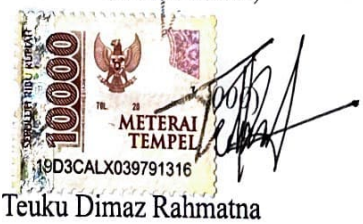

Teuku Dimaz Rahmatna

21511274

DEDICATION

This Research Paper is dedicated

To my beloved parents,
Dian Rohana and Boy Rachmat Mussanip,
whose endless love, support, and prayers have strengthened me throughout the ups and downs of my life's journey.

And

To the version of me,
who survived the hardest chapters of his life that could have stopped him, yet chose to rise, reclaimed the light, and kept moving forward, no matter how many times life tried to pull him down.

Pain is inevitable. Suffering is optional.
-Haruki Murakami

PREFACE

All praise and gratitude to Allah SWT., for His mercies and blessings, so that the author can complete the Final Project entitled *HEC-RAS 6.6 Dam Break Analysis with InaSAFE Disaster Impact Assessment Approach of Bili Bili Dam* as the requirements for obtaining a Bachelor's Degree in International Undergraduate Study Program of the Civil Engineering Department, Faculty of Civil Engineering and Planning, Universitas Islam Indonesia, Yogyakarta.

In the process of arranging and compiling this Final Project, the author encountered many challenges. But due to the advice, criticism, and encouragement from various parties, Alhamdulillah, this Final Project can be completed. In this regard, the Author would like to express his deepest gratitude to:

1. Mrs. Ir. Yunalia Muntafi S.T., M.T., Ph.D. (Eng), IPM, as the Head of the Civil Engineering Undergraduate Study Program,
2. Mr. Ir. Pradipta Nandhi Wardhana S.T., M.Eng., as the Supervisor and the Secretary of Civil Engineering International Program,
3. Mrs XXX as the Examiner Lecturer I,
4. Mrs XXX as the Examiner Lecturer II,
5. The Author's Father and Mother have helped the Author both materially and spiritually during and until the completion of the study, and
6. 21st Batch of Civil Engineering "International Program", who have helped and shared.

Finally, the Author hopes that this Final Project can be useful to all parties who read it.

Yogyakarta, May 2025
Author,

Teuku Dimaz Rahmatna
21511274

TABLE OF CONTENTS

LIST OF TABLES

LIST OF FIGURES

LIST OF ATTACHMENTS

NOTATION AND ABBREVIATION

1D	=	One-Dimensional
2D	=	Two-Dimensional
B_{avg}	=	Average breach width (m)
BBWS	=	Balai Besar Wilayah Sungai
BIG	=	Badan Informasi Geospasial
CRS	=	Coordinate Reference System
D.S.	=	Downstream
DEMNAS	=	Digital Elevation Model Nasional
Fr	=	Froude Number
g	=	Gravitational Force (9.81 m/s^2)
H_b	=	Height of the trapezoidal breach (m)
H_c	=	Critical Overtopping Depth
H_s	=	Threshold Breach Height (m)
H_w	=	Height of Water Above Breach Bottom at Time of Breach Initiation
HW	=	Headwater
InaSAFE	=	Indonesia Scenario Assessment for Emergency
k_H	=	Factor of Breach Height
k_M	=	Factor of Failure Mode
LULC	=	Land Use/Land Cover
LWD	=	Left Wing Dam
m	=	Breach Average Side Slope Ratio
MD	=	Main Dam
n	=	Manning's Roughness Coefficient
PMP	=	Probable Maximum Precipitation
Q_P	=	Predicted Dam Breach Peak Discharge
Q_{PMF}	=	Probable Maximum Flood Discharge (m^3/s)
Q_T	=	Return Period Discharge (m^3/s)
R	=	Hydraulic Radius (m)

RBI	=	*Rupa Bumi Indonesia*
RS	=	River Station
RWD	=	Right Wing Dam
S	=	Energy Grade Line Slope
SPF	=	Standard Project Flood
t_f	=	Breach Formation Time (s)
Tp	=	Time to Peak (h)
TW	=	Tailwater
U.S.	=	Upstream
V	=	Velocity (m/s)
V_w	=	Water Volume Above the Breach Bottom at Time of Failure (m^3)
W_{avg}	=	Average Width of the Embankment Between Toes of the Downstream and Upstream Slopes (m)
WSE	=	Water Surface Elevation (m)
z	=	Elevation (m)

ABSTRACT

Bili Bili Dam is a zoned rockfill embankment dam that plays a critical role in water supply, hydropower, and flood control for the Jeneberang River Basin. However, with an effective reservoir volume of 346 million m^3, the dam possesses a high hazard potential to the downstream area. In accordance with Permen PUPR No.27/PRT/M/2015, every dam is required to develop and periodically review its emergency action plan, particularly when changes occur in hydrology conditions, environmental factors, or the social conditions of the downstream. Therefore, a dam break analysis is essential to support emergency compilation and disaster-risk reduction for the Bili Bili Dam.

This study performs a comprehensive dam break analysis using HEC-RAS 6.6 through an integrated 1D-2D unsteady flow modelling approach. The 1D model represents the river channel hydrodynamics, while the 2D domain captures the floodplain propagation and inundation behaviour. Breach parameters were determined using the empirical equations of Froehlich (2016), and three piping-failure scenarios were simulated at breach-initiation elevations for both the Main Dam and the Right-Wing Dam. Hazard and exposure data processed in QGIS and analyzed using InaSAFE 5.0.7 to quantify potential impacts. Numerical stability was achieved through stepwise calibration of steady and unsteady simulations.

The simulation revealed that the highest peak discharge reached 30,635.40 m^3/s under the Right-Wing Dam top-piping scenario, while the most extensive inundation of 238.336 km^2 occurred in the middle-piping scenario. The results further showed that flood waves arrived in downstream settlements in less than 3 hours, with maximum depths in Makassar occurring within 3–6 hours. InaSAFE impact assessment indicated that up to 143,100 buildings, 2,017 km of road network, and 12,800 ha of farmland may be affected.

Keyword: Dam Break, Piping Failure, HEC-RAS, Flood Inundation, InaSAFE

CHAPTER I
INTRODUCTION

1.1 Background

A dam is a structure built across a river to retain water and form a reservoir that provides human necessities, such as water supply, hydroelectric power, and tourism. Reservoirs formed by dams modify the natural flow regime of a river by storing inflow and releasing it in a regulated manner. According to Chow (1988), reservoir storage affects the relationship between inflow and outflow through routing processes that reduce peak discharge and delay the time to peak. Similarly, Subramanya (2008) explains that flood control reservoirs function by attenuating flood hydrographs through temporary storage, thereby decreasing downstream flood magnitude. Therefore, dams play a significant role in regulating river discharge and mitigating flood impacts under normal operating conditions.

Despite the enormous benefits that a dam provides to the community, dams inherently store large volumes of water at considerable elevations, which introduces substantial potential hazard in the event of structural failure. When a dam fails, the sudden release of impounded water can generate a catastrophic flood wave with extremely high peak discharge within a short time. Such failure events may result from overtopping, internal erosion (piping), or structural malfunction (FEMA, 2013). The rapid propagation of the flood wave can threaten downstream communities, infrastructure, and environmental systems, causing severe economic losses and loss of life.

According to ICOLD (2019), statistical analyses of historical dam failures indicate that overtopping and internal erosion are among the most common causes of embankment dam collapse. In addition, through the regulatory framework established by the Kementrian Pekerjaan Umum dan Perumahan Rakyat (PUPR) in Permen PUPR No 27/PRT/M/2015, the Indonesian Ministry specifically states that the design of an emergency action plan must include a dam break analysis in Pasal 54 Ayat 4. This legal requirement underscores the need for a proactive approach in

managing disaster risk, ensuring that contingency plans are not merely theoretical but are based on scientific simulations of potential failure scenarios and their consequences. The framework further compels a dynamic approach to risk management, requiring dams to periodically reassess the plans, considering evolving environmental, hydrological, and social conditions in the downstream area as per Pasal 60 Ayat 1(PUPR, 2015).

Bili Bili Dam, located in Sulawesi Selatan, Kabupaten Gowa, approximately 30 km to the east of Kota Makassar, is a rockfill dam constructed in 1992 with an effective reservoir capacity of approximately 346 million m^3 and a dam height of 73 m. Considering its storage capacity and strategic location near densely populated areas, a hypothetical dam failure scenario may pose significant risks to downstream settlements, including Makassar City. Therefore, it is necessary to conduct a comprehensive dam break simulation integrated with disaster impact assessment to evaluate potential inundation areas and associated losses.

1.2 Problem Formulation

Problems formulated for this final project are as follows.

1. How large would the peak discharge be due to the Bili Bili Dam collapse?
2. How long would the breach flow take to reach peak discharge resulting from the Bili Bili Dam collapse event?
3. How extensive might the inundation area be due to the collapse of the Bili Bili Dam?
4. How quickly could the flooding reach the nearby village and Makassar City if the Bili Bili Dam collapses?
5. How deep would the inundation be due to the Bili Bili Dam collapse?
6. How severe might the impact be due to the Bili Bili Dam collapse?

1.3 Research Purposes

The purpose of this final project research is as follows.

1. To reveal the peak discharge due to the Bili Bili Dam collapse.
2. To find out the time to reach the peak discharge due to the Bili Bili Dam Collapse.

3. To predict the inundation area that occurred due to the collapse of the Bili Bili Dam.
4. To forecast the flooding duration to reach the nearby village and Makassar city if the Bili Bili Dam collapses.
5. To simulate the impact occurred due to Bili Bili Dam collapse.

1.4 Research Benefit

By conducting this dam break research using HEC-RAS 6.6, it can provide flood patterns due to the dam collapse in the downstream area. Furthermore, the losses that occur can be estimated using the InaSAFE approach towards the result of the HEC-RAS 6.6 analysis. Moreover, conducting this dam break research using HEC-RAS and InaSAFE is not merely an academic exercise but a critical compliance measure. It provides the foundational, data-driven evidence required to formulate effective evacuation routes, early warning systems, and mitigation strategies, thereby safeguarding downstream populations, infrastructure, and ecosystems from catastrophic flood waves resulting from a hypothetical dam failure.

1.5 Research Delimitation

To ensure the research is structured and organized, the following delimitations have been set for conducting this study.

1. The Bili Bili dam break analysis is only performed on the Main Dam (MD) and the Right-Wing Dam (RWD).
2. The Bili Bili dam break simulation is performed using HEC-RAS 6.6 with 1-dimensional river flow modelling.
3. The disaster impact estimation due to the Bili Bili dam collapse is performed using the InaSAFE QGIS plug-in.
4. This research only reviews the hydraulic analysis technical aspects.
5. The dam break is assumed to occur due to overtopping and/or piping.
6. The simulation ignores the structures across or parallel to the river, both upstream and downstream.
7. The simulation ignores the sediment along the river and the storage area.

8. The data used are Q_{PMF} discharge, dam technical data, river cross-section, and downstream area geometry, which are processed from DEMNAS data.
9. The terrain data used in this study were obtained from DEMNAS through the Ina-Geoportal of the Badan Informasi Geospasial (BIG), which provides elevation data with a spatial resolution of approximately 0.27 arcseconds, equivalent to about 8.1 meters.
10. The hydrology and hydraulic data used in this study analysis are obtained from the Balai Besar Wilayah Sungai (BBWS) Pompengan–Jeneberang's calculation from 2018.

CHAPTER II
LITERATURE OVERVIEW

2.1 General Overview

This chapter presents a comprehensive review of relevant literature that forms the theoretical and methodological foundation of this study. The purpose of this chapter is to define the conceptual framework, identify key variables and approaches, and compare this research development with the previous research.

To achieve this objective, a structured peer review was conducted on three international and four Indonesian publications closely related to this study. These selected references provide comparative insight into analytical methods, modelling approaches, and previous findings. Consequently, this chapter serves as the foundational basis for developing the research analysis and methodology, while also highlighting research gaps and justifying the approach adopted in this study.

2.2 "Dam Breach Analysis and Flood Inundation Mapping of Dire Dam, using HEC-HMS and HEC-RAS Models" (Tessema et al., 2024).

Tessema et al. (2024) conducted a study on dam breach analysis and flood inundation of the Dire Dam in Oromia Regional State, located 41 km from Addis Ababa City, Ethiopia. The Dire Dam is an embankment dam constructed with a zoned earth fill dam type that stores 19 million m^3 in its recent reservoir capacity. In addition, it was expected from the expansion project that the reservoir capacity would rise to 23.5 million m^3 by raising the dam crest height by 1.5 m from its previous level. Thus, this research sought to investigate the breach analysis of the Dire Dam concerning different inflow scenarios and failure modes, as well as to create flood inundation mapping for the downstream area of the dam. In this study, the hydraulic analysis was performed using HEC-RAS 2D simulations and HEC-HMS for the hydrology analysis of the Dire Dam. Moreover, Tessema et al. (2024) analyzed scenarios involving overtopping and piping failure modes by employing regression from five different breach parameters

Through the comparison of five different breach parameters, Tessema et al. (2024) selected the Von Thun and Gillette (1990) breach parameter empirical approach due to its highest peak discharge value among other breach parameters. This study indicated that the Dire Dam will experience breaching when the maximum flood reaches 7,073.02 m^3/s and 11,021.92 m^3/s due to overtopping and piping, respectively. The inundation map showed that 358.7 ha were affected by the flood hazard. Hence, Tessema et al. (2024) concluded that the piping failures were considered more hazardous than the overtopping failures on the dam breach of Dire Dam. The floodplain of the Dire Dam breach can be seen in Figure 2.1 on the next page.

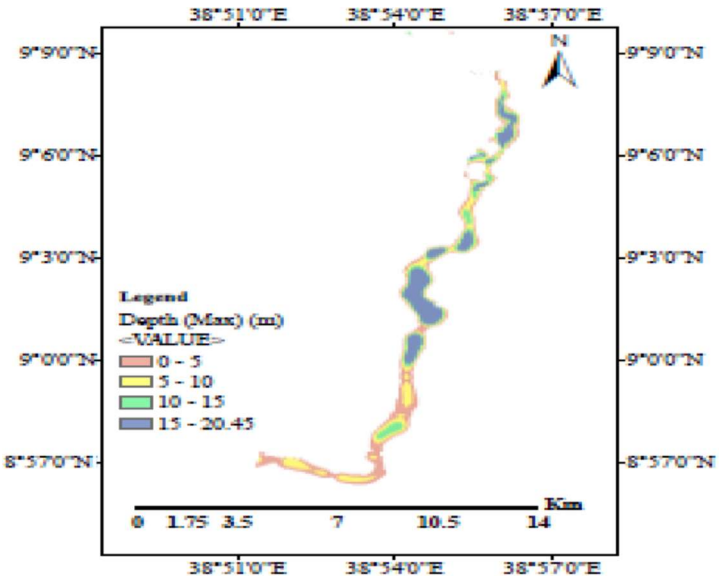

Figure 2. 1 Floodplain Depth Map of Dire Dam Breach
(Source: Tessema et al., 2024)

2.3 "Flood Hazard Analysis due to Overtopping of Dalaman Akköprü Dam: A Case Study" (Yilmaz et al., 2022).

Yilmaz et al. (2022) conducted a study on flood hazard analysis at the Akköprü Dam. The study object is located in the Dalaman River on the southwestern coast of Turkey. Akköprü Dam is a homogeneous earth-fill dam with 385.26 million m^3 at normal water surface elevation. This study aimed to assess the potential flood risk from hypothetical dam breaches and to develop mitigation measures for the affected areas. The analysis utilized HEC-RAS 2D simulations to

study dam failure with an overtopping mode. It implemented the dam breach parameters from Froehlich (2008). In addition, the flood hazard analysis used flood hazard and vulnerability thresholds set by Smith et al. (2014).

The result of this study showed that the average flood arrival time from upstream to the center city of Ortaca was 2 hours and 20 minutes, while to the center city of Dalaman it was 2 hours and 50 minutes. Thus, most inundated areas were considered unsafe for vehicles and people, with all buildings vulnerable to failure. Therefore, densely populated areas, roads, and Dalaman airport are at a high risk of potential flood inundation. The inundated area based on the flood hazard classification map can be seen in Figure 2.2 on the next page.

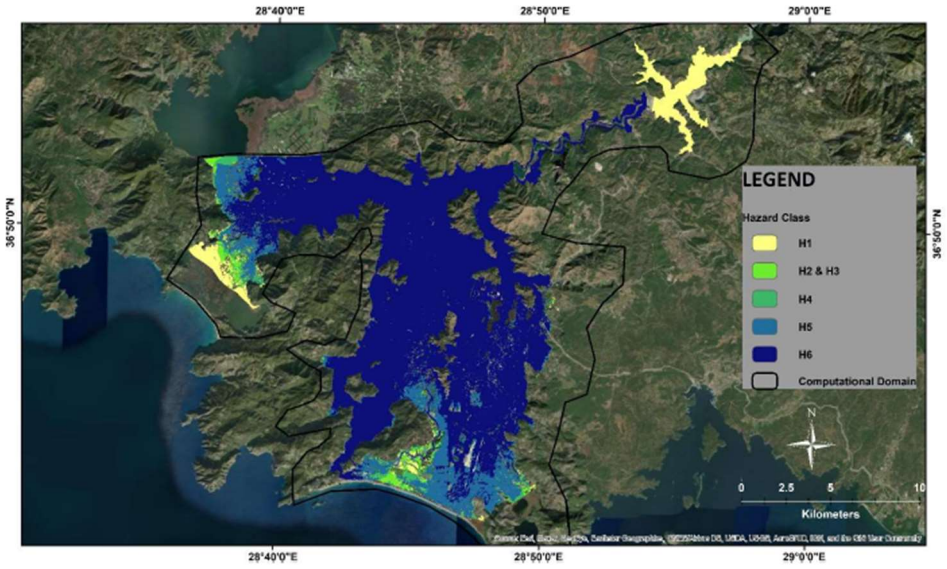

Figure 2. 2 Spatially Varied Hazard Mapping of the Inundated Area for the Case of Overtopping
(Source: Yilmaz et al., 2022)

2.4 "*Analisa Keruntuhan Bendungan Rukoh Kabupaten Pidie Menggunakan Aplikasi HEC-RAS dan Berbasis InaSAFE*" (Khairi et al. ,2022).

Khairi et al. (2022) conducted a study on dam break analysis and the hazard risk assessment of Rukoh Dam, which is located in Kabupaten Pidie, Provinsi Aceh. Rukoh Dam is a flood control and irrigation provider with a 125.7 million m^3 reservoir effective capacity. This study mainly aimed to reveal the hazards and estimate economic losses caused by the dam break of Rukoh Dam. The dam break

analysis in this study used HEC-RAS 5.0.7 through Froehlich's (2008) dam breach parameter approaches with six different piping failure mode scenarios, while the economic loss estimation utilized InaSAFE 5.0.1.

The findings of this study indicate that the largest inundated area among the various considered scenarios was 237.409 km^2, with a 21.94 m depth of flood. Consequently, approximately 68,100 residents would require evacuation and shelter, and an estimated IDR 573,068,311,480 in economic losses, including direct and indirect material damages as well as functional disruption that will be borne by the government and/or the dam operational management. Hence, the dam break of Rukoh Dam was classified as a high-hazard category. The flood distribution due to the dam break of Rukoh Dam can be seen in Figure 2.3 on the next page.

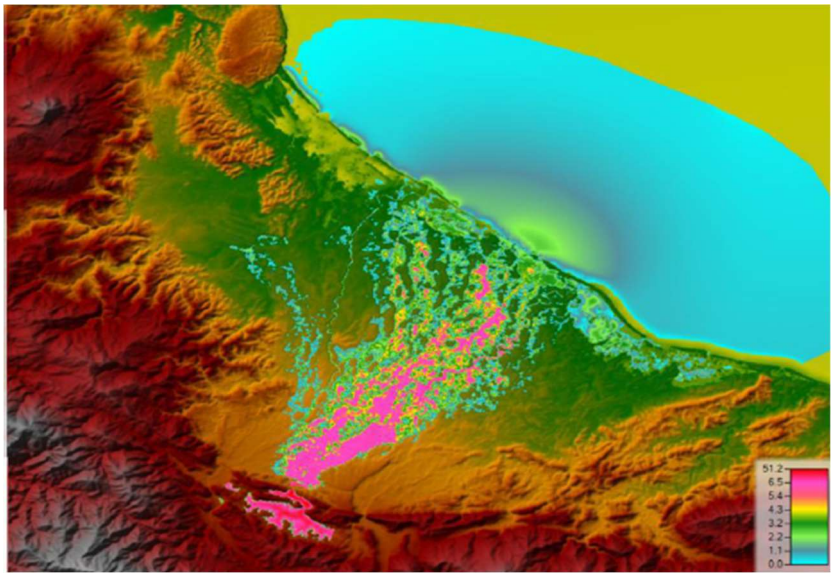

Figure 2. 3 Flood Distribution due to the Dam Break of Rukoh Dam
(Source: Khairi et al., 2022)

2.5 "Dam Break Analysis Using HEC-RAS and HEC-GeoRAS: A Case Study of Hidkal Dam, Karnataka State, India." (Bharath et al., 2021)

Bharath et al. (2021) conducted a study on the dam break analysis of Hidkal Dam, which is located in Karnataka State, India. Hidkal Dam is a composite structure of earthen embankment and masonry structure, which stores 51.00 TMC, or equally to 1,444.16 million m^3. The study objective was to estimate the maximum flood discharge and its corresponding stages, as well as the flood peak occurrence

time. In addition, the study aimed to model the peak flood hydrograph for various downstream segments along the river route. The dam break analysis in this study used HEC-RAS 5.0.1 and HEC-GeoRAS to create river geometry and inundation mapping, engaged piping and overtopping failure modes on 5 different downstream segments, namely 5 km, 10 km, 15 km, 20 km, and 22 km from the dam. Furthermore, Bharath et al. (2021) simulated the dam break with five various empirical methods for breach parameters on the piping failure mode and performed a sensitivity analysis on those breach parameters to reveal the peak flow and maximum stage.

Based on Bharath et al. (2021) study, the sensitivity analysis showed that breach depth, width, and formation time significantly influence the peak flow, while breach side slopes have less influence on the peak flow. The peak flow showed that at 22 km downstream of the dam was 72,085.45 m^3/s and 78,454.82 m^3/s with 75.224 km^2 and 79.205 km^2 of inundation area, respectively piping and overtopping failure scenarios. Bharath et al. (2021) concluded that overtopping failure was the critical failure mode due to the higher peak flow occurring at the downstream. Therefore, there were twenty villages affected, with seventeen of them severely affected by the flood hazard due to the dam break of Hidkal Dam. The inundation map with two different failure modes from this study can be seen in Figure 2.4 below.

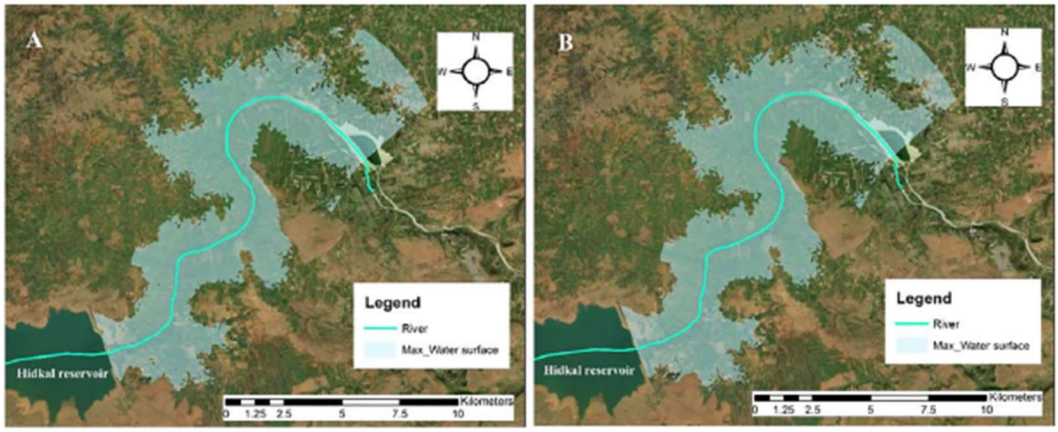

Figure 2. 4 Inundation Map for (A) Piping Failure, (B) Overtopping Failure
(Source: Bharath et al., 2021)

2.6 "Dam Breach Analysis Using HEC-RAS 5.0.7 and QGIS 3.16.7" (Amri, 2021).

Amri (2021) conducted a dam break analysis on Palasari Dam, which is located in Desa Ekasari, Kabupaten Jembrana, Bali. Palasari Dam is a rock-fill dam with a clay core, designed to store 450,000 m^3 of water in the reservoir. This dam break analysis was conducted to forecast the flood inundation of the downstream area due to the piping failure of the dam by employing HEC-RAS 5.0.7. Amri (2021) implemented the Froehlich (2008) dam breach parameters and estimated Manning's n roughness using the Cowan (1956) composite formula with Arcement and Schneider (1989) for each factor. Further, the dam break analysis was performed with four different breach formation times, namely, 0.46 hours, 1 hour, 2 hours, and 4 hours, as the analysis scenarios.

Amri's (2021) study had two peak flows that resulted from reservoir water volume and PMF. It showed that the shortest breach formation time scenario and reservoir volume wave gave the highest peak flow discharge among other breach formation scenarios, with the value of 8,733.17 m^3/s. Desa Ekasari had the largest flooded area, 152.39 ha, yet the proportion of the flooded area relative to the total district size was the smallest at 4.33 %. In contrast, Desa Warnasari had the highest percentage of flooded area at 13.36 %, although it's smaller than Desa Ekasari and Desa Nusasari. The flow hydrograph and maximum water surface elevation from varying scenarios are represented in Figures 2.5 and 2.6 below, respectively. The inundation map of the envelope scenario can be seen in Figure 2.7 on the next page.

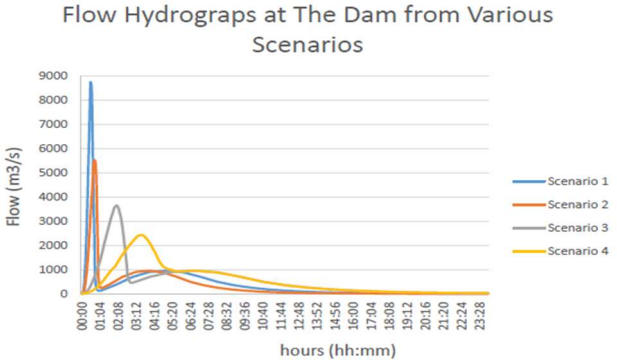

Figure 2. 5 Flow Hydrograph at Palasari Dam from Various Scenarios
(Source: Amri, 2021)

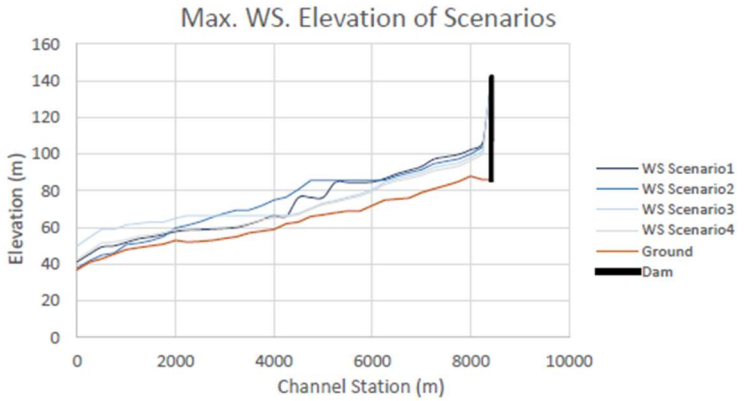

Figure 2. 6 Maximum Water Surface Elevation from Various Scenarios
(Source: Amri, 2021)

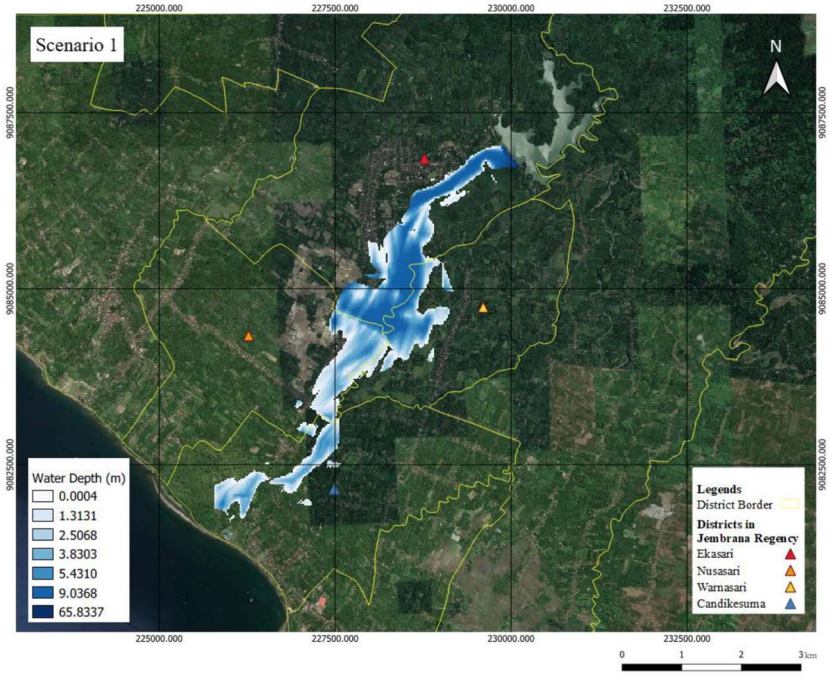

Figure 2. 7 Inundation Map of Palasari Dam Break
(Source: Amri, 2021)

2.7 "*Simulasi Keruntuhan Bendungan Bili Bili Kabupaten Gowa Provinsi Sulawesi Selatan*" (Rustan et al., 2019).

Rustan et al. (2019) conducted a dam break simulation on the Bili Bili Dam, which is located in Kabupaten Gowa, Provinsi Sulawesi Selatan, that is similar to this research object. This study was motivated by the highest water elevation due to a flash flood that happened throughout the Bili Bili Dam's operational life on

January 23rd, 2019. Rustan et al. (2019) intended to reveal the depth of inundation and distribution, and compared it to the water level that occurred on the Kembar Bridge based on the documentation picture. The dam breach was simulated using HEC-RAS 2D simulations by assuming a total and sudden collapse without implementing any empirical equations for the dam breach parameters.

Rustan et al. (2019) stated that the Kembar Bridge water elevation that occurred due to 3,464.98 m^3/s was similar to the water elevation that occurred due to a flash flood on January 23rd, 2019. Furthermore, this study revealed that the Bili Bili Dam collapsed in a 24,079.02 m^3/s flood discharge. The calibration model of the Kembar Bridge and the inundation area that occurred due to the Bili Bili Dam collapse can be seen in Figure 2.5 and Figure 2.6 below, respectively.

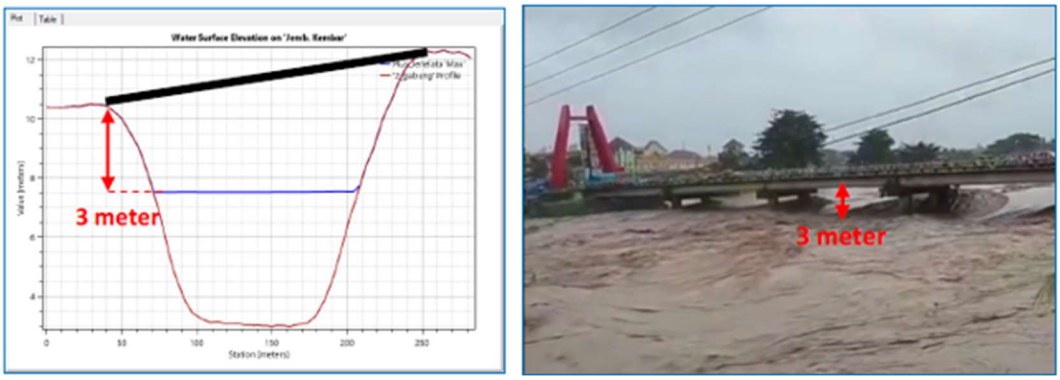

Figure 2. 8 (A) Calibration Model Result, (B) Real Event
(Source: Rustan et al., 2019)

Figure 2. 9 Maximum Condition of Dam Collapse
(Source: Rustan et al., 2019)

2.8 "*Analisa Hidrodinamik Keruntuhan Bendungan Cipanas*" (Ikromi ,2018).

Ikromi (2018) conducted a study on the hydrodynamic simulation of the dam breach on Cipanas Dam, which is located in Kecamatan Ujungjaya, Kabupaten Sumedang, Jawa Barat. Cipanas Dam is a rock-fill dam with a clay core, with 65 crest heights, and it was designed to accommodate 210 million m^3 of water in the reservoir. This study explored hydrodynamic behavior and inundation-affected areas due to the Cipanas Dam breach floods. This dam breach hydrodynamic simulation used HEC-RAS 5.0.5 by implementing the Froehlich (2008) dam breach parameters with the piping failure mode. Furthermore, the simulation was performed with 5 different breach formation times, respectively 1 hour, 1.78 hours, 2 hours, 3 hours, and 4 hours.

Through the five breach formation scenarios in this study, it was shown that the smallest breach formation times led to the flood peak discharge of 40,305.61 m^3/s among other scenarios. Consequently, the arrival time of the flood at the Cikopo-Palimanan Toll Road was 3 hours and 45 minutes, with 11 hours and 15 minutes for the receding time. On the other hand, the Kertajati Airport remained safe from the flood hazard. The hydrograph and maximum water surface elevation resulted from this dam breach, with varying breach formation times shown in Figure 2.10 and Figure 2.11, respectively. Moreover, the inundated area served by this study simulation can be seen in Figure 2.12 below.

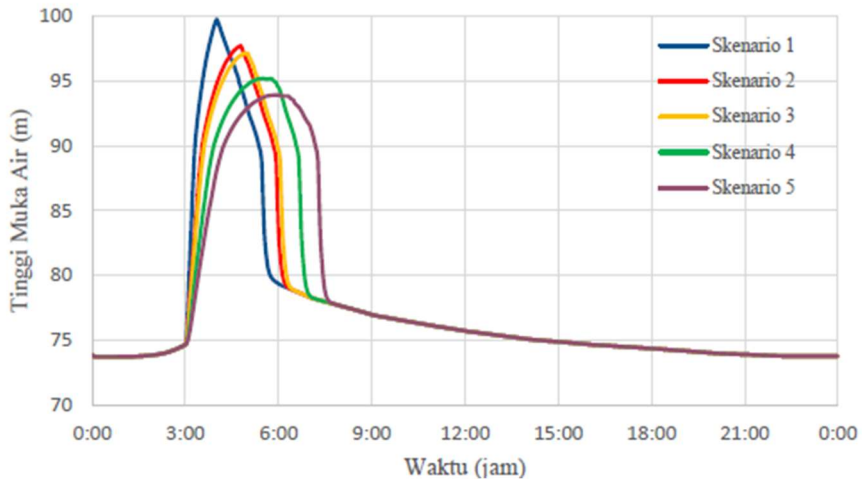

Figure 2. 10 Hydrograph of Water Surface from Various Scenarios
(Source: Ikromi, 2018)

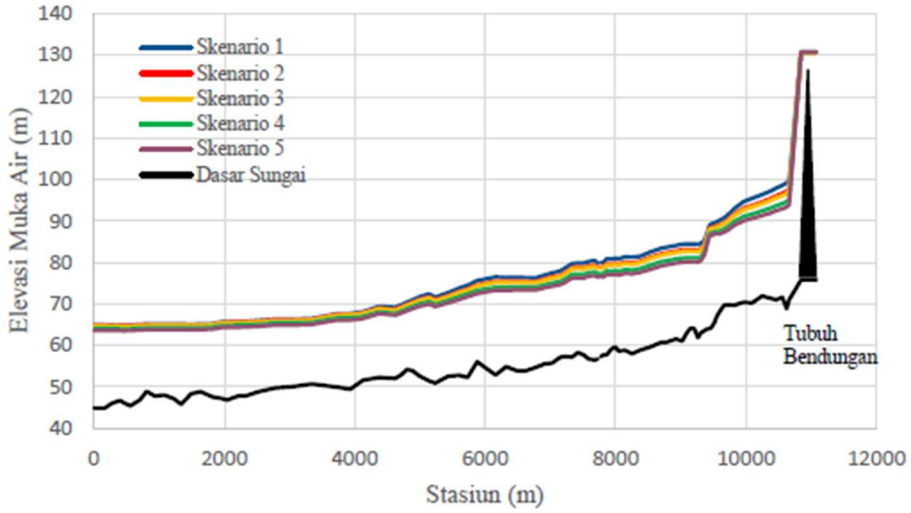

Figure 2. 11 Maximum Water Surface Elevation of Various Scenarios
(Source: Ikromi, 2018)

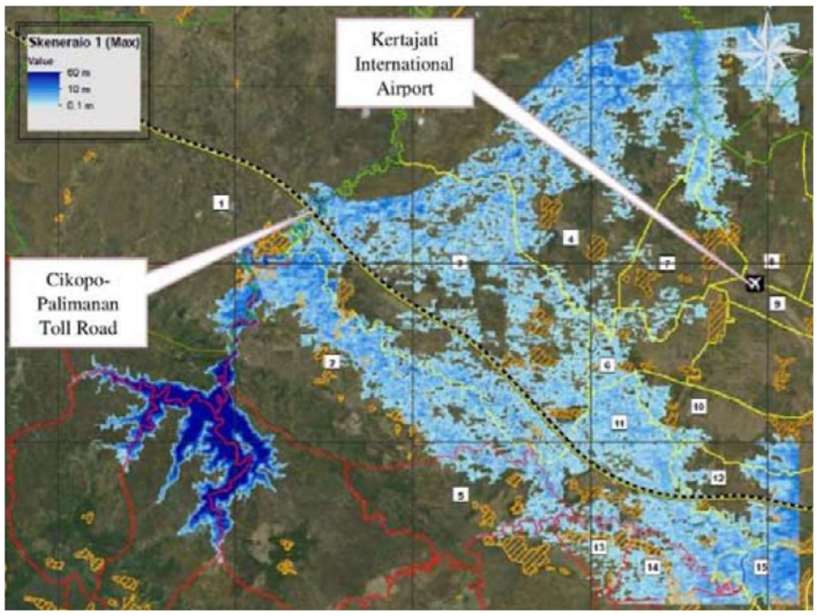

Figure 2. 12 Cipanas Dam Breach Inundation Area Simulation Results
(Source: Ikromi, 2018)

2.9 Research Authenticity

This study sought to identify the impacted areas and potential losses resulting from dam failure due to overtopping and piping failure modes, using the breach parameters established by Froehlich (2016). To assess the worst-case scenarios, three collapse scenarios were simulated, focused particularly on the piping failure at the right-wing dam, the main dam, and the left-wing dam.

Although previous studies had used similar methods and parameters, notably using HEC-RAS to analyze dam break and estimate flood impacts. However, this approach had not been applied to the Bili Bili Dam prior to this research. Consequently, the objectives of comparable studies at the Bili Bili Dam remained unknown.

Research by Rustan et al. (2019) that analyzed the dam break of Bili Bili Dam assumed total and sudden collapse without specifying breach parameters in its analysis. In contrast to this research, Rustan et al. (2019) aimed to validate the discharge that occurred on January 23rd, 2019, by comparing the results with the flood level at the Kembar Bridge and revealed the discharge that hypothetically caused the collapse of the Bili Bili Dam. The earlier relevant research is summarized in Table 2.1 to highlight the contrast with current research.

Table 2. 1 Previous Research Review Recapitulation

No.	Aspect	**Tessema et al. (2024)**	**Yilmaz et al. (2022)**	**Khairi et al. (2022)**	**Bharath et al. (2021)**	**Amri (2021)**	**Rustan et al. (2019)**	**Ikromi (2018)**	**Rahmatna (2026)**
1	Title	Dam breach analysis and flood inundation mapping of Dire Dam, using HEC-HMS and HEC-RAS models	Flood Hazard Analysis due to Overtopping of Dalaman Akköprü Dam: A Case Study	*Analisa Keruntuhan Bendungan Rukoh Kabupaten Pidie Menggunakan Aplikasi HEC-RAS dan Berbasis InaSAFE*	Dam break analysis using HEC-RAS and HEC-GeoRAS: A case study of Hidkal dam, Karnataka state, India	Dam Breach Analysis Using HEC-RAS 5.0.7 and QGIS 3.16.7	*Simulasi Keruntuhan Bendungan Bili Bili Kabupaten Gowa Provinsi Sulawesi Selatan*	*Analisa Hidrodinamik Keruntuhan Bendungan Cipanas*	HEC-RAS 6.6 Dam Break Analysis With InaSAFE Disaster Impact Assessment Approach of Bili Bili Dam
2	Dam Object	Dire Dam Oromia Regional State, Ethiopia	Akköprü Dam Muğla Province, Turkey	Rukoh Dam Pidie District, Aceh	Hidkal Dam Karnataka state, India	Palasari Dam Ekasari District, Bali	Bili Bili Dam Gowa District, South Sulawesi	Cipanas Dam Sumedang District, West Java	Bili Bili Dam Gowa District, South Sulawesi
3	Dam Type	Earth-fill	Earth-fill	Earth-fill	Earth-fill	Earth-fill	Earth-fill	Earth-fill	Earth-fill
4	Failure Mode	Piping & Overtopping	Overtopping	Piping	Piping & Overtopping	Piping	Total and Sudden	Piping	Piping
5	Program Modelling	HEC-RAS	HEC-RAS 2D	HEC-RAS 5.0.7	HEC-RAS 5.0.1	HEC-RAS 5.0.7	HEC-RAS 2D	HEC-RAS 5.0.7	HEC-RAS 6.6
6	Reservoir Volume	19 hm^3	385.26 hm^3	125.7 hm^3	1444.16 hm^3	6 hm^3	375 hm^3	210 hm^3	375 hm^3

Continuation of Table 2.1 Previous Research Review

No.	Aspect	**Tessema et al. (2024)**	**Yilmaz et al. (2022)**	**Khairi et al. (2022)**	**Bharath et al. (2021)**	**Amri (2021)**	**Rustan et al. (2019)**	**Ikromi (2018)**	**Rahmatna (2025)**
7	Research Purpose	- Investigate the breach analysis of the Dire Dam concerning different inflow scenarios and failure modes, - Create flood inundation mapping for the downstream area of the dam.	- Determine the possible flood risk due to a hypothetical dam breach, - Develop mitigation measures for the affected areas.	- Reveal the hazards and estimate economic losses caused by the dam break of Rukoh Dam.	- Estimate the maximum flood discharge and its correspondin g stages, - Estimate the flood peak occurrence time.	- Obtain the hydrograph from the dam breach analysis from the determined locations - Identify the arrival time of the flood in affected areas. - Inundation mapping for the downstream area	- Reveal the depth of inundation and distribution, - Compare it to the water level that occurred on the Kembar Bridge.	- Explore the hydrodynami c behavior due to the Cipanas Dam break - Inundation-affected areas due to the Cipanas Dam break	- Identify the impacted areas due to the Bili Bili Dam break, - Identify potential losses resulting from Bili Bili Dam break.
8	Research Results	The Dire Dam will experience breaching when the maximum flood reaches 7,073.02 m3/s and 11,021.92 m3s-1 due to overtopping and piping, respectively.	The average flood arrival time from upstream to the center city of Ortaca is 2 hours and 20 minutes, while to the center city of Dalaman is 2 hours and 50 minutes	The largest inundated area among the various considered scenarios is 237.409 km2, and is estimated at IDR 573,068,311,48 0 in economic losses	The peak flow shows that 72,085.45 m3/s and 78,454.82 m3/s with 75.224 km2 and 79.205 km2 of inundation area, respectively piping and overtopping scenarios.	The shortest breach formation time scenario gives the highest peak flow discharge among other breach formation scenarios, with the value of 8733.17 m3/s.	The Kembar Bridge water elevation that occurred due to 3464.98 m3s-1 is similar to the water elevation that occurred due to a flash flood on January 23rd, 2019.	It shows that the smallest breach formation times lead to the flood peak discharge of 40,305.61 m3/s among other scenarios.	-

CHAPTER III
THEORETICAL BASIS

3.1 Design Flood

Based on Chow et al. (1988), the objectives of planning and managing water resources could generally be divided into two main categories, namely water control and water use. The difference between the two purposes is that design for water control is usually concerned with extreme events of short duration, such as the instantaneous peak discharge during a flood, or the minimum flow over a period of a few days during a dry period, while design for water use is concerned with the complete flow hydrograph over a period of years. The design variable, such as the design discharge, required a selected value to determine the inflow to the system. The ideal magnitude for design achieves a balance between cost and safety concerns.

Novak et al. (2007) pointed out that in a dam structure, there must be a spillway to discharge excess flows to the downstream safely. The design of the spillway is primarily determined by the design flood, type of dam, site location, and the size and operation of the reservoir. The approaches for determining design floods differed across various countries and are found in codes and guidelines. In numerous situations, the highest standard is using the possible maximum flood. In Indonesia, the determination of design flood was stated in Standar Nasional Indonesia 03-3432-1994 and later updated in Standar Nasional Indonesia 3432-2020, shown in Table 3.1.

Table 3. 1 Design Flood of Old Dam

Dam Type	Dam Size	Dam Height (meters)	Old Dam	
			High Consequence Level	Low Consequence Level
			Design Flood (Inflow)	Design Flood (Inflow)
Embankment Dam	Small	$h \leq 5$ m	Q100	Q100
		$5 < h \leq 10$ m	Q100	Q100
		$10 < h \leq 15$ m	Q1000 or 0.5 PMF	Q500

Continuation of Table 3.1 Design Flood of Old Dam

Dam Type	Dam Size	Dam Height (meters)	Old Dam	
			High Consequence Level	Low Consequence Level
			Design Flood (Inflow)	Design Flood (Inflow)
Embankment Dam	Large	15 < h ≤ 40 m	Q1000 or 0.5 PMF	Q1000 or 0.5 PMF
		40 < h ≤ 80 m	Q1000 or 0.5 PMF	Q1000 or 0.5 PMF
		h > 80 m	Q1000 or 0.5 PMF	Q1000 or 0.5 PMF
Concrete Dam	—	—	Q100	Q100

Source: SNI 3432-2020

Table 3. 2 Design Flood of New Dam

Dam Type	Dam Size	Dam Height (meters)	New Dam	
			High Consequence Level	Low Consequence Level
			Design Flood (Inflow)	Design Flood (Inflow)
Embankment Dam	Small	h ≤ 5 m	Q100	Q100
		5 < h ≤ 10 m	Q1000 or 0.5 PMF	Q500
		10 < h ≤ 15 m	Q1000 or 0.5 PMF	Q500
	Large	15 < h ≤ 40 m	PMF	0.5 PMF
		40 < h ≤ 80 m	PMF	0.75 PMF
		h > 80 m	PMF	PMF
Concrete Dam	—	—	Q1000	Q1000

Source: SNI 3432-2020

Several existing hydrology and hydraulic applications textbooks universally prescribe that there are two different design floods for designing a spillway: (a) probable maximum flood (PMF) for high-hazard dams; and (b) return period events or commonly called standard project flood (SPF) for lower-hazard dams (Chow et al., 1988; Novak et al., 2007; Subramanya, 2008).

1. Probable Maximum Flood (Q_{PMF})

   The probable maximum flood is the largest hypothetical flood that can happen due to the highest precipitation. Chow et al. (1988) defined probable maximum flood as “the greatest flood to be expected assuming complete coincidence of all factors that would produce the heaviest rainfall and maximum runoff”, and Subramanya (2008) defined probable maximum flood as “the extreme flood

that is physically possible in a region as a result of severemost combinations, including rare combinations of meteorological and hydrological factors.”. Both specified that the probable maximum flood is derived from probable maximum precipitation (PMP).

2. Return Period Flood (Q_T)

   A return period flood is a hydrological event of a specific peak discharge that has a statistical probability of occurrence once every T period, through the frequency and intensity of flooding events, based on historical data. Chow et al. (1988) expressed the return period through an extreme event of a random variable X that is greater than or equal to some level x_T. While $_T$ is the time interval between occurrences of $X \geq x_T$.

3.2 Flood Hydrograph

A hydrograph is a curve that represents the relationship between streamflow and time parameters (Triatmodjo, 2019). Subramanya (2008) defined a hydrograph as “a plot of the discharge in a stream plotted against time chronologically”. Chow (1959) in Chow et al. (1988), stated that the hydrograph is "an integral expression of the physiographic and climatic characteristics that govern the relations between rainfall and runoff of a particular drainage basin". The interpretation may vary based on the specific time frame being considered; therefore, four types of hydrographs can be produced (Subramanya, 2008), namely:

1. Annual Hydrographs

   Showing the variation of daily or weekly, or 10 daily mean flows over a year.

2. Monthly Hydrographs

   Showing the variation of daily mean flows over a month.

3. Seasonal Hydrographs

   Depicting the variation of the discharge in a particular season, such as the monsoon season or the dry season.

4. Flood Hydrographs

   Represents stream flow due to a storm event over a catchment.

A hydrograph essentially has three characteristic regions: (1) the rising limb, (2) the crest or inflection segment, and (3) the recession or falling limb, which shows the dynamic of how a specific catchment responds to rainfall. It represents the flow from three types of runoffs: surface runoff, subsurface flow, and base flow. The hydrograph reflects the combined effects of various factors related to the catchment area and the rainfall, which can interact in complicated ways. As a result, two different storms in the same catchment will create different visualizations of hydrographs and conversely. Hence, the interactions between storms and catchments are complex (Subramanya, 2008). Therefore, the flood hydrograph components are represented in Figure 3.1 below.

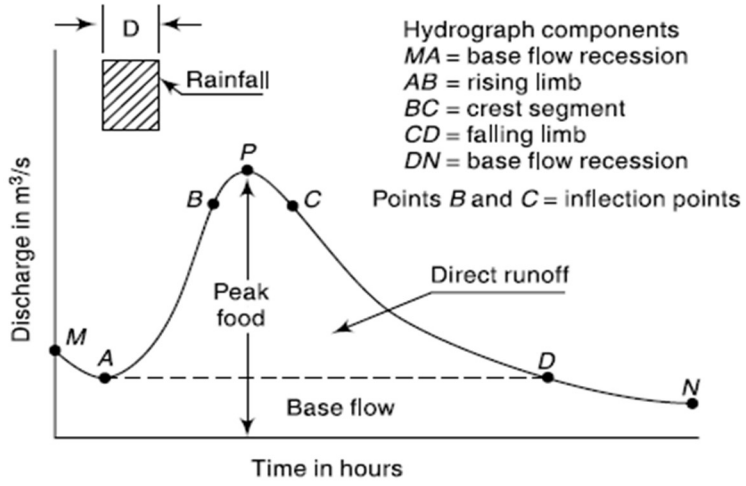

Figure 3. 1 Elements of a Flood Hydrograph
(Source: Subramanya, 2008)

The main components of a Flood Hydrograph are explained below.

1. Rising Limb

   The rising limb (point *A*-*B* in Figure 3.1), also called the concentration curve, shows how discharge increases as water builds up in the channel and over the catchment area. During the early stages of a storm, initial losses and high rates of water soaking into the ground cause the discharge to rise slowly. As the storm continues, infiltration losses will decrease and create the overland flow; consequently, more water from distant areas flows toward the basin outlet. (Subramanya, 2008).

2. Crest Segment

   The crest segment (point *B*-*C* in Figure 3.1) is a key part of a hydrograph because it shows the peak flow (point *P* in Figure 3.1). The peak flow occurs when water runoff from various areas of the catchment converges simultaneously, resulting in the highest flow at the basin outlet. For large catchments, peak flow usually occurs after the rain has stopped (Subramanya, 2008).

3. Falling Limb

   The recession limb (point *C*-*D* in Figure 3.1) extends from the point of inflection at the end of the crest segment (point *C* in Figure 3.1) to the start of the natural groundwater flow (point *D* in Figure 3.1). The falling limb represents the water accumulated in the earlier phases of the hydrograph is decreasing over time. The point of inflection represents the condition of maximum storage (Subramanya, 2008).

3.3 Flood Routing

A flood flow that moves through the reach will undergo a configuration change due to various factors, such as channel irregularities, resistance, and lateral addition. When a flood flow passes through a reservoir, its peak will be attenuated, and the time base is enlarged due to the effect of storage (Chow et al., 1988; Subramanya, 2008). The impact of the configuration change will decrease the peak inflow from upstream as it moves to the downstream as outflow.

Flood routing refers to the analysis of flood wave transformation along a watercourse. Two types of methods: (1) lumped system (hydrologic) routing, and (2) distribution system (hydraulic) routing. Hydrologic routing calculates the flow as a function of time alone at a particular location. Hydraulic routing calculates the flow as a function of space and time throughout the system (Chow et al. 1988).

Chow (1959) pointed out that the hydrologic route method is generally simpler than the hydraulic route, but it fails to give satisfactory results for floods through long rivers with complex geometry, especially when the backwater and

surges case occurs. Therefore, those cases can only be accurately assessed using the hydraulic method, rather than the hydrologic method.

Hence, the hydraulic routing will be used in HEC-RAS for the dam break study. This tool can perform flood routing to predict downstream flow behaviour using either one-dimensional or two-dimensional unsteady flow methods, providing accurate results for both breach and non-breach scenarios. It can provide the water surface slope through the pool as the inflow hydrograph propagates, along with variations in water surface slope that occur during a dam breach (Brunner, 2024). Further explanation of HEC-RAS will be provided later in this chapter.

3.4 Manning's Roughness Coefficient

Manning's roughness was introduced by Robert Manning, who expressed the flow resistance of the channel through an empirical formula. The roughness coefficient was once a dimensional formula of *C* and was adopted into a modern Manning's formula through a dimensionless coefficient of *n*. Based on Chow (1959), the formula derived from Strickler (1923) is universally known as:

$$V = \frac{1}{n} R^{2/3} S^{1/2} \quad (3.1)$$

where,

V = Velocity (m/s)

n = Manning roughness coefficient ($s/m^{1/3}$)

R = Hydraulic radius (m)

S = Energy slope or equivalent to channel bed slope

In Manning's formula, other parameters must be determined, whereas the identification of the roughness coefficient *n* is the main concern, as there is no exact method to determine the *n* value. Defining a specific value of *n* essentially involves assessing the resistance to flow within a particular channel, which fundamentally concerns factors that are not easily expressed or measured as a quantity (Chow, 1959). Chow (1959) underscored that when choosing the *n* coefficient, professional

engineers may rely on engineering judgment, while for beginners, it would be a guess, and different individuals may lead to different outputs.

Manning's *n* values for typical channels are widely written in hydraulic books. A key reference for roughness coefficients in streams and floodplains is Chow's (1959), which provides an authoritative compilation of these values. Brunner (2024) excerpted from Manning's *n* from Chow (1959), which included *n* values for the most common channel types, are presented in the table below.

Table 3. 3 Most Common Manning's *n* Value for Natural Stream

Type of Channel and Description	Min (n)	Normal (n)	Max (n)
A. Natural Streams			
1. Main Channels			
a. Clean, straight, full, no rifts or deep pools	0.025	0.030	0.033
b. Same as above, but with more stones and weeds	0.030	0.035	0.040
c. Clean, winding, some pools and shoals	0.033	0.040	0.045
d. Same as above, but some weeds and stones	0.035	0.045	0.050
e. Same as above, lower stages, more ineffective slopes	0.040	0.048	0.055
f. Same as "d" but more stones	0.045	0.050	0.060
g. Sluggish reaches, weedy, deep pools	0.050	0.070	0.080
h. Very weedy reaches, deep pools, or floodways with heavy timber/brush	0.070	0.100	0.150
2. Flood Plains			
a. Pasture, no brush			
1) Short grass	0.025	0.030	0.035
2) High grass	0.030	0.035	0.050
b. Cultivated areas			
1) No crop	0.020	0.030	0.040
2) Mature row crops	0.025	0.035	0.045
3) Mature field crops	0.030	0.040	0.050
c. Brush			
1) Scattered brush, heavy weeds	0.035	0.050	0.070
2) Light brush and trees, winter	0.035	0.050	0.060
3) Light brush and trees, summer	0.040	0.060	0.080
4) Medium to dense brush, winter	0.045	0.070	0.110
5) Medium to dense brush, summer	0.070	0.100	0.160
d. Trees			
1) Cleared land with tree stumps, no sprouts	0.030	0.040	0.050
2) Same as above, but heavy sprouts	0.050	0.060	0.080
3) Heavy stand of timber, few down trees, little undergrowth, flow below branches	0.080	0.100	0.120
4) Same as above, but with flow into branches	0.100	0.120	0.160
5) Dense willows, summer, straight	0.110	0.150	0.200
3. Mountain Streams (no vegetation in channel, steep banks)			
a. Gravels, cobbles, a few boulders	0.030	0.040	0.050
b. Cobbles with large boulders	0.040	0.050	0.070

Source: Brunner (2024)

The recommended Manning's roughness values for the global LULC 2020-ESRI dataset were derived from a comprehensive study by Soliman et al. (2022). The study compared the LULC 2020-ESRI dataset with the NLCD 2019 dataset, achieving an overall accuracy of 72%. The proposed Manning's values were calibrated and validated using HEC-RAS 2D modelling across nine catchments in the conterminous United States, demonstrating acceptable accuracy with an average peak flow error of 5.22% and RMSE in depth of 2.7 cm. The weighted average method was identified as the most effective for determining roughness values, particularly for biased classes like trees, grass, and built areas (Soliman et al. 2022).

Table 3. 4 Recommended Manning's Roughness (n) Values for the Global LULC ESRI Topologies

LULC 2020-ESRI Classification		Suggested Roughness Values		
LULC-Value	Description	Minimum (n)	Maximum (n)	Average (n)
1	Water	0.025	0.05	0.038
2	Trees	0.079	0.174	0.126
3	Grass	0.025	0.05	0.038
4	Flooded Vegetation	0.05	0.085	0.061
5	Crops	0.02	0.05	0.035
6	Scrub/shrub	0.07	0.16	0.115
7	Built Area	0.064	0.119	0.092
8	Bare ground	0.023	0.03	0.027

Source: Soliman et al. (2022)

3.5 Dam Breach

3.5.1 Breach Formation

Three empirical breach models of breach formation are widely employed in dam failure analysis (i.e., Model A, Model B, and Model C). Each model presumes that a breach initiates at the upper part of a dam, and the breach opening gradually widens over time into either a triangular or trapezoidal shape (Froehlich, 2008).

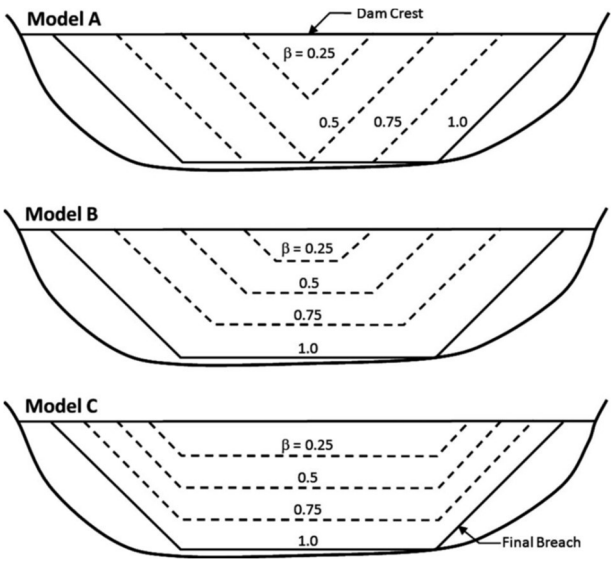

Figure 3. 2 Schematic Representation of Three Empirical Breach Formation Models
(Source: Froehlich, 2008)

The breach's characteristics include height, average width, and side slope of the trapezoidal opening in the dam. In Model A, breaches start as triangles until the bottom reaches its lowest point, after which they expand laterally into a trapezoidal shape. Model B shows a linearly increasing base width as the breach deepens, with maximum height and width achieved simultaneously. In Model C, the bottom width remains constant. Historical dam failure observations suggest that Model A best represents breach development (Froehlich, 2008).

3.5.2 Failure Modes

A dam can experience failure due to various factors, which depend on the specific type of dam and the conditions at the site. Moreover, the shape of the breach and the timing of a dam's failure can differ based on the dam's classification. For example, concrete gravity dams often exhibit a partial breach, where one or more sections constructed during the building process collapse, whereas concrete arch dams commonly fail suddenly and completely. In contrast, embankment dams usually breach until the reservoir is drained or the materials that have breached become resistant to erosion, such as at the base of the dam (FEMA, 2013).

ICOLD (2019) reported that embankment dams have a dominant number of dams that failed among other dam types from pre-1900 to post-2000, with the most

frequent cause of failure being due to internal erosion and overtopping. A study by Zhong et al. (2021) compiled the historical records of embankment dam failures up to 2020, showing that embankment dams fail with 48% due to overtopping, 35% due to piping, 4% due to sliding, and 13% other causes. Brunner (2024) adopts potential failure modes from Costa (1985) and Atallah (2002) for different types of dams, which are listed in Table 3.5.

Table 3. 5 Possible Failure Modes for Various Dam Types

Failure Mode	Earthen/ Embankment	Concrete Gravity	Concrete Arch	Concrete Buttress	Concrete Multi-Arch
Overtopping	**X**	**X**	**X**	**X**	**X**
Piping/Seepage	**X**	**X**	**X**	**X**	**X**
Foundation Defects	**X**	**X**	**X**	**X**	**X**
Sliding	**X**	**X**		**X**	
Overturning		**X**	**X**		
Cracking	**X**	**X**	**X**	**X**	**X**
Equipment Failure	**X**	**X**	**X**	**X**	**X**

Source: Brunner (2024)

1. Overtopping Failure

   Overtopping happens when the water level in the reservoir surpasses the height of the dam and flows over the dam face. The overflow water continues to erode the face of the dam from the top downstream dam as it reaches the foundation base. Overtopping typically results from an insufficient design of the spillway capacity to handle the resulting flooding event. A failure may also occur when a reservoir's outlet system malfunctions (FEMA, 2013). The overtopping failure stage process on an embankment dam is represented in Figure 3.3

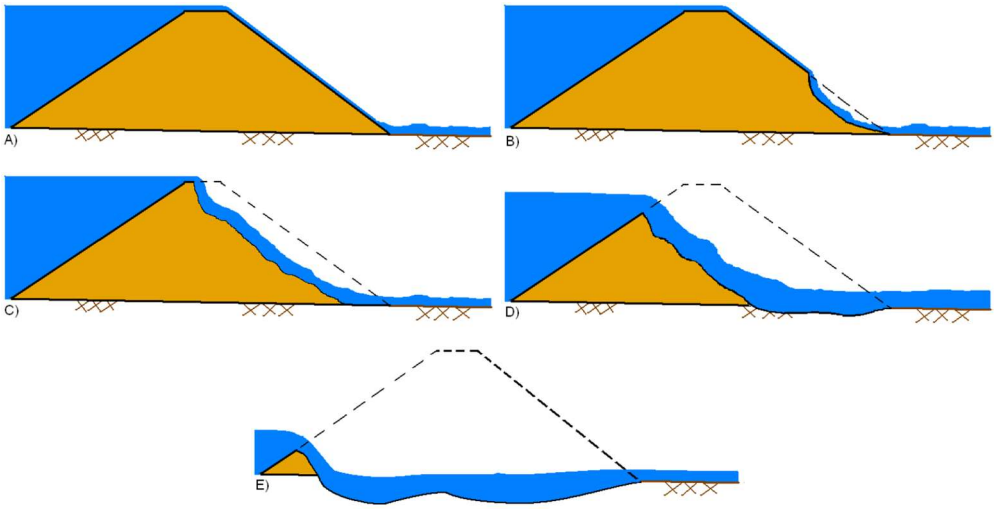

Figure 3. 3 Overtopping Failure Process of Earthen Dam
(Source: Brunner, 2024)

2. Piping Failure

Piping happens when concentrated seepage erodes an embankment dam, forming large voids in the soil. The process starts as water seeping through the dam core accelerates in speed and volume, eroding fine sediments. If enough material had been removed, a direct connection forms from the reservoir to the dam face, making failure nearly inevitable (FEMA, 2013). The piping failure stage process on an embankment dam is represented in Figure 3.4.

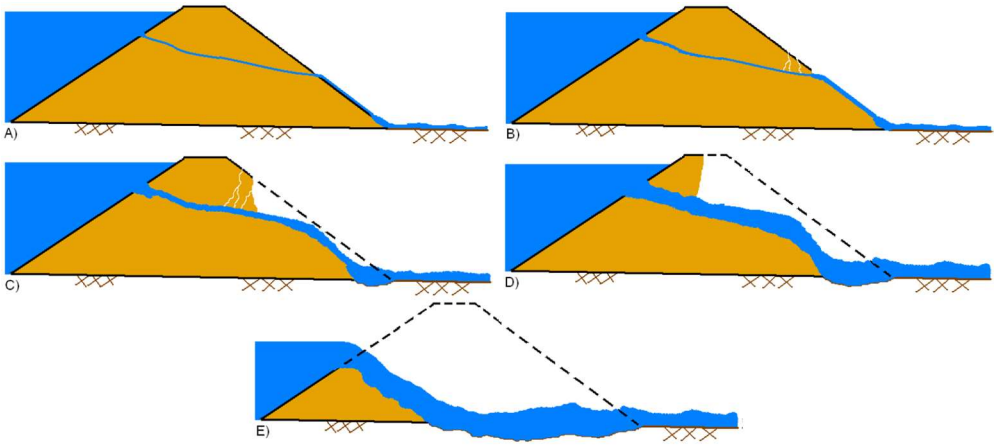

Figure 3. 4 Piping Failure Process of Earthen Dam
(Source: Brunner, 2024)

3.5.3 Breach Parameters

Breach parameters are the key characteristics that describe the geometry and time development of a dam breach. These parameters are critical inputs for hydraulic modelling of a dam break study. Hence, there are several sets of empirical and semi-theoretical formulas to predict breach parameters of a dam. As one of them, Froehlich (2016) has continuously developed the dam breach parameters in 1995, 2008, and 2016, which are the most recent breach parameters developed by Froehlich (2016). Therefore, Froehlich's (2016) breach parameters were used in this study. The final geometry of the trapezoidal dam breach is illustrated in the following Figure 3.5.

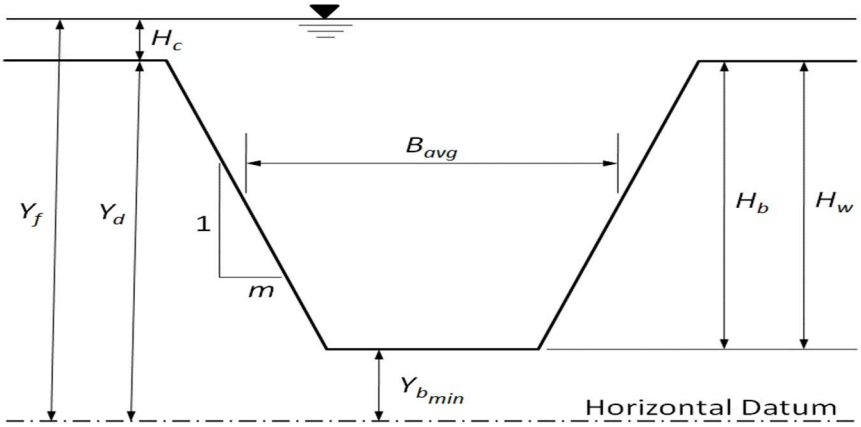

Figure 3. 5 Dimension of a Trapezoidal Dam Breach Approximation
(Source: Froehlich, 2016)

In earlier research, Froehlich (1995) analyzed data from 63 embankment dam failures through an empirical model of breach formation using multiple regression to estimate the height, average width, side slope ratio, and formation time (Froehlich, 1995). In a later study in 2008, Froehlich expanded the data up to 73 embankment dam failures utilizing the same empirical model and method from 1995 (Froehlich, 2008). Further, in Froehlich's (2016) latest development, the empirical model of breach formation was analyzed using multivariate nonlinear modelling, which involved 110 embankment dam failures.

The mathematical expression of breach parameters by Froehlich (2016) is presented as follows.

1. Average breach width

   The average breach width (B_{avg}) equation defines the final cross-sectional opening of the dam, which primarily controls the peak discharge of the released flood wave. This formula is presented in Equation 3.2.

$$B_{avg} = 0.28 \times k_M \times k_H \times {V_w}^{1/3} \times {W_{avg}}^{-1/6} \times {H_b}^{1/6} \quad (3.2)$$

   where,

$$k_M = \begin{cases} 1.0, & \text{for internal erosion failures} \\ 1.5, & \text{for overtopping failures} \end{cases},$$

$$k_H = \begin{cases} \left(\frac{H_b}{H_s}\right)^{1/2}, & \text{for } H_b < H_s, \text{ and} \\ 1.0, & \text{for } H_b \geq H_s \end{cases}$$

$$H_s = \begin{cases} 6.1 \text{ m}, & \text{for SI units} \\ 20 \text{ ft}, & \text{for U.S. customary units} \end{cases},$$

   The equation indicates that the average breach width (B_{avg}) rises with an increase in both the volume of stored water (V_w) and the height of the breach (H_b), while it decreases with wider embankment widths (W_{avg}) (Froehlich, 2016a).

2. Breach formation time

   The breach formation time (t_f) estimates the duration required for the breach to develop fully from its initial to final cross-section. This parameter is critical to express the reservoir water level recession and influence the outflow hydrograph shape. This equation is presented in Equation 3.3.

$$t_f = 50 \times \sqrt{\frac{V_w}{g{H_b}^2}} \times \left(\frac{W_{avg}}{H_b}\right)^{1/4} \quad (3.3)$$

   The equation shows that the breach formation time (t_f) increases with a larger volume of stored water (V_w) and average embankment widths (W_{avg}), while it decreases as the embankment height rises (Froehlich, 2016).

3. Average side slope ratio

   The average side slope ratio (m) is a constant value that defines whether the breach sides remain relatively steep or flatten out as the failure progresses. This

constant parameter is assigned based on the failure mode of the dam breach as follows.

$$m = \begin{cases} 0.6, & \text{for internal erosion failures} \\ 1.0, & \text{for overtopping failures} \end{cases},$$

3.6 HEC-RAS Open Channel

Flow in an open channel is classified as steady if the flow depth remains unchanged or can be assumed to be constant during the relevant time. Flow is considered unsteady if the depth varies over time. In scenarios such as floods and surges, which serve as typical examples of unsteady flow, the flow stage changes rapidly as the waves move through, making the timing aspect crucial in the design of control structures (Chow, 1959).

Brunner (2024) stated that the HEC-RAS modelling system can simulate different types of water flow in open channels. It handles one-dimensional unsteady flow, two-dimensional unsteady flow, or a combination of both. The one-dimensional flow equation solver, adapted from Dr. Robert L. Barkau's UNET model (Barkau, 1992, and HEC,1997), is mainly used for calculations involving subcritical flow. The two-dimensional flow solver was developed at HEC and is directly integrated into the HEC-RAS unsteady flow engine to allow for combined 1D and 2D hydrodynamic modelling.

3.6.1 One-Dimensional Unsteady Flow Hydrodynamics

The physical principles that govern the water flow in a stream are the conservation of mass (continuity), the conservation of momentum. These principles are represented mathematically through partial differential equations, which later will be referred to as the continuity and momentum equations (Brunner, 2024).

1. Continuity Equation

   The elementary control volume used to derive the continuity equation is illustrated in Figure 3.6 below.

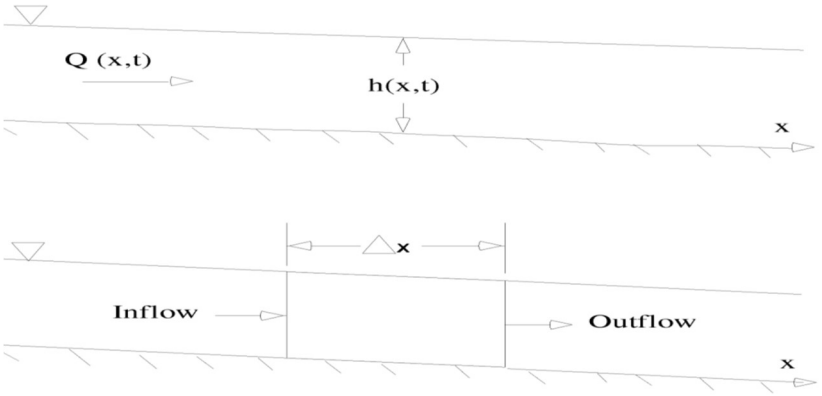

Figure 3. 6 Elementary Control Volume
(Source: Brunner, 2024)

The distance x is measured along the channel as shown. In the middle of this area, the flow rate is called $Q(x,t)$, and the total flow area is called A_T. The total flow area consists of the active area A and the off-channel storage area S. Furthermore, the principle of mass conservation for a control volume indicates that the total flow entering the volume is equal to the rate at which mass is changing within the volume. The derived equation presented below is based on Mahmoud and Yevjevich (1975) in Brunner (2024).

The rate of inflow is

$$Q - \frac{\partial Q}{\partial x}\frac{\Delta x}{2} \tag{3. 4}$$

The rate of outflow is

$$Q + \frac{\partial Q}{\partial x}\frac{\Delta x}{2} \tag{3. 5}$$

The rate of change in storage as

$$\frac{\partial A_T}{\partial t}\Delta x \tag{3. 6}$$

If we assume that Δx is small, then the change in mass within the control volume is equal to

$$\rho\frac{\partial A_T}{\partial t}\Delta x = \rho\left[\left(Q - \frac{\partial Q}{\partial x}\frac{\Delta x}{2}\right) - \left(Q + \frac{\partial Q}{\partial x}\frac{\Delta x}{2}\right) + Q_t\right] \tag{3. 7}$$

Breaking it down and dividing by ρ results in the conclusive expression of the continuity equation.

$$\frac{\partial A_T}{\partial t} + \frac{\partial Q}{\partial x} = q_t \tag{3. 8}$$

2. Momentum Equation

Newton's second law expresses conservation of momentum as

$$\sum F_x = \frac{d}{dt}\vec{M} \tag{3. 9}$$

The principle of momentum conservation for a control volume indicates that the total rate of momentum entering the volume (momentum flux), combined with the total of all external forces acting on the volume, equals the rate at which momentum is changing within the volume. The momentum flux (MV) is calculated as the product of fluid mass and the velocity vector in the flow direction. Three forces will be considered in the momentum conservation principle, namely, pressure, gravity, and boundary drag, or friction force.

a) Pressure force

Pressure forces at the upstream are

$$F_P - \frac{\partial F_P}{\partial x}\frac{\Delta_x}{2} \tag{3. 10}$$

Pressure forces at the downstream are

$$F_P + \frac{\partial F_P}{\partial x}\frac{\Delta_x}{2} \tag{3. 11}$$

Net pressure force is

$$F_g = -\rho g A \frac{\partial h}{\partial x}\Delta x \tag{3. 12}$$

b) Gravitational force

$$F_g = -\rho g A \frac{\partial z_0}{\partial x}\Delta x \tag{3. 13}$$

The derived gravitational force will be positive for negative bed slopes.

c) Boundary drag/Friction force

$$F_f = -\rho g A S_f \Delta_x \quad (3.14)$$

Friction slope

$$s_f = \frac{Q|Q| \times n^2}{2.208 R^{4/3} A^2} \quad (3.15)$$

d) Momentum flux

Flux entering the control volume

$$\rho \left[QV - \frac{\partial QV}{\partial x} \frac{\Delta_x}{2} \right] \quad (3.16)$$

Flux leaving the control volume

$$\rho \left[QV + \frac{\partial QV}{\partial x} \frac{\Delta_x}{2} \right] \quad (3.17)$$

The Net rate of momentum flux entering the control volume is

$$-\rho \frac{\partial QV}{\partial x} \Delta_x \quad (3.18)$$

The net rate of momentum flux plus the sum of all forces acting on the volume is equal to the rate of accumulation of momentum. Therefore, it can be expressed as

$$\rho \Delta x \frac{\partial Q}{\partial t} = -\rho \frac{\partial (QV)}{\partial x} \Delta_x - \rho g A \frac{\partial h}{\partial x} \Delta x - \rho g A \frac{\partial z_0}{\partial x} \Delta x - \rho g A S_f \Delta_x \quad (3.19)$$

While the elevation of the water surface z is equal to $z_0 + h$, therefore

$$\frac{\partial z_2}{\partial x} = \frac{\partial h}{\sigma x} + \frac{\partial z_0}{\partial x} \quad (3.20)$$

Final Form

$$\frac{\partial Q}{\partial t} + \frac{\partial (QV)}{\partial x} + gA \left(\frac{\partial z_s}{\partial x} + S_{\dot{f}} \right) = 0 \quad (3.21)$$

3.6.2 Dam Break Inflow Flood Routing

HEC-RAS provides two primary methods for routing the reservoir inflow during a dam break event, which are (1) full dynamic wave (unsteady flow) routing and (2) level pool routing. The differences between each method through a reservoir

can be complex to measure (Brunner, 2024). The concept of both methods can be briefly explained as follows.

1. Full Dynamic Wave Routing

Full dynamic wave routing is the most accurate method for simulating a reservoir pool, especially in record pool levels and outflows on long and narrow reservoirs. In HEC-RAS, it has the option to model the pool using 1D cross sections throughout the entire reservoir, similar to how a typical river reach would be approached, or alternatively, the reservoir pool can be represented as a single 2D flow area (Brunner, 2024). The illustration of the full dynamic wave (unsteady flow) routing modelling can be seen in Figure 3.7.

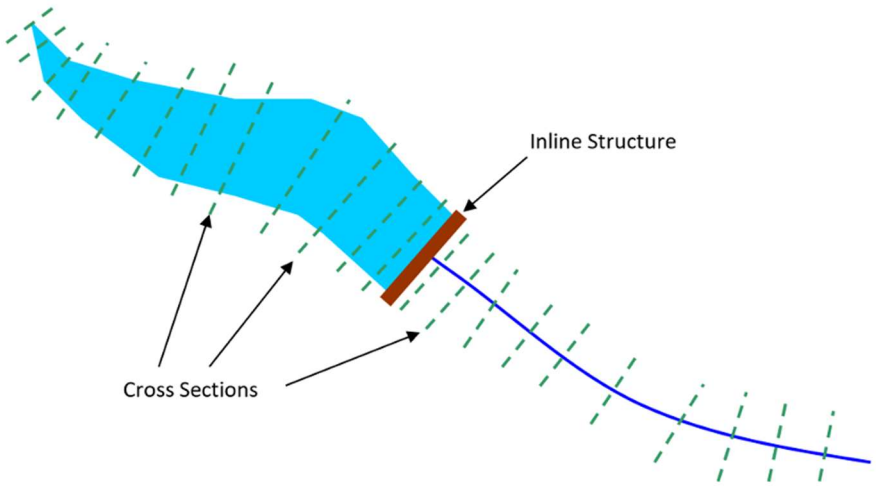

Figure 3. 7 Schematic View of Full Dynamic Wave Routing
(Source: Brunner, 2024)

2. Level Pool Routing

Level pool routing treats the pool area as a storage area. When a dam break is modelled using this method, the breach discharge is computed by using the same equations as the full dynamic wave method. The key difference is that the water from the dam comes from the storage area. As the water flows out of the breach, the storage area elevation will drop to a level pool. This method is more accurate in capturing the pool elevations and discharge of wide and short reservoirs (Brunner, 2024). The illustration of the level pool routing modelling can be seen in Figure 3.8.

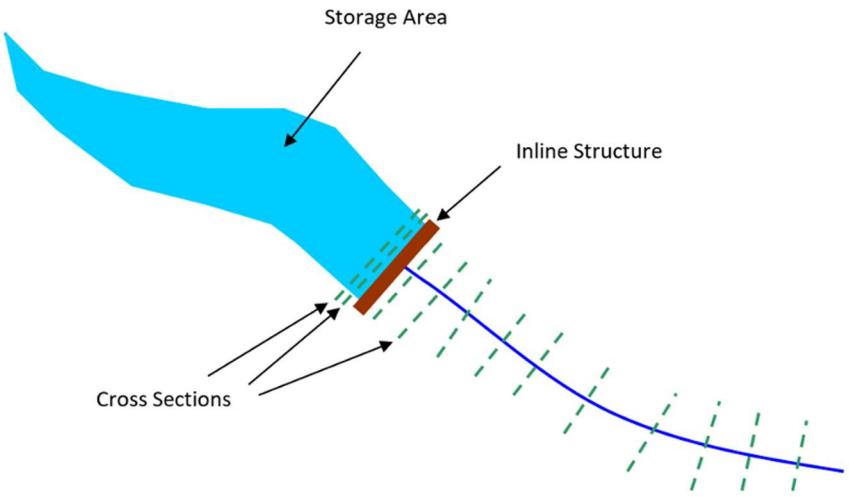

Figure 3. 8 Schematic View of Level Pool Routing
(Source: Brunner, 2024)

The selection of an appropriate flood routing method is a critical step in modelling a dam breach event, as it directly influences the accuracy of the resulting downstream hydrograph. The key parameters provided by Brunner (2024) that must be considered on choosing the appropriate flood routing in a dam break study are briefly explained as follows.

1. Proximity of Downstream Population

   The "level pool" method may be sufficient when the downstream population is located a significant distance from the dam. It is because the flood wave will spread out and lose energy as it travels, making the exact details of its initial shape less critical by the time it reaches the distant location. The "full dynamic" method is essential for the concerned downstream population immediately near the dam, as it accurately captures the critical peak discharge and timing of the flood wave, which influences immediate impacts.

2. Data Availability

   The "level pool" method is preferred when the detailed bathymetric data for the reservoir pool is unavailable or has low resolution, which does not represent the actual elevation-volume. The "full dynamic" method can be used when the detailed bathymetric data has good resolution, as it represents the actual reservoir's elevation-volume and produces more accurate results.

3. Tributary River

The “level pool” method may be applied in reservoir systems that are hydraulically simple, specifically those with no significant tributaries entering the pool. In this method, the entire reservoir is treated as a single, lumped storage volume. The “full dynamic” method is necessary if there are major tributaries that enter the reservoir. This method is uniquely capable of dynamically modelling the two-directional interactions between the main pool and its tributaries. It can simulate the backwater storage up the tributary channels as the reservoir fills and the subsequent contribution of this stored water during the drawdown phase. Furthermore, it can accurately route the tributary's inflow hydrograph through the system.

3.7 InaSAFE Risk Assessment

InaSAFE is an open-source application to facilitate and assist with better planning and mitigation in disasters. The initial focus was on Indonesia, a country vulnerable to disasters such as floods, tsunamis, volcanoes, earthquakes, as well as localized disasters such as landslides, forest fires, etc. Further, InaSAFE has been adopted by other countries (InaSAFE, 2017).

InaSAFE combines an exposure data layer with a hazard layer to produce a spatial impact layer of the disaster, along with summary statistical information and questions for action. InaSAFE can also provide impact results by administrative boundary and provide detailed information related to the gender and age of the affected population (InaSAFE, 2017).

The InaSAFE operational workflow for generating a disaster impact assessment is illustrated in Figure 3.9, which outlines the key stages from data input to the final output of the InaSAFE features.

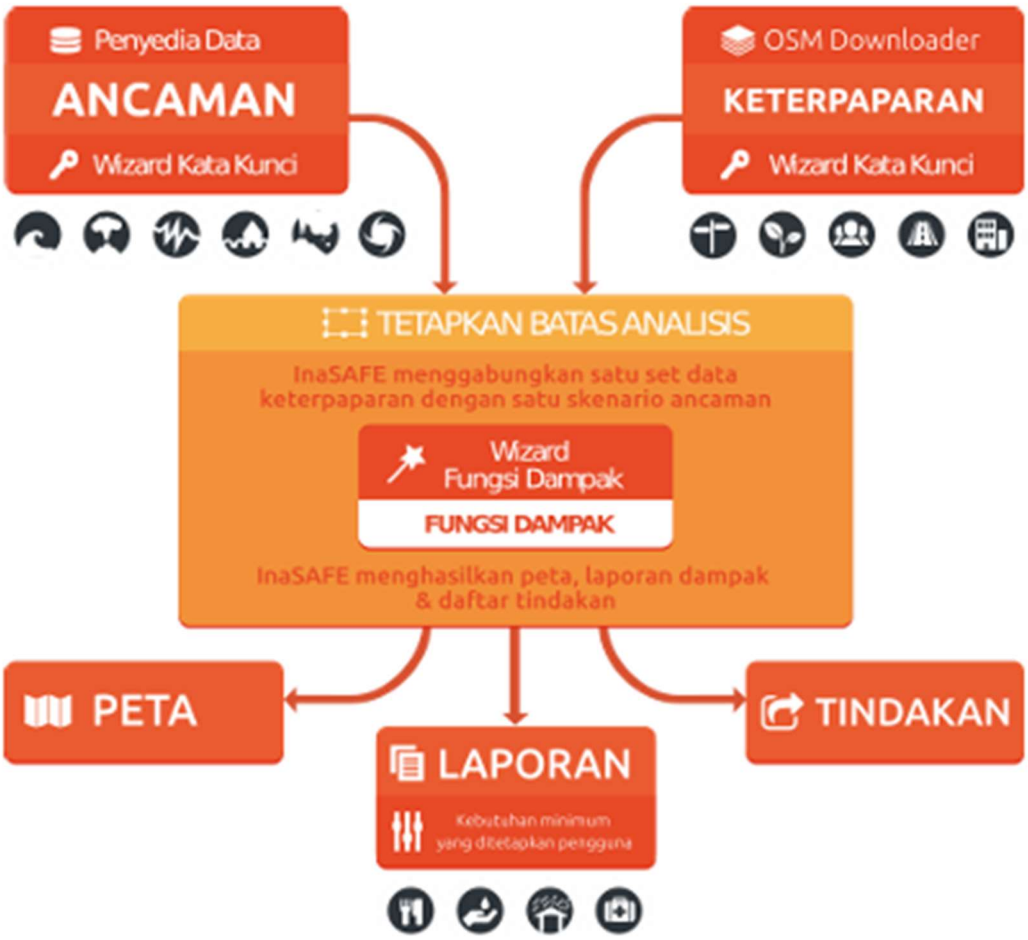

Figure 3. 9 Flowchart of InaSAFE
(Source: InaSAFE, 2017)

The key components of the InaSAFE flowchart are explained below.

1. Hazard (*Ancaman*)

   Based on InaSAFE (2017), a hazard is a natural or human-caused event or a series of events that harms the population, infrastructure, or resources of a certain area. Hazard can be classified into two types: single-event and multiple-event hazard data. Single-event hazards represent a specific disaster that occurs within a short, defined time, and are used for the potential impact of a particular historical or hypothetical event. In contrast, multiple-event hazards represent disasters that occur repeatedly over a long period in the same area, and are mainly used for long-term disaster risk reduction and management planning.

2. Exposure (*Keterpaparan*)

   Based on InaSAFE (2017), exposure relates to the people, infrastructure, or land use areas that could be impacted by a disaster event. Currently, InaSAFE can support four types of exposure data:

   a. roads
   b. buildings
   c. population
   d. land cover

3. Impact Function (*Fungsi Dampak*)

   An impact function is software code in InaSAFE that implements a specific algorithm to determine the impact of a hazard on specific exposure data. The impact function can be run if the necessary data related to the hazard type is already included. Each impact function will produce an impact map layer, an impact analysis report, minimum needs data, and an action list (InaSAFE, 2017).

4. Impact Layer Map (*Peta Dampak*)

   The impact layer is a new GIS dataset generated as a result of the impact function analysis calculation. This usually represents the exposure layer. For instance, InaSAFE will apply its symbology to the impact layer output to provide information on where buildings are affected (InaSAFE, 2017).

5. Impact Summary (*Laporan Dampak*)

   The impact analysis report is produced from the impact function analysis. It includes various tables and additional textual information detailing the number of buildings, roads, or individuals affected. Moreover, it contains essential details such as a description of minimum requirements, an action list, and a summary (InaSAFE, 2017).

6. Action List (*Tindakan*)

   The action list consists of questions created for disaster managers to consider when implementing disaster management. The action list produced by InaSAFE aims to develop discussion and stimulate the importance of contingency plans (InaSAFE, 2017).

The impact function that can be employed based on the available data are represents in Table 3.6.

Table 3. 6 Supported Data on each Hazard Type in InaSAFE

Impact Function	Hazard Type	Supported Data Type
Earthquake Impact Function	**Hazard**	Continuous raster, classified raster, or classified polygons
	Exposed Population	Continuous raster with per-pixel population values
	Affected Buildings	Classified polygons or points with type attributes
Flood Impact Functions	**Hazard**	Continuous raster or classified polygons
	Exposed Population	Continuous raster with per-pixel population values
	Affected Buildings	Classified polygons or points with type attributes
	Exposed Road Network	Line classifications with type attributes
Tsunami Impact Functions	**Hazard**	Continuous raster or classified polygons
	Exposed Population	Continuous raster with per-pixel population values
	Affected Buildings	Classified polygons with type attributes
	Exposed Road Network	Line classifications with type attributes
Volcano Impact Functions	**Hazard**	Continuous polygons, classified polygons, or points
	Exposed Population	Continuous raster with per-pixel population values
	Affected Buildings	Classified polygons with type attributes
Volcanic Ash Impact Functions	**Hazard**	Classified polygons or continuous raster
	Exposed Population	Continuous raster with per-pixel population values
	Affected Buildings	Classified polygons with type attributes
Cyclone Impact Functions	**Hazard**	Classified polygons or continuous raster
	Exposed Population	Classified polygons with type attributes
Generic Impact Functions	**Hazard**	Classified polygons, classified raster, or continuous raster
	Exposed Population	Continuous raster with per-pixel population values
	Affected Buildings	Classified polygons with type attributes
	Exposed Landcover	Classified polygons with type attributes
Dam Break Impact Functions	**Hazard**	Continuous raster or classified polygons
	Exposed Population	Continuous raster with per-pixel population values
	Affected Buildings	Classified polygons or points with type attributes
	Exposed Road Network	Line classifications with type attributes

Source: InaSAFE (2017)

The inundation class used for the InaSAFE impact function in this study was instructed by Badan Nasional Penanggulangan Bencana (BNPB) in Perka BNPB No. 12 Tahun 2012. Although there is no specific hazard class for dam breaks mentioned in the guideline. However, this guideline is the most recent regulation and remains the official national guideline for disaster risk assessment.

Consequently, the inundation depth vulnerability threshold used in this study is the flood hazard class, which serves as the foundational framework. Therefore, the threshold only uses the depth and the vulnerability class, leaving the vulnerability value, weight percentage, and score. Furthermore, the inundation depth-based vulnerability is translated into Table 3.7 below.

Table 3. 7 Inundation Depth Vulnerability Class

Depth (m)	Class	Value	Weight (%)	Score
< 0.76	Low	1	100	0.333333
0.76 - 1.5	Moderate	2		0.666667
> 1.5	High	3		1.000000

Source: BNPB (2012)

CHAPTER IV
METHODOLOGY

4.1 Research Object Location

Bili Bili Dam was constructed in Sulawesi Selatan, Kabupaten Gowa, approximately 30 km to the east of Kota Makassar and 31 km from the Jeneberang River estuary, which is geographically located at 5°16'39.67"S and 119°35'4.57"E. This dam was designed with three parts of the dam body using a zoned rockfill-type dam, namely (a) main dam, (b) left wing dam, and (c) right wing dam, with a body height of 73 m, 42 m, and 52 m, respectively, from the foundation. Bili Bili Dam crosses the Jeneberang River and generates an effective reservoir volume capacity of 346 million m^3 with 18.5 km^2, submerging parts of Desa Moncongloe, on Kecamatan Manuju, as well as Desa Bontoparang on Kecamatan Parangloe.

Bili Bili Dam location, Jeneberang river basin map, and Bili Bili watershed map are presented in Figure 4.1, Figure 4.2, and Figure 4.3, respectively.

Figure 4. 1 Bili Bili Dam Location
(Source: Google Earth Pro)

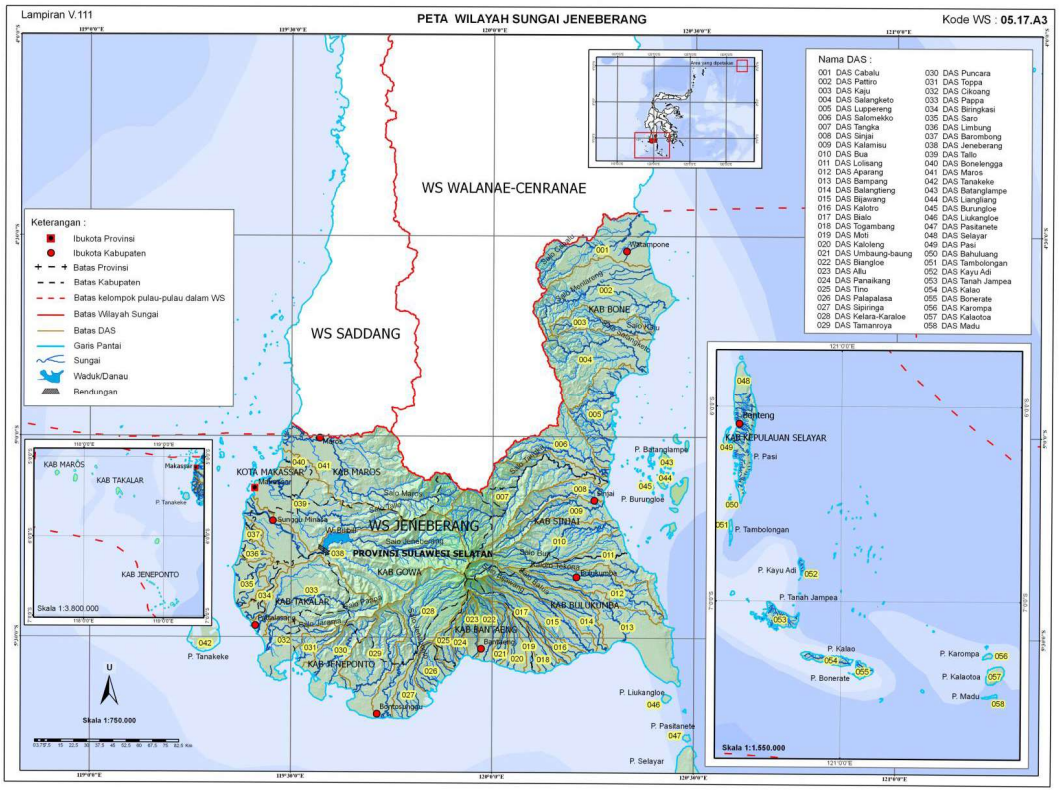

Figure 4. 2 Jeneberang River Basin Map
(Source: BBWS Pompengan – Jeneberang, 2019)

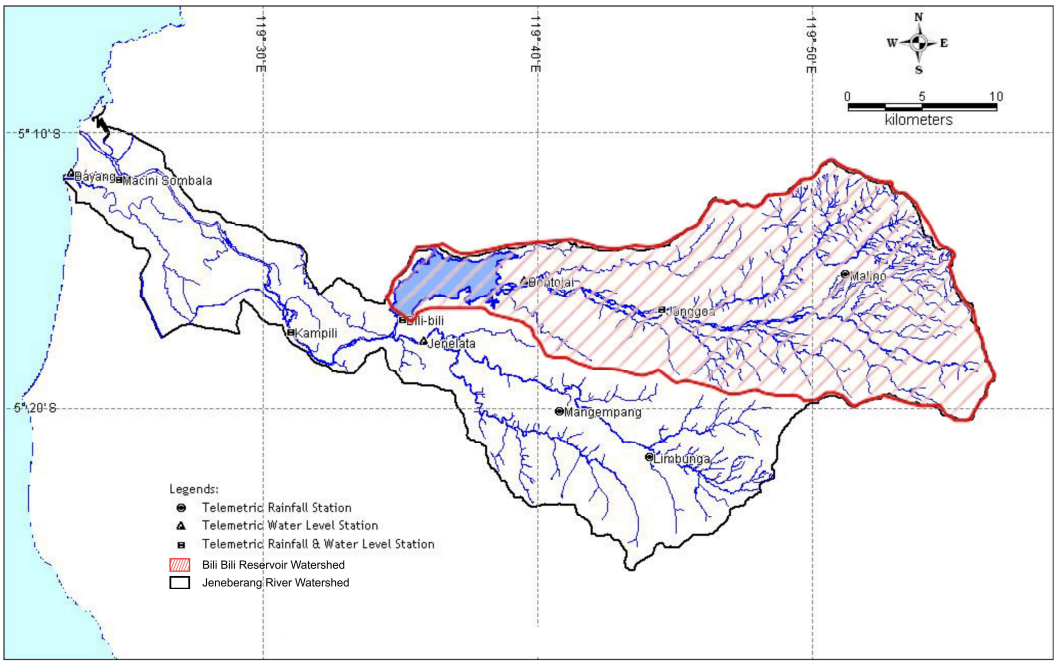

Figure 4. 3 Jeneberang River Watershed Map
(Source: BBWS Pompengan – Jeneberang, 2019)

4.2 Research Method

Dam break analysis with disaster impact assessment is a quantitative research approach. This research aims to determine the impacted areas and potential losses resulting from dam failure due to overtopping and/or piping failure modes, utilizing the latest empirical approach of the breach parameters established by Froehlich (2016); while the failure mode feasibility is evaluated through the HEC-RAS unsteady flow analysis.

To reveal the most harmful and detrimental impact, three initial piping elevation scenarios were simulated at the right-wing dam and the main dam. The breach scenarios were defined by varying the initial piping location into three elevations using an equal-interval approach: top piping, middle piping, and bottom piping. Accordingly, the breach opening initiates at different elevations relative to the dam's maximum water surface elevation (WSE) and bottom reservoir elevation, allowing systematic evaluation of outflow sensitivity and downstream impact under alternative piping initiation levels.

The impact assessment in this study was carried out using InaSAFE, which integrates the floodplain areas with the exposure parameters. The analysis applies the BNPB (2012) flood hazard threshold to estimate the quantitative impact on the downstream inundation extents.

4.3 Research Data

The necessary data will need to be collected to perform this research and will be processed to achieve this research purpose. The data used in this research were as follows.

1. Dam Technical Data
   a. Dam geometry
   b. Reservoir elevation-volume-area curve (characteristics curve)
   c. Probable maximum flood discharge (Q_{PMF})

   These data are collected from Balai Besar Wilayah Sungai (BBWS) Pompengan - Jeneberang
2. Terrain Map

Terrain data was used from the Digital Elevation Model (DEM) of DEMNAS. These data are collected from the Ina-Geoportal of Badan Informasi Geospasial with 0.27 arcseconds or 8.1m resolution.

3. Infrastructure Map

   The infrastructure map used was collected from OpenStreetMap (OSM), 2025.

4. Administrative Map

   This data was collected from the Ina-Geoportal of Badan Informasi Geospasial, 2022.

5. Land Use/Land Cover (LULC) Map

   a. Manning's n based on the LULC classification Map

      This data was collected from ESRI, which uses Sentinel-2 satellite imagery with 10m resolution.

   b. Land Use Map

      The Land Use map used was collected from OpenStreetMap (OSM), 2025.

4.4 Research Tools

In this research, tools or software were used to perform analysis as follows.

1. HEC-RAS 6.6
2. QGIS 3.40.13 Bratislava
3. InaSAFE 5.0.7
4. Microsoft Excel

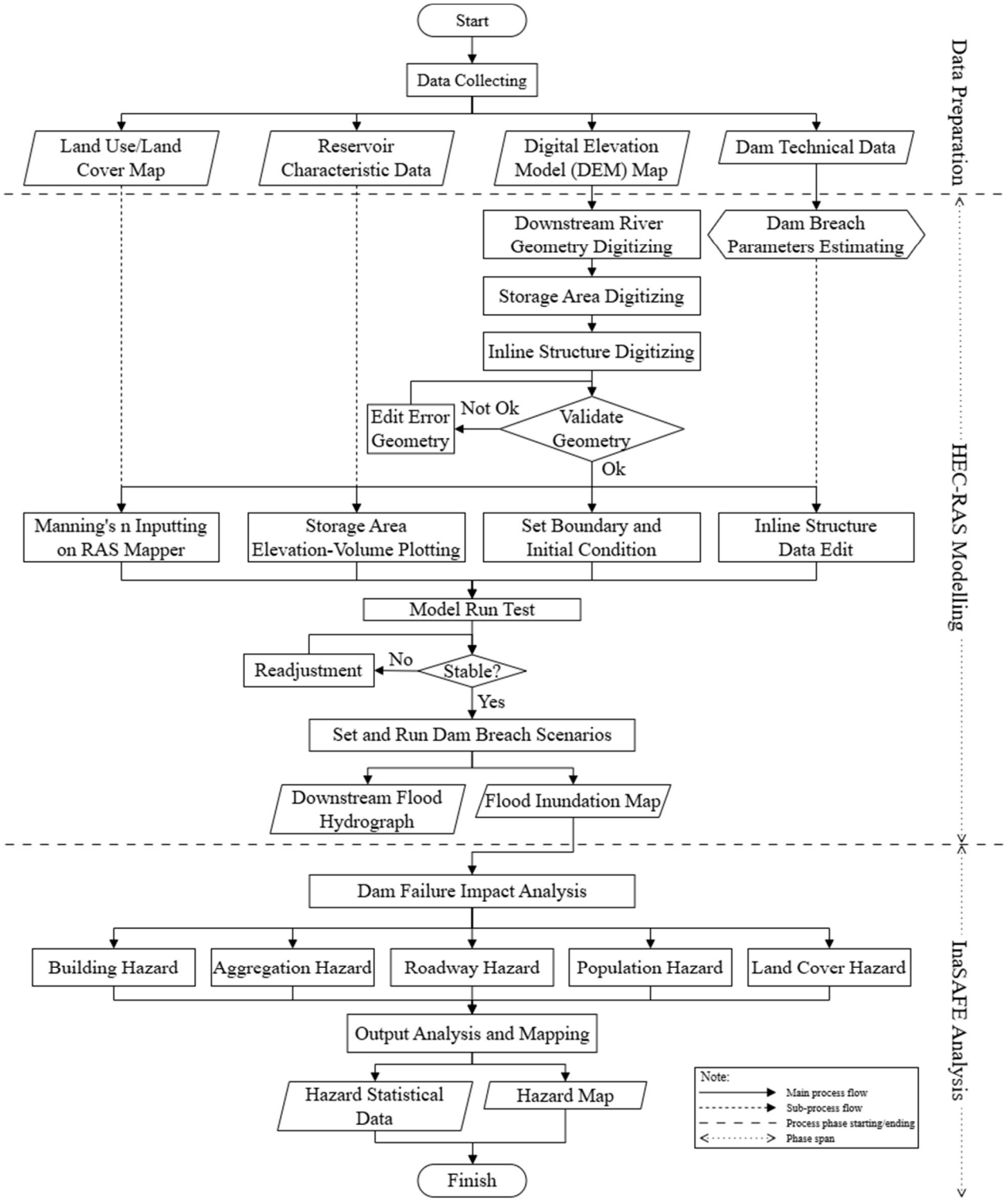

Figure 4. 4 Research Procedures Flowchart

CHAPTER V
ANALYSIS AND DISCUSSION

5.1 Data

The integrity and outcomes of this dam break analysis are fundamentally dependent on the quality, accuracy, and comprehensiveness of the underlying input data. The necessary data as a reference for this study analysis and simulations are categorized into technical data, hydraulic data, and breach parameters, which will be derived empirically to define the failure scenarios and produce an accurate analytical workflow in this study.

5.1.1 Technical Data

These technical data of Bili Bili Dam served as the primary input for breach parameter estimation and were used for digitizing the dam and reservoir within the HEC-RAS model. The data set was acquired from the Balai Besar Wilayah Sungai (BBWS) Pompengan Jeneberang.

The general layout of Bili Bili Dam presents the fundamental reference for the dam structure layout, as presented in Figure 5.1 below.

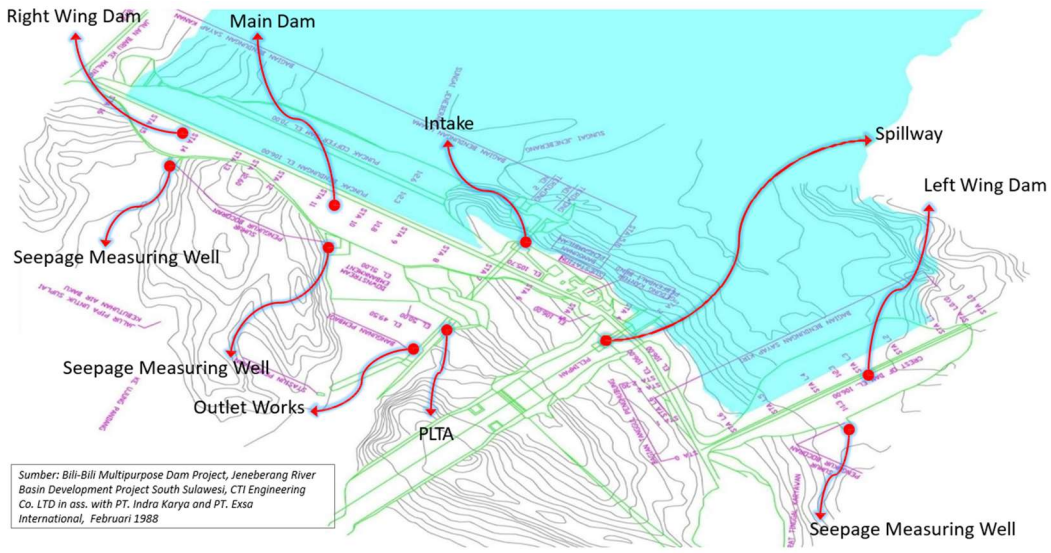

Figure 5. 1 General Layout of Bili Bili Dam
(Source: BBWS Pompengan – Jeneberang, 2019)

From the general layout, Bili Bili Dam is divided into three (3) different dam bodies, namely, the main dam, the right-wing dam, and the left-wing dam. The cross-sectional details of each dam body can be seen in Figure 5.2, Figure 5.3, and Figure 5.4 below, and they can also be found in the Attachments section.

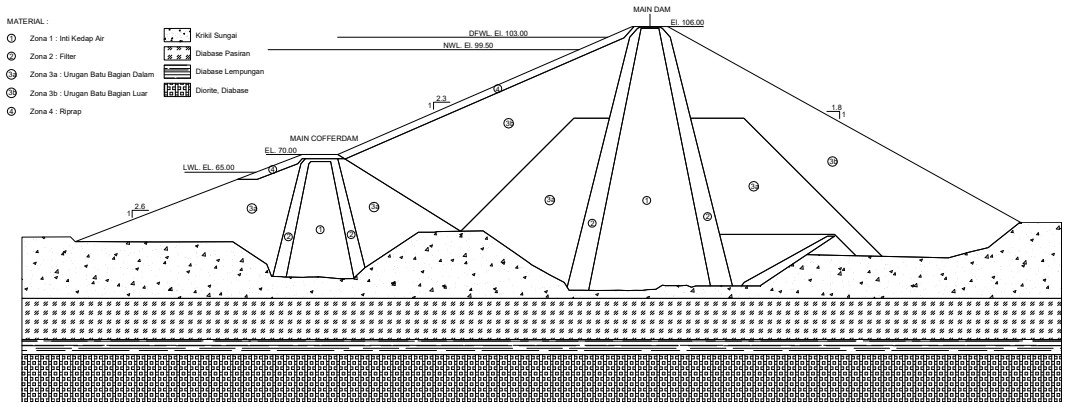

Figure 5. 2 Main Dam Cross-Section
(Source: BBWS Pompengan – Jeneberang, 2019)

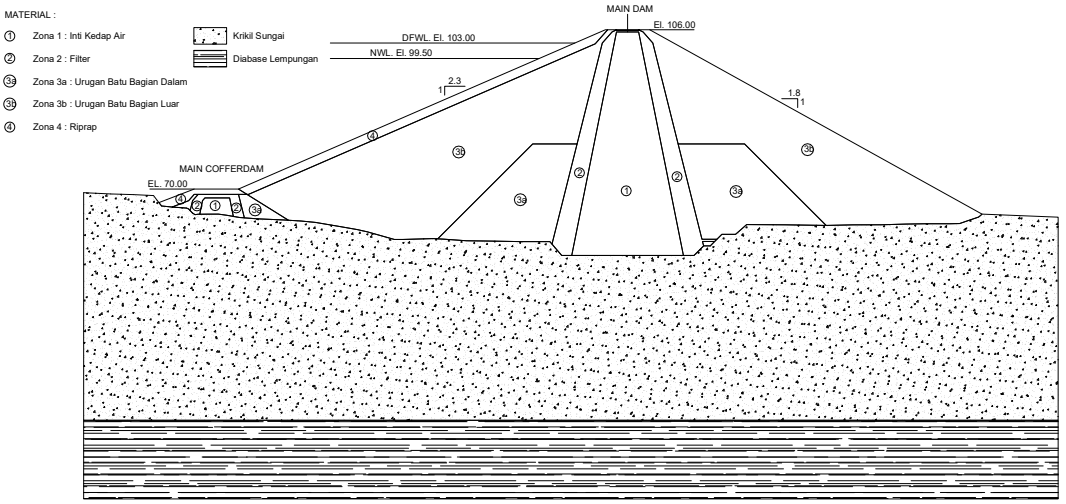

Figure 5. 3 Right-Wing Dam Cross-Section
(Source: BBWS Pompengan – Jeneberang, 2019)

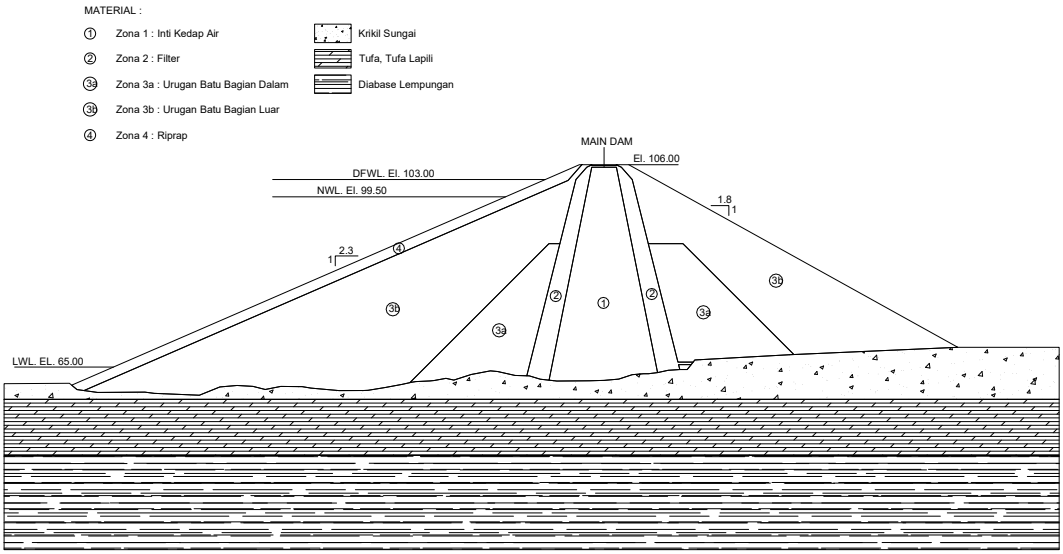

Figure 5. 4 Left-Wing Dam Cross-Section
(Source: BBWS Pompengan – Jeneberang, 2019)

The general reservoir properties data are summarized in Table 5.1 below.

Table 5. 1 Reservoir Properties

No.	Reservoir Properties	Unit	Value
1	Water Catchment Area	km^2	384.4
2	Design Flood Water Level (DFWL)	m	+103
3	Normal Water Level (NWL)	m	+99.5
4	Low Water Level (LWL)	m	+65
5	Total Storage Capacity	m^3	375,000,000
6	Effective Storage Capacity	m^3	346,000,000

Source: BBWS Pompengan – Jeneberang (2019)

With a Rockfill with Core dam type, the Bili Bili dam properties are summarized in Table 5.2 below.

Table 5. 2 Embankment Properties

No.	Properties	Main Dam	Right-Wing Dam	Left-Wing Dam
1	Height from Foundation (m)	73	42	52
2	Crest Length (m)	750	412	646
3	Crest Width (m)	10	10	10
4	Crest Elevation (m)	+106	+106	+106
5	D.S. Embankment Elevation (m)	+46	+70	+60
6	Upstream Slope	1V:2.3H	1V:2.3H	1V:2.3H
7	Downstream Slope	1V:1.8H	1V:1.8H	1V:1.8H

Source: BBWS Pompengan – Jeneberang (2019)

In addition, the spillway properties of the Bili Bili Dam are summarized in Table 5.3 below.

Table 5. 3 Spillway Gates Properties

No.	Properties	Unit	Free Flow Crest	Gated Crest
1	Crest Elevation	m	+99.5	+91.8
2	Crest Width	m	70	14

Source: BBWS Pompengan – Jeneberang (2019)

5.1.2 Hydraulic Data

The hydraulic data of Bili Bili Dam are used as boundary condition inputs for the upstream and downstream within the HEC-RAS unsteady flow modelling. The hydraulic data set was obtained from the Balai Besar Wilayah Sungai (BBWS) Pompengan Jeneberang measurement and calculation.

1. Reservoir Characteristics Curve

   As explained in 3.6.2, the HEC-RAS flood routing method selection has several key parameters. Since the reservoir topographic data was acquired from DEMNAS with only 8.1 meters resolution, which is insufficient to define the detailed cross-sections required for a full unsteady. Moreover, the unavailability of detailed upstream hydrologic inflow data makes the development of a complex unsteady model unfeasible and potentially unreliable. The reservoir has no significant tributary inflows, and the primary population centers at risk are situated a considerable distance downstream, where the flood wave spreads out. Consequently, the analysis utilizes an elevation-volume-area (characteristic) curve in the level pool routing method in HEC-RAS. Thus, the characteristic curve of the Bili Bili reservoir can be seen in Figure 5.5 below.

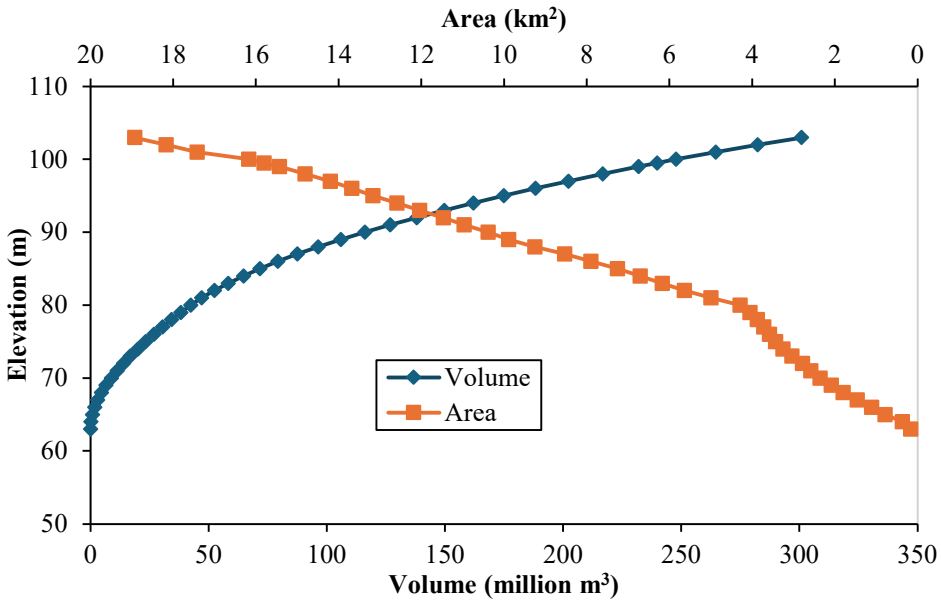

Figure 5. 5 Characteristic Curve of Bili Bili Reservoir
(Source: BBWS Pompengan – Jeneberang, 2019)

The characteristic curve above was obtained from the reservoir bathymetry measurement by Balai Besar Wilayah Sungai (BBWS) Pompengan Jeneberang in 2018. The reservoir bathymetry measurement produced an elevation-area-volume data that can be seen in Table 5.4 below.

Table 5. 4 Elevation – Area – Volume of Bili Bili Reservoir

Elevation	Area	Volume
m	km^2	x 10^6 m^3
63	0.165	0.000
64	0.366	0.259
65	0.789	0.823
66	1.112	1.768
67	1.459	3.050
68	1.801	4.676
69	2.086	6.618
70	2.357	8.838
71	2.585	11.308
72	2.783	13.991
73	3.038	16.901
74	3.254	20.046
75	3.431	23.388

Continuation of Table 5.4 Elevation – Area – Volume of Bili Bili Reservoir

Elevation	Area	Volume
m	km^2	x 10^6 m^3
76	3.577	26.891
77	3.723	30.541
78	3.874	34.339
79	4.050	38.301
80	4.290	42.471
81	4.996	47.109
82	5.641	52.424
83	6.170	58.327
84	6.707	64.763
85	7.260	71.745
86	7.902	79.323
87	8.534	87.539
88	9.254	96.431
89	9.890	106.001
90	10.380	116.135
91	10.965	126.806
92	11.469	138.022
93	12.037	149.774
94	12.590	162.087
95	13.173	174.967
96	13.680	188.393
97	14.196	202.330
98	14.813	216.834
99	15.432	231.955
99.5	15.803	239.764
100	16.174	247.758
101	17.416	264.549
102	18.167	282.339
103	18.929	300.886

Source: BBWS Pompengan – Jeneberang (2019)

3. Probable Maximum Flood (Q_{PMF}) Hydrograph

In this study, the reservoir inflow discharge is using the probable maximum flood discharge (Q_{PMF}) obtained from the BBWS Pompengan – Jeneberang 2019 calculations, which represents the most severe inflow scenario for the Bili Bili Reservoir. Furthermore, this probable maximum flood

(PMF) is applied as the critical value of the upstream boundary condition within the HEC-RAS dam break modelling. Thus, the probable maximum flood (PMF) reservoir inflow, the spillway with gate operations outflow, and the reservoir water surface level (WSL) served in a hydrograph, which is presented in Figure 5.6 below.

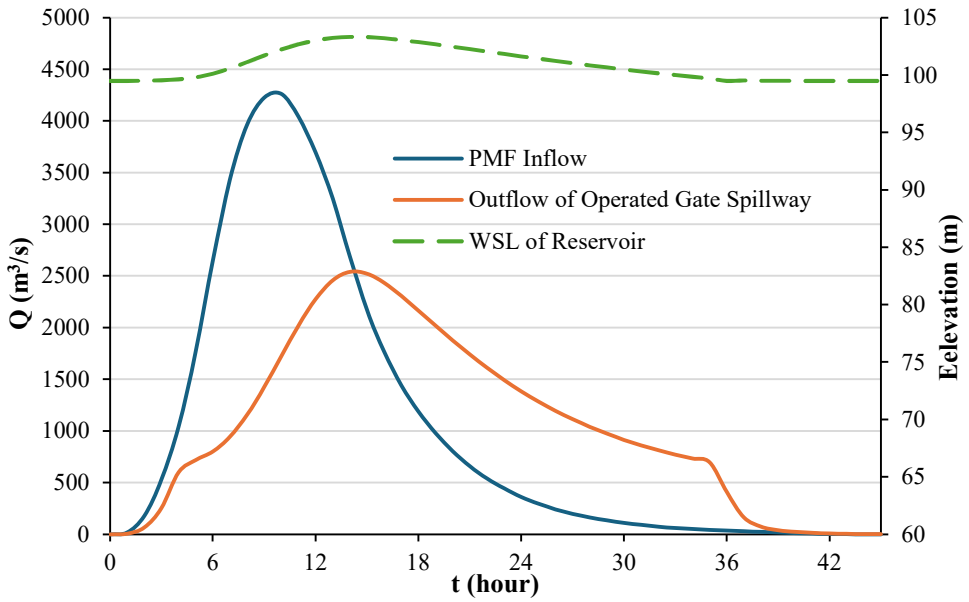

Figure 5. 6 Flood Hydrograph of Bili Bili Reservoir
(Source: BBWS Pompengan – Jeneberang, 2019)

The probable maximum flood (PMF) hydrograph above was obtained from the Bili Bili Reservoir flood routing in 2018 by Balai Besar Wilayah Sungai (BBWS) Pompengan-Jeneberang. Therefore, the probable maximum flood (PMF) hydrograph shows that the peak inflow occurred at hour 10 with 4261.71 m^3/s, and the peak outflow of the spillway with gate operations remained at hour 14 with 2541.08 m^3/s. The flood routing result of the Bili Bili Reservoir is shown in Table 5.5 on the following page.

Table 5. 5 Flood Routing of Bili Bili Reservoir

t (hours)	Q_{PMF} (m^3/s)	Q_{OUT} (m^3/s)	Elevation (m)	H (m)
0	0.00	0.00	99.50	0.00
1	16.81	5.49	99.50	0.00
2	179.96	66.16	99.52	0.02
3	528.87	254.35	99.56	0.06
4	1043.19	601.48	99.64	0.14
5	1766.44	719.17	99.81	0.31
6	2652.82	801.53	100.13	0.63
7	3432.70	944.17	100.59	1.09
8	3966.63	1156.47	101.15	1.65
9	4225.65	1423.53	101.72	2.20
10	4261.71	1726.52	102.25	2.75
11	4040.68	2022.51	102.69	3.19
12	3695.27	2275.67	103.03	3.53
13	3246.77	2459.88	103.25	3.75
14	2690.42	2541.08	103.34	3.84
15	2168.54	2522.67	103.32	3.82
16	1767.60	2435.01	103.22	3.72
17	1441.32	2307.11	103.06	3.56
18	1188.13	2164.98	102.88	3.38
19	979.56	2019.76	102.69	3.19
20	805.70	1877.76	102.48	2.98
21	657.56	1741.65	102.27	2.77
22	540.01	1614.07	102.06	2.56
23	443.89	1494.00	101.85	2.35
24	361.19	1383.88	101.64	2.14
25	296.28	1284.14	101.44	1.94
26	242.13	1194.88	101.24	1.74
27	198.40	1114.85	101.05	1.55
28	163.54	1041.23	100.86	1.36
29	133.81	974.18	100.68	1.18
30	110.23	914.61	100.50	1.00
31	90.35	861.45	100.33	0.83
32	73.51	814.13	100.17	0.67
33	60.71	771.53	100.02	0.52
34	50.32	732.14	99.86	0.36
35	42.69	696.62	99.71	0.21

Continuation of Table 5.5 Flood Routing of Bili Bili Reservoir

t (hours)	Q_{PMF} (m^3/s)	Q_{OUT} (m^3/s)	Elevation (m)	H (m)
36	35.92	406.63	99.50	0.09
37	29.40	162.47	99.54	0.04
38	23.19	73.56	99.52	0.02
39	17.61	38.85	99.51	0.01
40	12.20	23.22	99.51	0.01
41	6.86	14.28	99.50	0.00
42	2.11	7.88	99.50	0.00
43	0.72	3.66	99.50	0.00
44	0.24	1.58	99.50	0.00
45	0.00	0.63	99.50	0.00

Source: BBWS Pompengan – Jeneberang (2019)

5.1.3 Breach Parameters

In this study, the breach parameters employed the latest empirical breach parameter equations developed by Froehlich (2016), which are based on a multivariate nonlinear analysis of 110 historical dam failures.

The primary inputs defining the dam failure mechanism in the HEC-RAS model are the breach parameters, calculated based on the dam failure scenarios. HEC-RAS breach data input required the (2) final bottom width (B_b), which was derived from the (1) average breach width (B_{avg}), and the (3) breach formation time (t_f). Thus, the initial data required for these calculations include the reservoir water volume (V_w), the average embankment width (W_{avg}), and the breach height (H_b).

To specify the calculation steps of the breach parameter, the overtopping failure will be used since this failure mode occurs at least at the dam crest elevation. Thus, the reservoir water volume uses the highest water volume data in +105, which is 340.755 million m^3; and the crest length of the Main Dam and the Right-Wing Dam is 750 m and 412 m, respectively.

1. Average breach width (B_{avg})

   The average breach width (B_{avg}) is a key empirical output used to derive the final geometry of the breach. However, the average breach width (B_{avg}) was not directly input into HEC-RAS. It served as a critical pre-processing

parameter to calculate the final bottom width of the trapezoidal breach, which is then specified in the breach data in the HEC-RAS model. The example calculation steps for overtopping breach scenarios in the main dam were performed as follows.

a. Factor of failure mode (k_M)

   As mentioned in Equation 3.2, this constant number is used based on the breach failure mode in the dam breach scenario. Thus, the failure mode factor (k_M) for piping failure has a constant value of 1.0, and for overtopping failure has 1.5.

b. Breach height (H_b)

   The possible height of breach is presumed using the dam crest elevation difference from the highest elevation between the downstream elevation and the upstream elevation of the embankment toe. This assumption is used because this study ignored the sediment in the storage area. Thus, the sediment is considered the ground elevation of the reservoir and the upstream elevation of the embankment. Based on Table 5.2, the crest elevation of Bili Bili Dam is +106 m. Furthermore, the upstream elevation in the data is using the lowest elevation of the reservoir characteristic curve, which is +63 m as it the highest elevation between downstream and upstream toe elevation. So, the breach height (H_b) would be as follows.

   H_b = z (crest) – z (highest of D.S/U.S toe)
   = 106 – 63
   = 43 m

c. Factor of breach height (k_H)

   As the main dam has a 43 m possible breach height (H_b), which is greater than the breach height threshold (Hs) of 6.1 m ($H_b > Hs$). Therefore, based on Equation 3.2, the breach height factor (k_H) would be 1.0.

d. Average embankment width (W_{avg})

   Due to the limited access to the design engineering drawing (DED) of the Bili Bili Dam, the average embankment width cannot be determined using--the embankment width toes of the downstream and upstream slopes

(Froehlich, 2016). Consequently, in this study, the average embankment width (W_{avg}) data is used from the crest length of each dam body.

Therefore, after the factor of failure mode (k_M), the breach height (H_b), and the factor of breach height (k_H) are determined, the average breach width (B_{avg}) for the Main Dam can be calculated using Equation 3.2 as follows.

$$\begin{aligned} B_{avg} &= 0.28 \times k_M \times k_H \times V_w^{1/3} \times W_{avg}^{-1/6} \times H_b^{1/6} \\ &= 0.28 \times 15 \times 1.0 \times (340.755 \times 10^6)^{1/3} \times 750^{-1/6} \times 43^{1/6} \\ &= 182.16 \text{ m} \end{aligned}$$

The average breach width (B_{avg}) calculation for the Main Dam and Right-Wing Dam applied in the overtopping failure mode is summarized in Table 5.6.

Table 5. 6 Recapitulation of Overtopping Average Breach Width (B_{avg})

Description	Main Dam (MD)	Right-Wing Dam (RWD)	Unit
Crest Elevation	+106	+106	m
U.S. Elevation	+63	+63	m
D.S. Elevation	+46	+60	m
H_b	43	43	m
H_s	6.1	6.1	m
k_M Overtopping	1.5	1.5	-
k_H	1.00	1.00	-
V_w (+105 m)	340,755,000	340,755,000	m^3
W_{avg}	750	412	m
B_{avg} Overtopping	182.16	201.29	m

2. Final bottom width (B_b)

After the average breach width (B_{avg}) was obtained, the final bottom width can be determined, as the HEC-RAS dam breach modelling required the final bottom width data to represent the breach formation geometry. The calculation of the final bottom width (B_b) uses 0.6 and 1 average side slope ratios (m) for the piping breach scenarios and overtopping breach scenarios, respectively. The example calculation of the final bottom width (B_b) for overtopping breach scenarios in the main dam was performed as follows.

$$B_{bottom} = B_{avg} - 2\left(\frac{H_b}{2} \times \frac{m}{1}\right)$$
$$= 182.16 - 2\left(\frac{43}{2} \times \frac{1}{1}\right)$$
$$= 139.16 \text{ m}$$

The final bottom width (B_b) calculation for the main dam and the left-wing dam, of overtopping scenarios, is summarized in Table 5.7 below.

Table 5. 7 Recapitulation of Overtopping Final Bottom Width (B_b)

Description	Main Dam (MD)	Right-Wing Dam (RWD)	Unit
B_b Overtopping	139.16	158.29	m

3. Breach formation time (t_f)

Using equation 3.3 in the previous chapter, the breach formation time (t_f) can be determined to fulfill the breach data input in HEC-RAS dam break modelling. The example calculation of the breach formation time (t_f) for piping breach scenarios in the main dam is as follows.

$$t_f = 50 \times \sqrt{\frac{V_w}{gH_b}} \times \left(\frac{W_{avg}}{H_b}\right)^{1/4}$$
$$= 50 \times \sqrt{\frac{340.755 \times 10^6}{9.81 \times 43}} \times \left(\frac{750}{43}\right)^{1/4}$$
$$= 14005.10 \text{ s}$$
$$= 3.89 \text{ hours}$$

Using the same approach, the breach formation time (t_f) for the main dam, the right-wing dam, and the left-wing dam is summarized in Table 5.8 below.

Table 5. 8 Recapitulation of Overtopping Breach Formation Time (t_f)

Description	Main Dam (MD)	Right-Wing Dam (RWD)	Unit
t_f	14005.10	12057.17	s
	3.89	3.35	h

The calculation of the average breach width (B_{avg}), the final bottom width (B_b), and the breach formation time (t_f) for the piping failure mode can only be continued if the maximum water surface elevation (WSE) during the PMF inflow on the HEC-RAS Unsteady Flow modelling to know which reservoir water volume (V_w) data will be use in the breach parameter calculation. Consequently, the recapitulation will later be summarized in the 5.2.3 Breach Scenarios Simulation.

5.2 HEC-RAS Modelling

The reliability of a dam break simulation fundamentally depends on the stability of the hydraulic model. Therefore, the simulation model was gradually structured to build and calibrate a stable and accurate numerical representation of the Jeneberang River system. To achieve a precise simulation result of the complex analysis process, the modelling and the simulation are separated into three parts, namely steady flow, unsteady flow using 1D analysis, and the breach simulation using 1D-2D coupling analysis. Thus, the model instability would be easier to identify. In sequence, the HEC-RAS modelling in this study is as follows.

5.2.1 Steady Flow Analysis

Downstream boundary conditions are frequently a major source of model error and numerical instability because the true stage corresponding to the downstream end of the river is often unknown. To address this uncertainty, either a "Normal Depth" or a "Rating Curve" derived from a steady flow simulation is being used for unsteady flow (Brunner, 2024). In this context, the main purpose of performing a steady flow analysis is to generate a reliable downstream rating curve from a series of Possible Maximum Flood (PMF) flows up to the peak.

In addition, a rating curve is a relationship between stage and flow rate. The rating curve that will be used for the downstream boundary condition of the unsteady flow analysis is extracted from the very downstream of the river station, which is RS 1. The rating curve data can be seen in Table 5.9 and the rating curve plot in Figure 5.7.

Table 5. 9 Downstream Rating Curve

Flow	Downstream Elevation	Stage
(m^3/s)	(m)	(m)
0.00	-2.83	0.00
16.81	-2.33	0.50
179.96	-1.59	1.24
528.87	-0.73	2.10
1043.19	+0.16	2.99
1766.44	+1.11	3.94
2652.82	+1.84	4.67
3432.70	+2.41	5.24
3966.63	+2.74	5.57
4225.65	+2.89	5.72
4261.71	+2.92	5.75

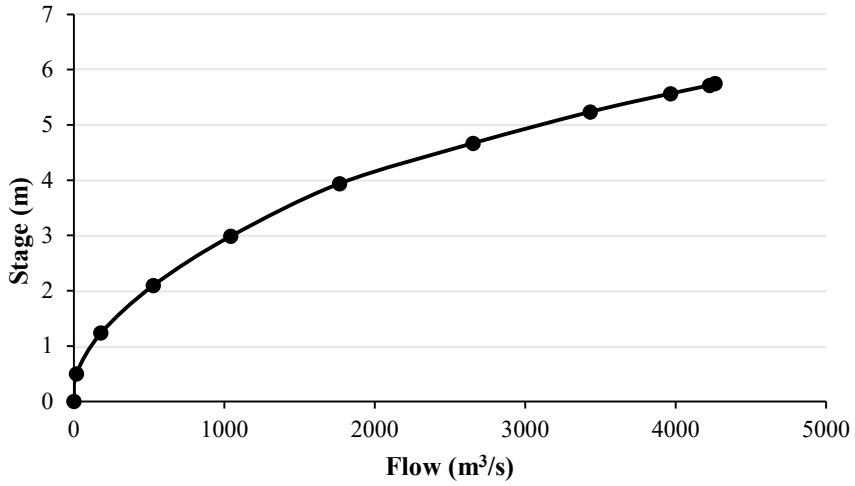

Figure 5. 7 Downstream Rating Curve

5.2.2 Unsteady Flow Analysis

The unsteady flow analysis was conducted to identify the model instability, evaluate model sensitivity, and validate the hydraulic connectivity of the river system under dynamic conditions. Unlike steady flow, unsteady flow analysis introduces time-dependent changes in discharge and stage through the Saint-Venant equations (continuity and momentum), Brunner (2024), which can expose weaknesses in the geometry setup.

The stable model result was successfully achieved by effectively addressing the instability. The adjusted model runtime messages are shown in Figure 5.8

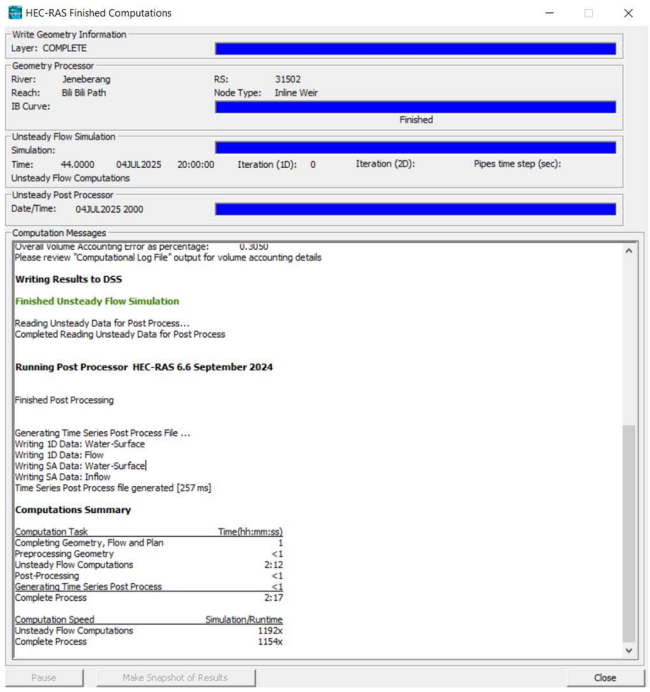

Figure 5. 8 Unsteady Flow Analysis – Adjusted Runtime Messages

Meanwhile, the stable model profile plot of the Jeneberang River, which was simulated under the non-breach PMF inflow hydrograph, can be seen in Figure 5.9.

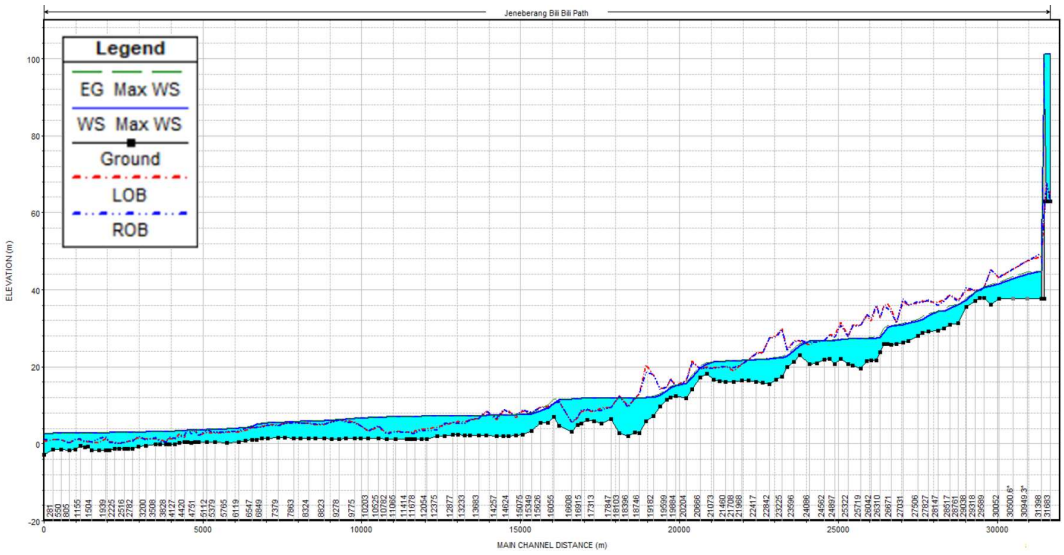

Figure 5. 9 Profile Plot Result – Max Water Surface of Stable Model

The downstream boundary condition in this unsteady flow analysis uses the "Rating Curve" produced from the steady flow in Table 5.9. In addition, the storage area boundary condition uses the "Lateral Inflow Hydrograph" from Probable Maximum Flood (PMF) inflow hydrograph data in Table 5.5.

After the model achieved numerical stability, the reservoir routing through the inline structure attenuated the incoming PMF hydrograph, resulting in a reduced and delayed peak at the outlet. The peak inflow to the reservoir reached 4261.57 m^3/s at the 10^{th} hour from the start, while the peak outflow through the inline structure was 872.25 m^3/s at the 19^{th} hour from the start, confirming that the flood routing occurred aligned with the storage effects and hydraulic controls effectively reduced the downstream discharge. The hydrograph of reservoir PMF inflow and Bili Bili Dam spillway outflow comparison on this model is shown in Figure 5.10.

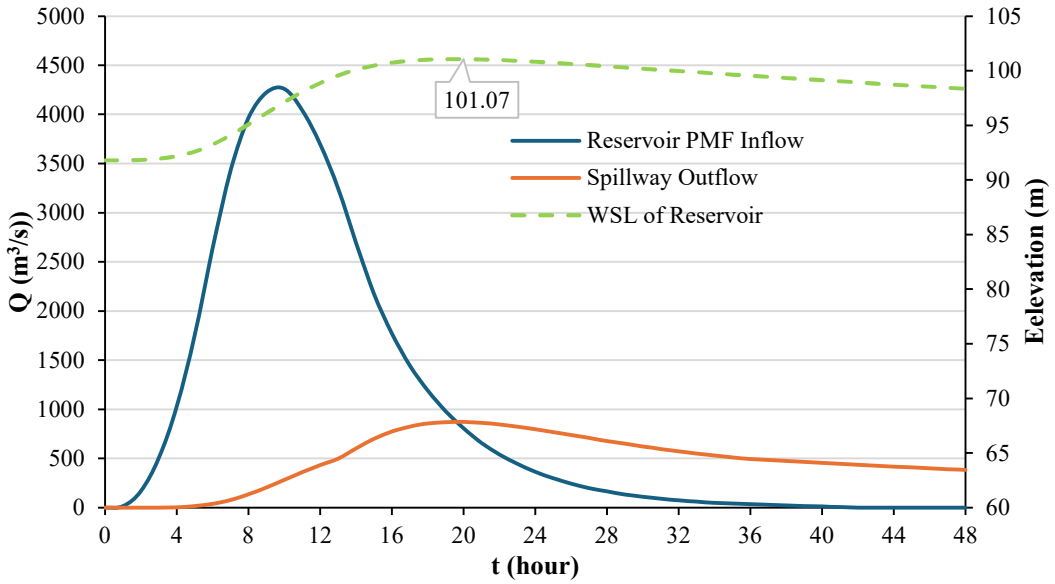

Figure 5. 10 PMF Inflow vs Dam Outflow Hydrograph

Consistent with this reduced outflow, the maximum water surface elevation (WSE) at Bili Bili Dam is +101.07 m showing at the 20^{th} hours from the start of the simulation, which remains below the crest elevation of +106 m, therefore indicating that no overtopping occurs under the non-breach PMF condition; thus, the overtopping failure mode cannot be performed for the dam break simulation in this study. Hence, the piping failure mode will presumably happen for further

investigation. The maximum water surface elevation (WSE) of Bili Bili Dam can be seen in Figure 5.11.

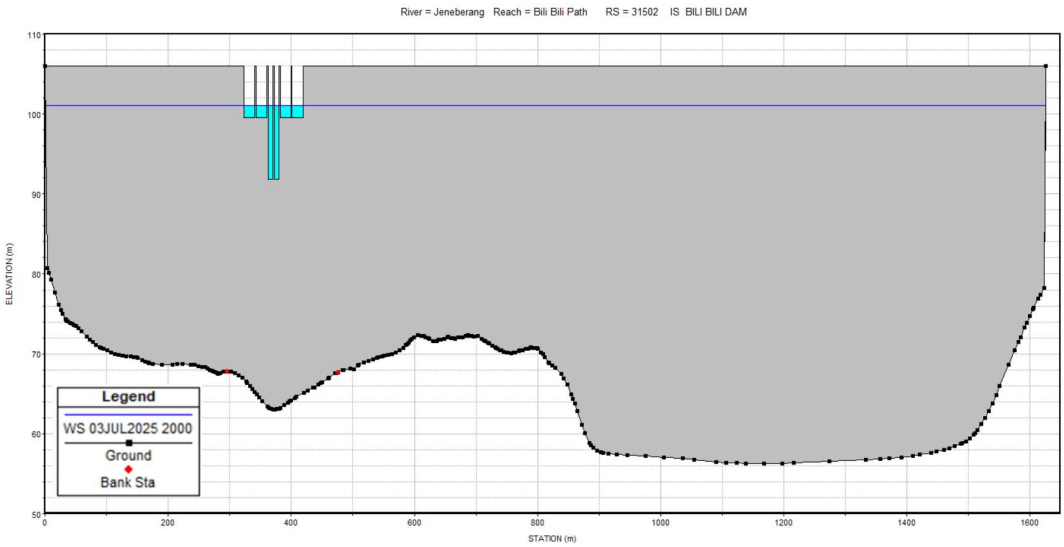

Figure 5. 11 Inline Structure Cross-Section Plot – Max WSE PMF

5.2.3 Breach Scenarios Simulation

The breach scenarios in this study exclude overtopping because the non-breach run shows no overflow at the dam crest. Accordingly, the failure modes focus on the internal erosion/piping failure mode, which may occur under these study conditions. The breach trigger is presumably set at the 20th hour from the simulation start, which corresponds to the time of the highest reservoir WSE observed in the non-breach PMF run. Applying the same sequence as 5.1.3 Breach Parameters, the breach parameters for piping failure mode are summarized in Table 5.10 below.

Table 5. 10 Recapitulation of Piping Breach Parameters

Description	Main Dam (MD)	Right-Wing Dam (RWD)	Unit
Center Station	1000	1470	m
Crest Elevation	+106	+106	m
U.S. Elevation	+63	+63	m
D.S. Elevation	+46	+60	m
H_b	43	43	m

Continuation of Table 5.10 Recapitulation of Piping Breach Parameters

Description	Main Dam (MD)	Right-Wing Dam (RWD)	Unit
H_s	6.1	6.1	m
k_M Piping	1.0	1.0	-
k_H	1.00	1.00	-
W_{avg}	750	412	m
V_w (+101 m)	264,549,000	264,549,000	m^3
B_{avg} Piping	111.62	123.34	m
B_b Piping	85.82	97.54	m
tf	3.43	2.95	h

Scenario variations are constructed by varying the "Initial Piping Elevation", by determining the piping elevation interval using the water height from the reservoir elevation of +63 m to the maximum water surface elevation (WSL) of +101 m that rounded from +101.07 m; which is proposed to be divided into three (3) scenarios. Starting at +63 m, which was previously used as the highest elevation of D.S/U.S toe, or in this case, it serves as the lowest piping point (bottom piping); and ending at +101 m as the maximum water surface elevation (WSL). The scenario's determination is as follows.

$$\text{Piping Height Interval} = \frac{\text{Max water height}}{\text{Number of piping location} - 1}$$

$$= \frac{101 - 63}{3 - 1}$$

$$= 19 \text{ m}$$

Therefore, using the determined interval, the scenarios for both the Main Dam and the Right-Wing Dam are summarized as indicated in Table 5.11 below.

Table 5. 11 Breach Scenarios

Initial Piping Elevation	Main Dam (MD)	Right-Wing Dam (RWD)
1st Scenario (Bottom Piping)	+63 m	+63 m
2nd Scenario (Middle Piping)	+82 m	+82 m
3rd Scenario (Top Piping)	+101 m	+101 m

After configuring the breach plan, the simulation was executed. During the simulation, numerical instability may occur due to the Courant number. Therefore, if the high Courant numbers were identified, adjusting the computation interval divisor iteratively may help to stabilize the solution. In addition, a very small error in the cross-section and the overall volume accounting may be ignored. The runtime messages of the breach scenario running can be seen in Figure 5.12 below.

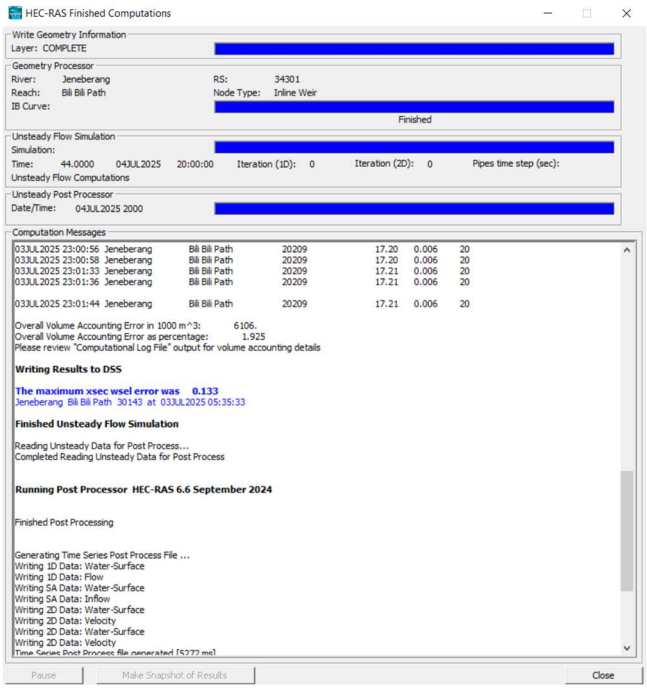

Figure 5. 12 Unsteady Flow Analysis – Breach Plan Runtime Messages

The visualization of the initial piping opening formation for each scenario, 30 minutes after the piping starts forming, can be seen in Figure 5.13 and Figure 5.14.

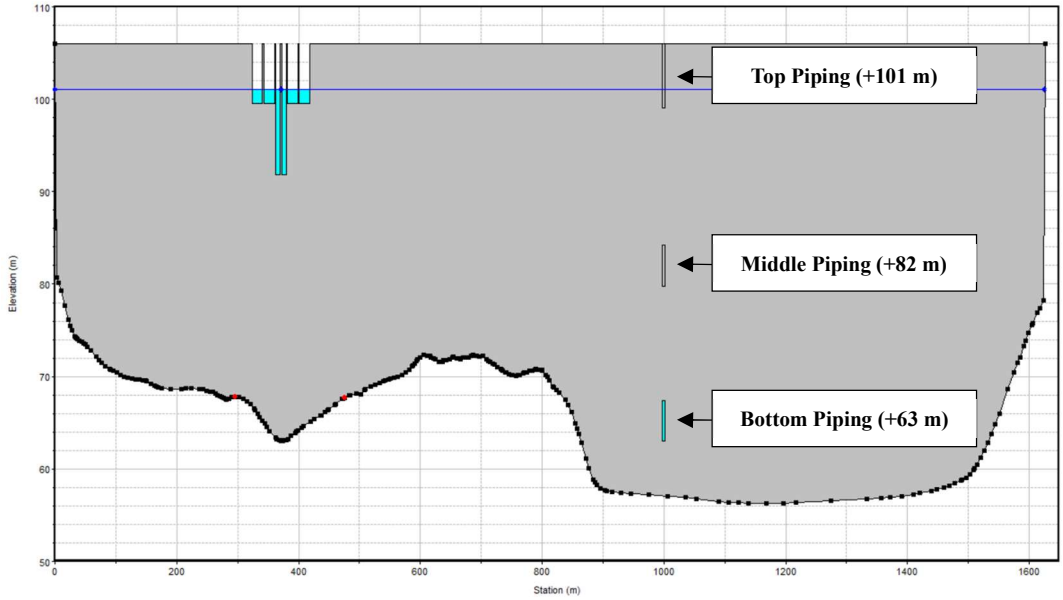

Figure 5. 13 Main Dam Piping Formation Comparison

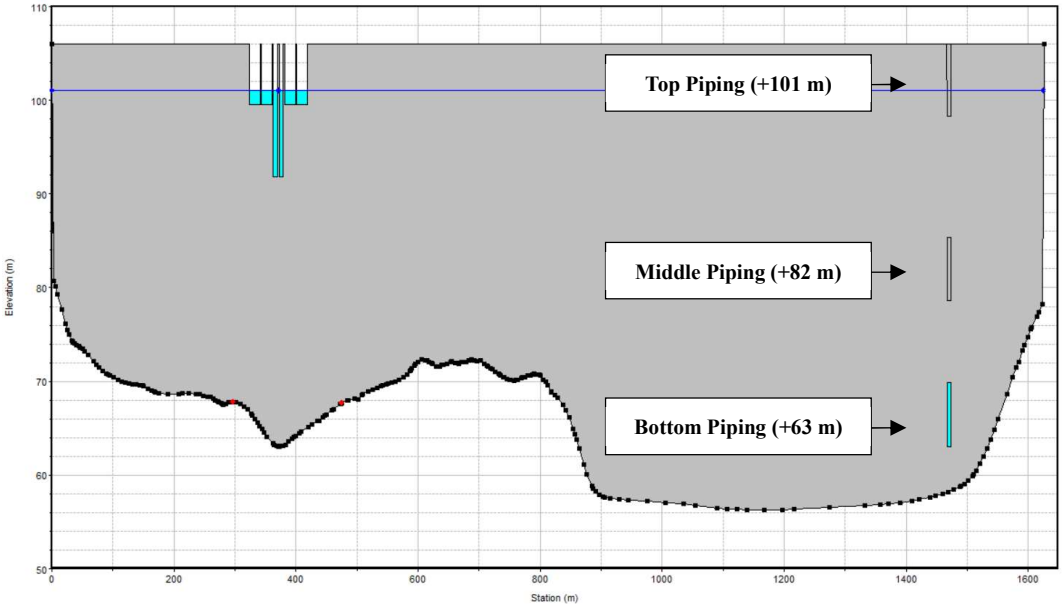

Figure 5. 14 Right Wing Dam Piping Formation Comparison

5.3 InaSAFE Analysis

The InaSAFE analysis is primarily conducted to produce a disaster impact assessment from the dam failure. InaSAFE performs four core analyses for dam break impact functions, namely, (1) estimation of exposed population, (2) counting affected buildings, (3) measuring exposed road network, and (4) exposed land cover. Whereas using Table 3. 7 of the inundation depth threshold to perform each InaSAFE hazard impact function.

The hazard inputs to InaSAFE are the maximum inundation depth exported from HEC-RAS breach simulations in raster or vector format. In addition, the hazard used is the middle piping failure scenario, which produced the most extensive inundation among the assigned scenarios, indicating a more dominant flood propagation pattern that is suitable for representing worst-case conditions of both the Main Dam and Right-Wing Dam.

Whereas the exposure data include building footprints, road networks, and land-cover polygons entered in QGIS and configured with the required InaSAFE keywords creation. Although a population density raster was available, its coarse resolution resulted in zero calculated exposed population during the impact analysis. Consequently, population impact estimation was not considered reliable in this study.

5.4 Results

The dam failure simulation results were built upon the maximum reservoir water surface elevation, which is +101.7 m occurred in 20 hours from the simulation beginning. This condition served as the hydraulic condition for all breach scenario determinations on the Main Dam (MD) and the Right-Wing Dam (RWD). Based on this condition, the parameter was estimated and entered using the water volume (Vw) and the failure trigger related to that elevation.

The hydrodynamic behaviour resulting from the Main Dam piping failure shows a different peak discharge evidence response for each differents piping initial elevation scenarios. For the bottom-piping failure, the model produces a peak discharge of 24,739.57 m^3/s, which occurs 2 hours and 40 minutes after the breach

begins, whereas the middle-piping failure results in a peak discharge of 24,837.16-m^3/s at the same time of occurrence as the bottom-piping. Meanwhile, the top-piping failure generates the highest peak discharge among the three Main Dam scenarios, which is 26,885.72 m^3/s in 3 hours and 10 minutes after the breach starts.

A similar analysis is carried out for the Right-Wing Dam, and the results also show clear variations among the three failure modes. The bottom-piping failure produces a peak discharge of 27,907.21 m^3/s, occurring 2 hours and 20 minutes after the breach, and with the same time occurrence, the middle-piping failure reaches a peak discharge of 28,029.29 m^3/s. In addition, the top-piping failure generates the highest release among the Right-Wing Dam scenarios, with a peak discharge of 30,635.40 m^3/s that occurs 2 hours and 40 minutes after failure.

In this study, it is revealed that the highest discharge among the three piping scenarios doesn't produce the largest inundation area. The inundation mapping results show clear differences in the flooded area among the three piping scenarios. For the Main Dam, the bottom-piping and middle-piping scenarios produced slightly larger inundation extents compared to the top-piping case, with the middle-piping scenario giving the widest overall spread. In addition, a similar pattern appears for the Right-Wing Dam. Even so, the relatively small difference between those results may occurred due to the time to peak and duration of the flood hydrograph.

To provide clear evidence of these findings, the corresponding figures show both the hydrograph and the maximum water surface elevation (WSE) profile for each scenario for the Main Dam (MD).

The hydrograph of the Main Dam (MD) produced from the bottom piping scenario can be seen in Figure 5.15 below.

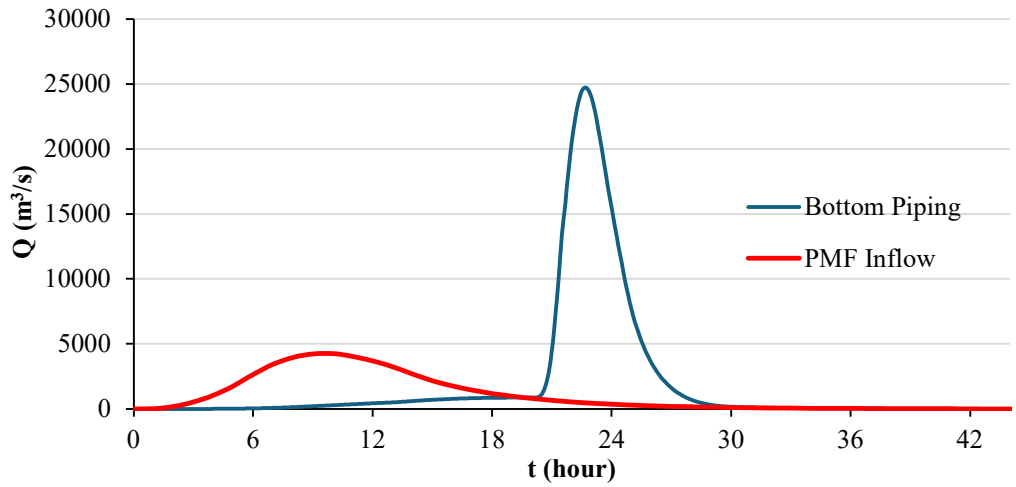

Figure 5. 15 Main Dam (MD) – Bottom Piping Scenario Hydrograph

The maximum water surface elevation (WSE) of the Main Dam (MD) resulting from the bottom piping scenario shown in Figure 5.16 below.

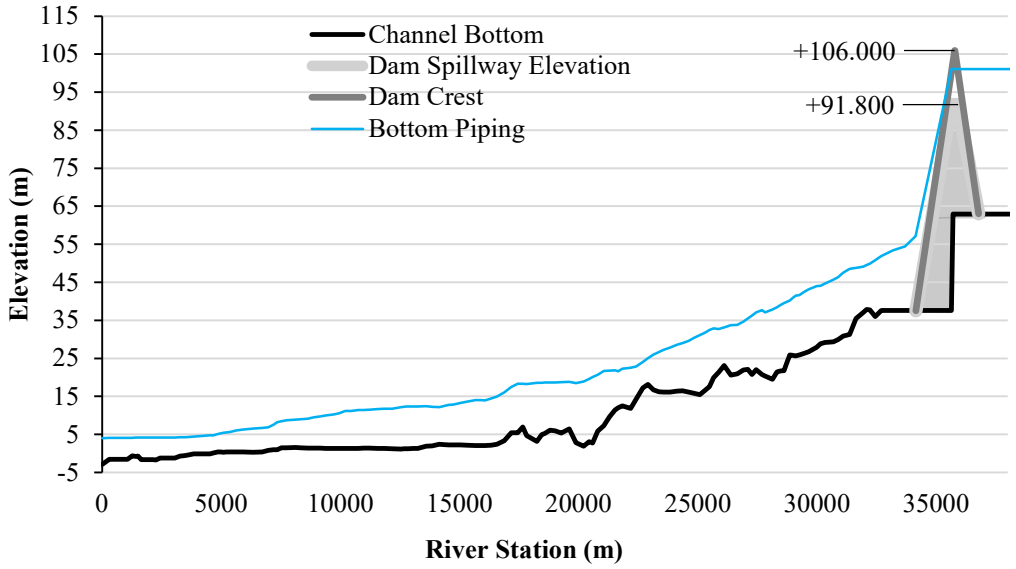

Figure 5. 16 Main Dam (MD) – Bottom Piping Maximum WSE Profile

The hydrograph of the Main Dam (MD) produced from the middle piping scenario can be seen in Figure 5.17 below.

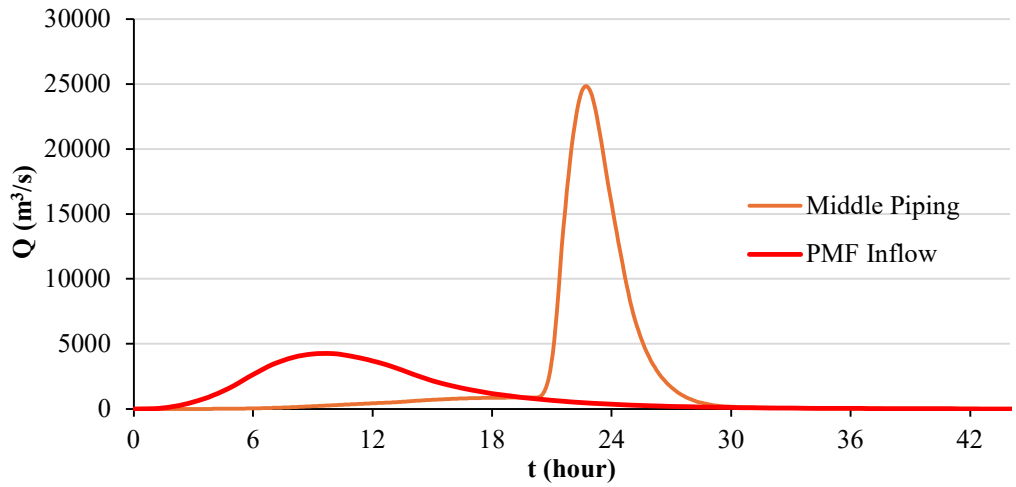

Figure 5. 17 Main Dam (MD) – Middle Piping Scenario Hydrograph

The maximum water surface elevation (WSE) of the Main Dam (MD) resulting from the middle piping scenario is shown in Figure 5.18 below.

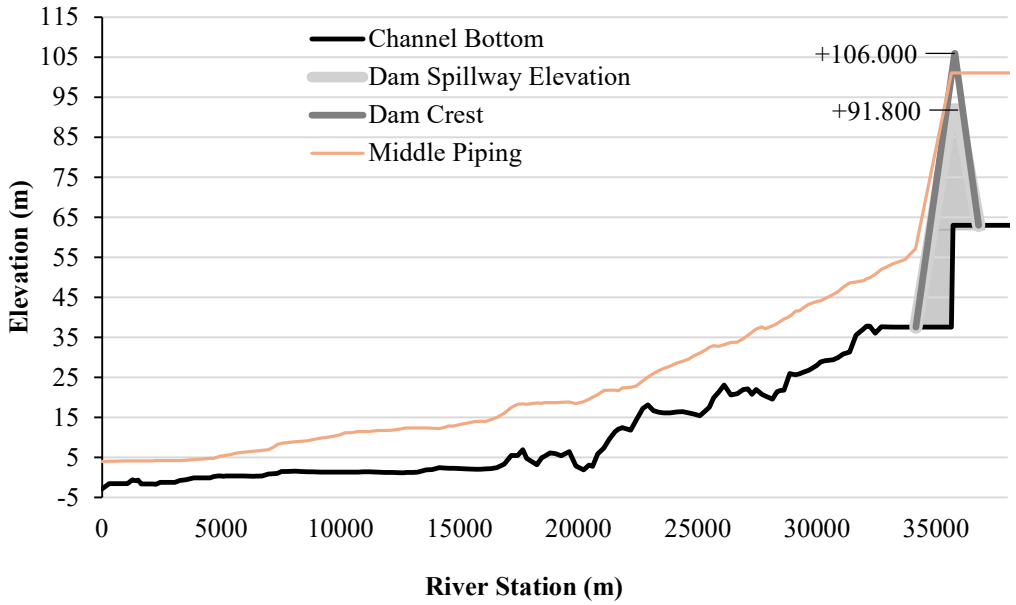

Figure 5. 18 Main Dam (MD) – Middle Piping Maximum WSE Profile

The hydrograph of the Main Dam (MD) produced from the top piping scenario can be seen in Figure 5.19 below.

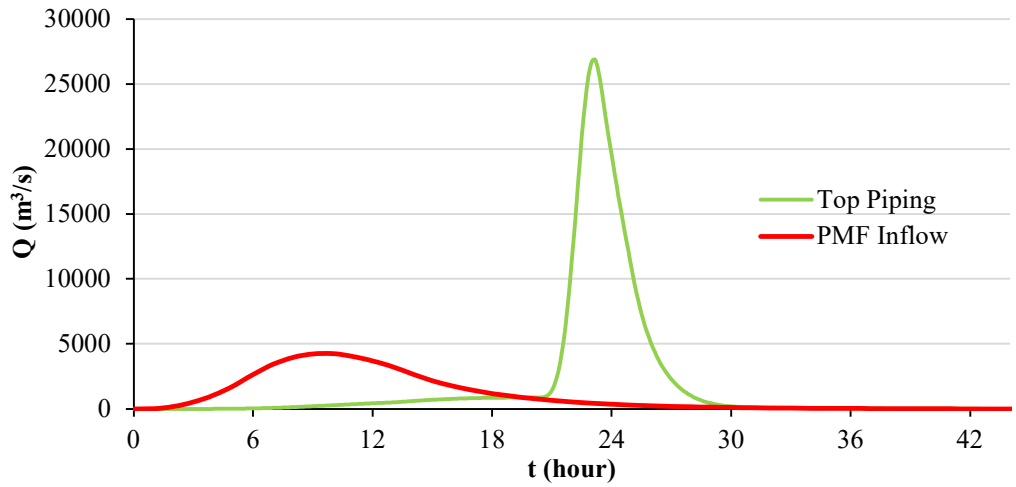

Figure 5. 19 Main Dam (MD) – Top Piping Scenario Hydrograph

The maximum water surface elevation (WSE) of the Main Dam (MD) resulting from the top piping scenario is shown in Figure 5.10 below.

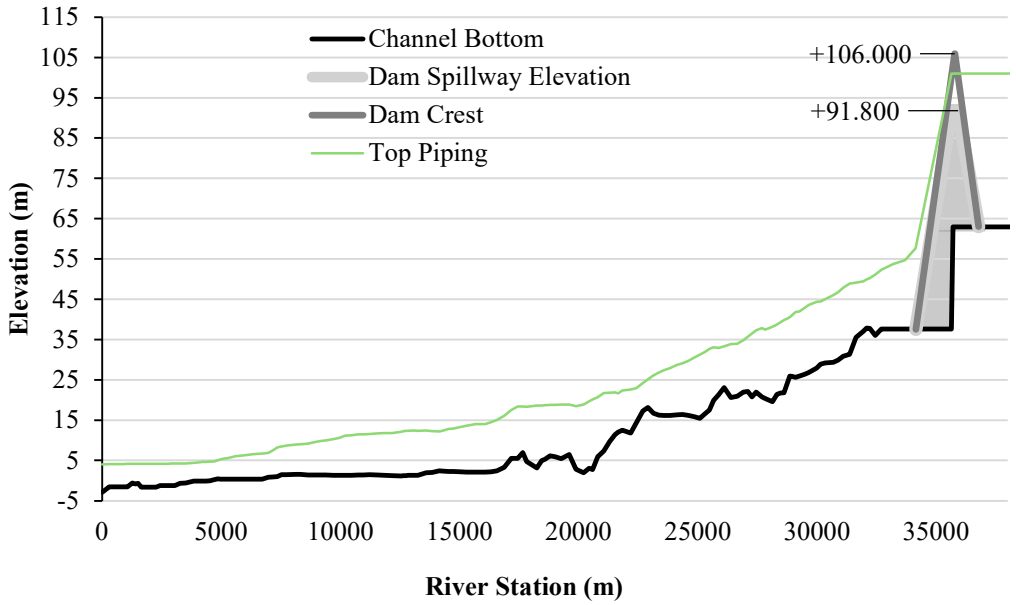

Figure 5. 20 Main Dam (MD) – Top Piping Maximum WSE Profile

The comparison hydrograph of the Main Dam (MD) between the bottom piping scenario, the middle piping scenario, and the top piping scenario can be seen in Figure 5.21 below.

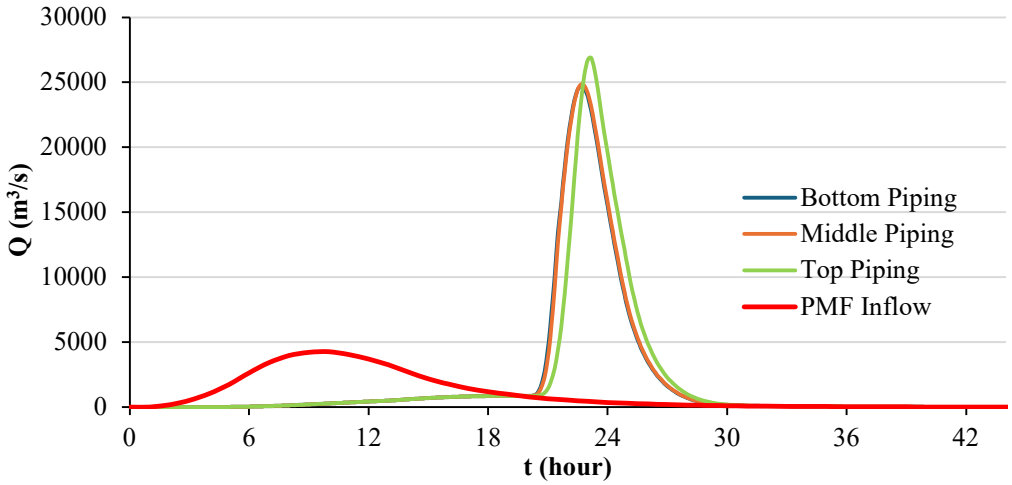

Figure 5. 21 Main Dam (MD) – Scenarios Hydrograph Comparison

The maximum water surface elevation (WSE) comparison of the Main Dam (MD) between the bottom piping scenario, the middle piping scenario, and the top piping scenario is shown in Figure 5.22 below.

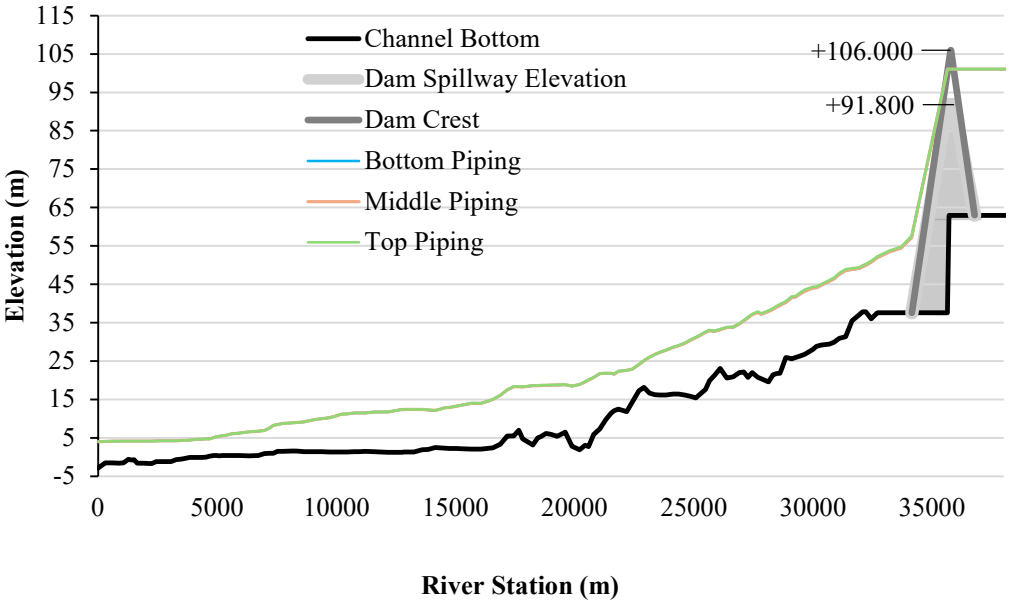

Figure 5. 22 Main Dam (MD) – Maximum WSE Profile Comparison

Furthermore, the corresponding figures also provided to show the evidence from both the hydrograph and the maximum water surface elevation (WSE) profile for each scenario for the Right-Wing Dam (RWD).

The hydrograph of the Right-Wing Dam (RWD) produced from the bottom piping scenario can be seen in Figure 5.23 below.

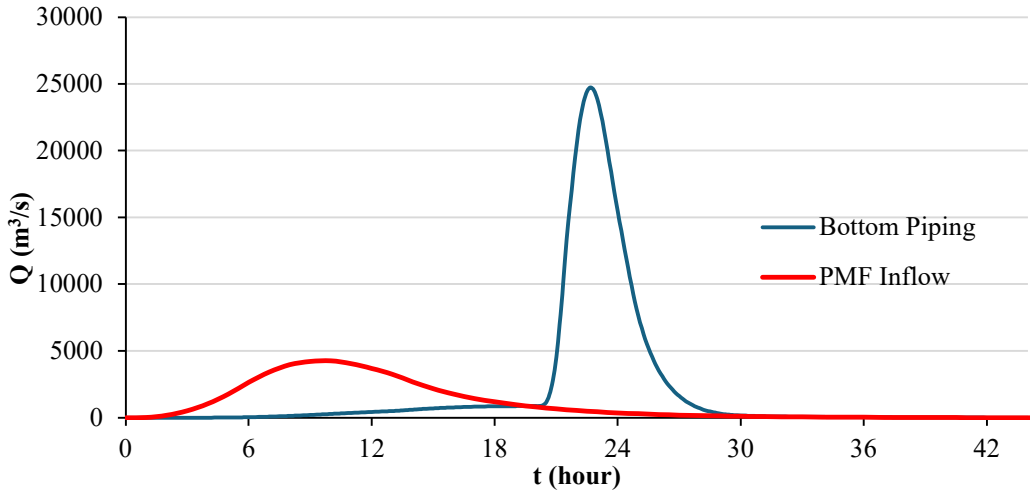

Figure 5. 23 Right-Wing Dam (RWD) – Bottom Piping Scenario Hydrograph

The maximum water surface elevation (WSE) of the Right-Wing Dam (RWD) resulting from the bottom piping scenario is shown in Figure 5.24 below.

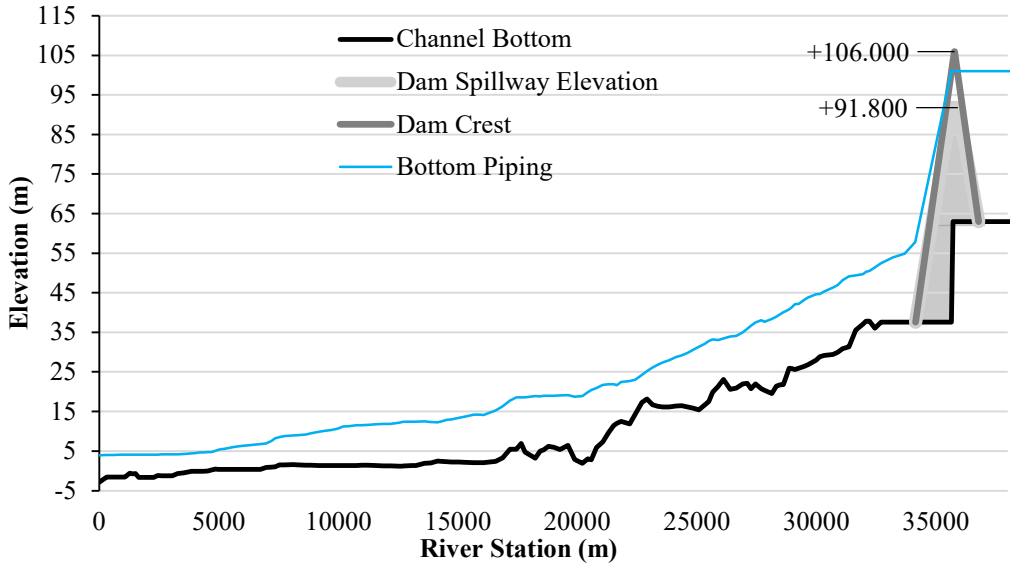

Figure 5. 24 Right-Wing Dam (RWD) – Bottom Piping Max WSE Profile

The hydrograph of the Right-Wing Dam (RWD) produced from the middle piping scenario can be seen in Figure 5.25 below.

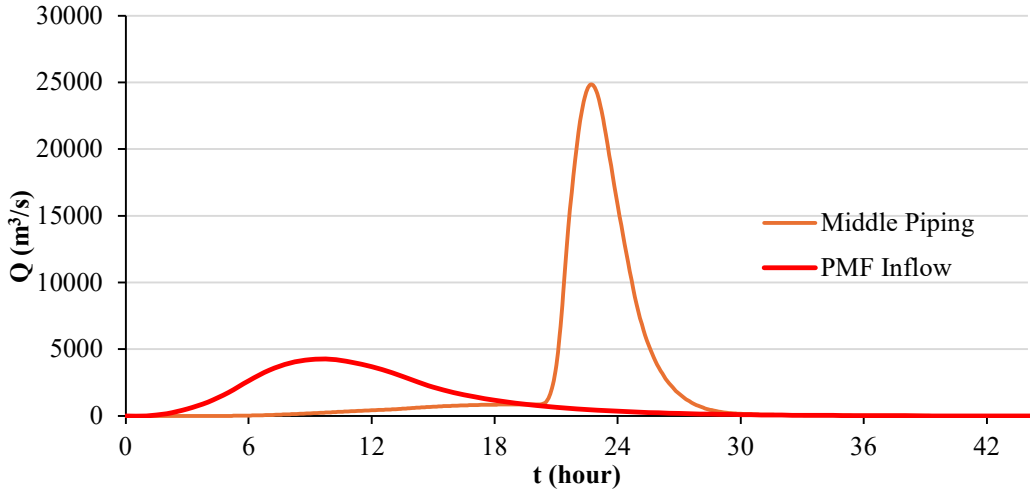

Figure 5. 25 Right-Wing Dam (RWD) – Middle Piping Scenario Hydrograph

The maximum water surface elevation (WSE) of the Right-Wing Dam (RWD) resulting from the middle piping scenario is shown in Figure 5.26 below.

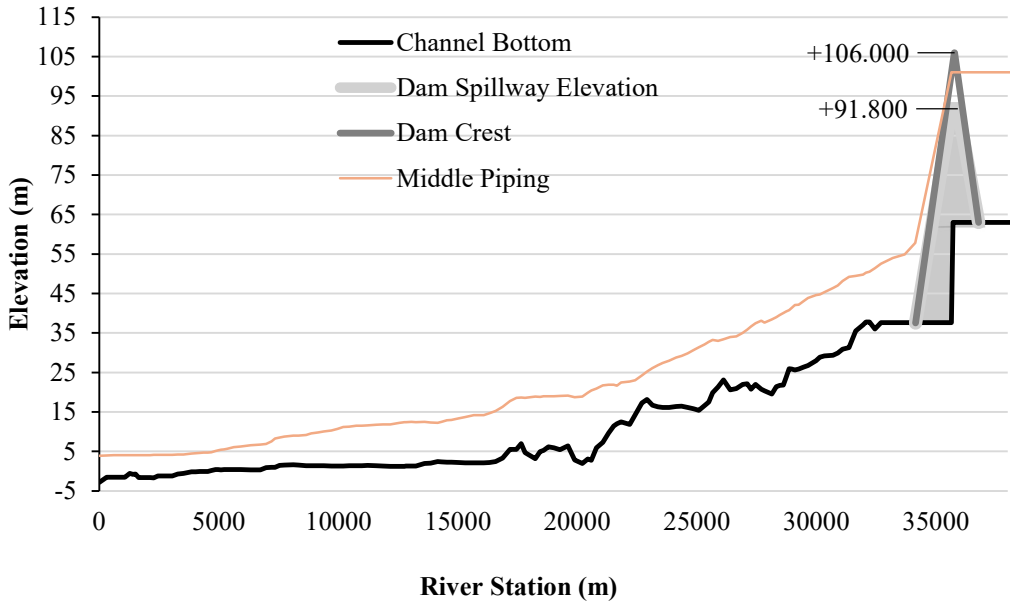

Figure 5. 26 Right-Wing Dam (RWD) – Middle Piping Max WSE Profile

The hydrograph of the Right-Wing Dam (RWD) produced from the top piping scenario can be seen in Figure 5.27 below.

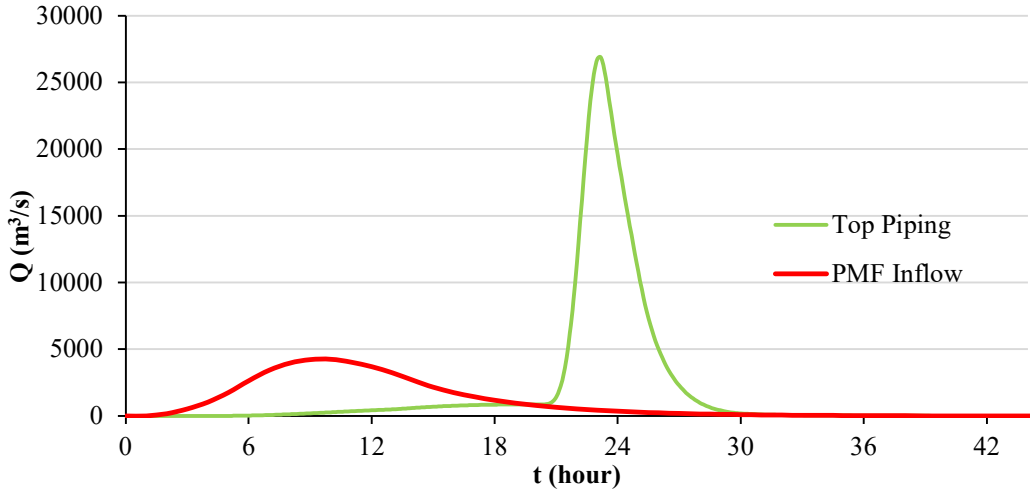

Figure 5. 27 Right-Wing Dam (RWD) – Top Piping Scenario Hydrograph

The maximum water surface elevation (WSE) of the Right-Wing Dam (RWD) resulting from the middle piping scenario is shown in Figure 5.28 below.

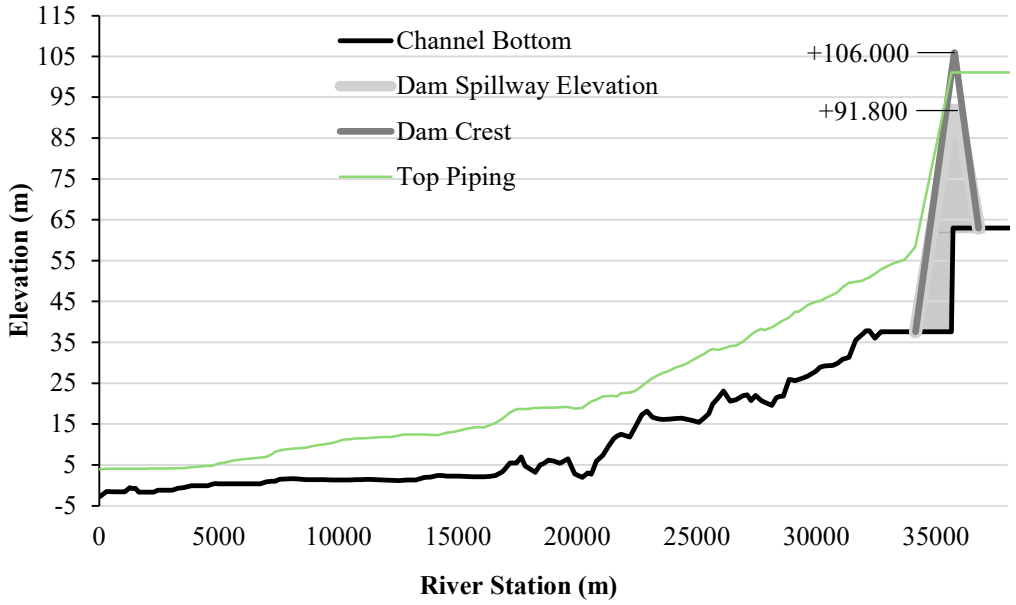

Figure 5. 28 Right-Wing Dam (RWD) – Top Piping Max WSE Profile

The comparison hydrograph of the Right-Wing Dam (RWD) between the bottom piping scenario, the middle piping scenario, and the top piping scenario can be seen in Figure 5.29 below.

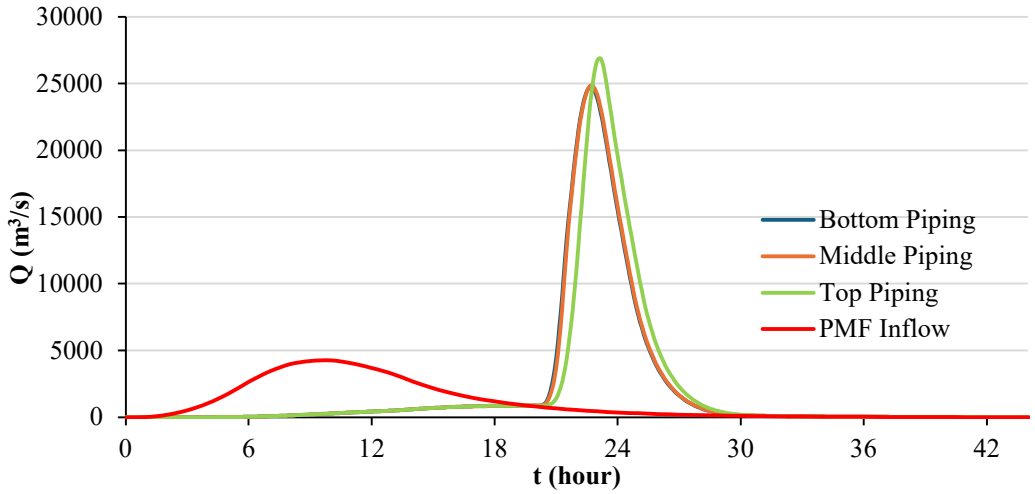

Figure 5. 29 Right-Wing Dam (RWD) – Scenarios Hydrograph Comparison

The maximum water surface elevation (WSE) comparison of the Right-Wing Dam (MD) between the bottom piping scenario, the middle piping scenario, and the top piping scenario is shown in Figure 5.30 below.

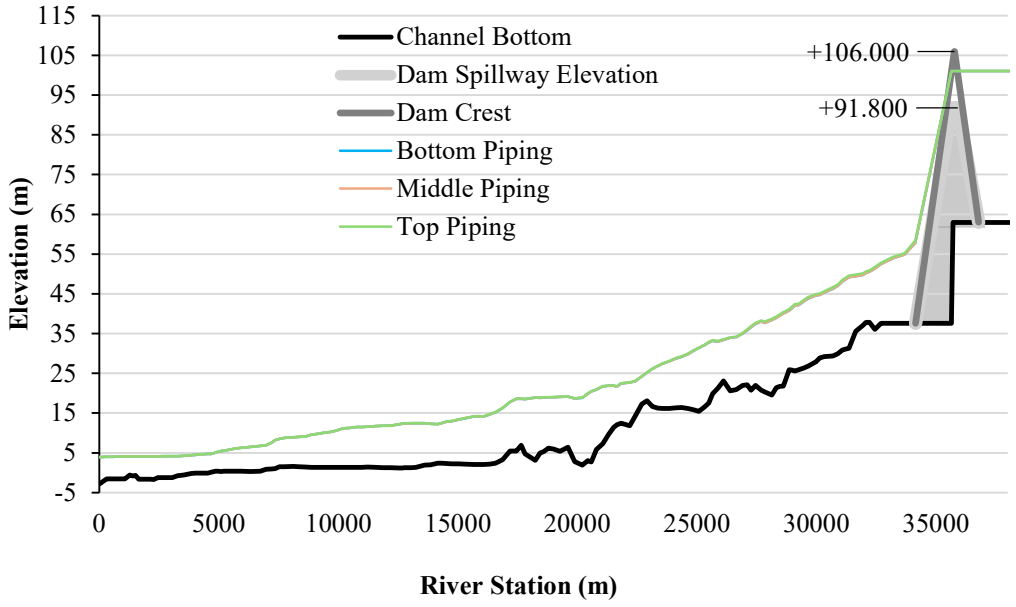

Figure 5. 30 Right-Wing Dam (RWD) –Maximum WSE Profile Comparison

To show the clear evidence of the peak discharge (Qp) and the time to peak (Tp) behaviour of the Main Dam (MD) between the bottom piping scenario, the middle piping scenario, and the top piping scenario. The peak discharge (Qp) and the time to peak (Tp) comparison is shown in Figure 5.31 below.

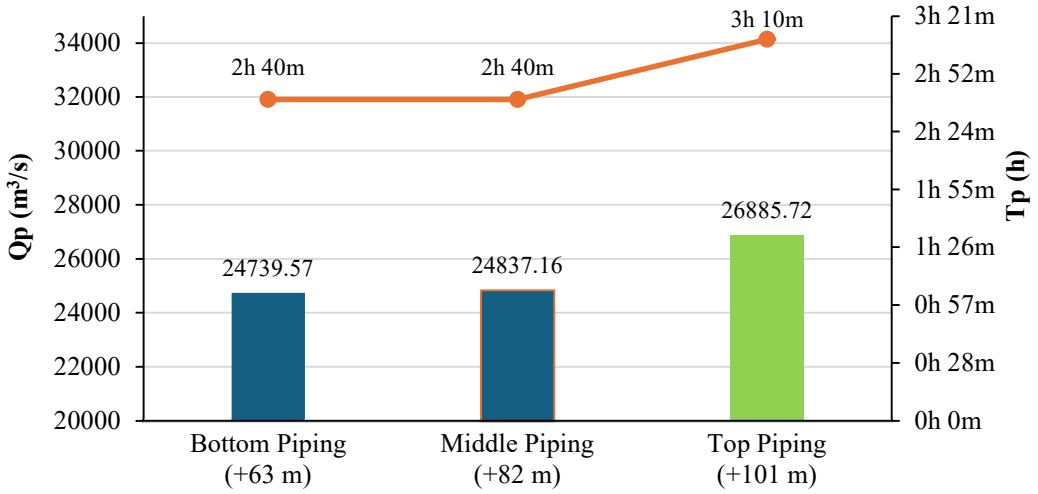

Figure 5. 31 Main Dam (MD) – Scenarios Peak Discharge Comparison

Likewise, the peak discharge (Qp) and the time to peak (Tp) behaviour of the Right-Wing Dam (MD) between the bottom piping scenario, the middle piping scenario, and the top piping scenario is shown in Figure 5.32 below.

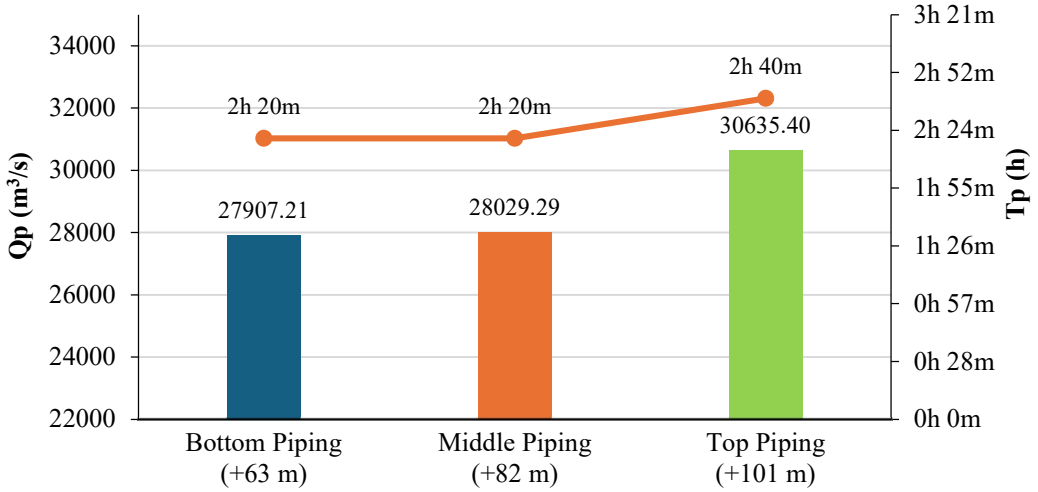

Figure 5. 32 Right-Wing Dam (RWD) – Scenarios Peak Discharge Comparison

To further highlight the differences between the Main Dam (MD) and the Right-Wing Dam (RWD). The peak discharge (Qp) comparison of the Main Dam (MD) and Right-Wing Dam for applied scenarios is shown in Figure 5.33 below.

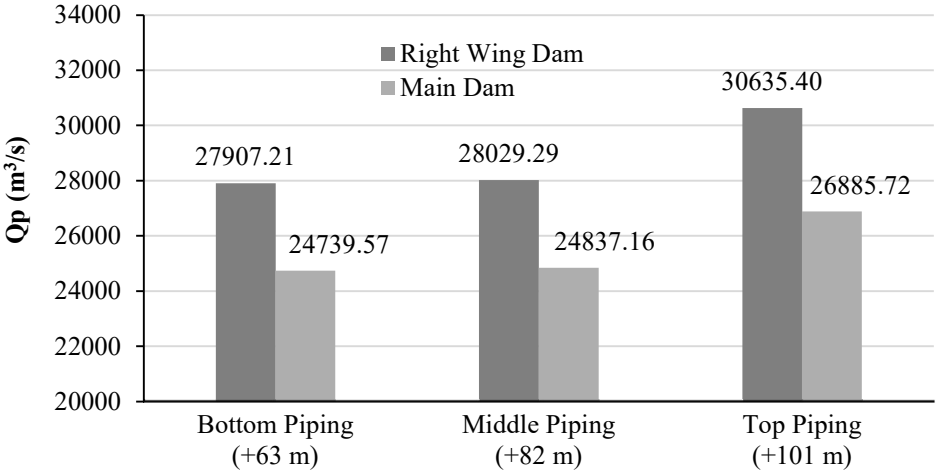

Figure 5. 33 Peak Discharge Comparison

The hydraulic simulation result obtained from HEC-RAS 6.6 is further presented in the form of spatial maps. The spatial maps correspond to the middle piping scenario of both the Main Dam (MD) and the Right-Wing Dam (RWD), which produces the largest inundation extent and is therefore considered the worst-case condition among other scenarios.

In addition, Figure 5.34 and Figure 5.35 illustrate the spatial distribution of maximum inundation depth with an interval of 1 meter, showing how high the maximum water would be due to the middle piping dam breach of Bili Bili Dam; Figure 5.36 and Figure 5.37 illustrate the maximum water arrival time, showing the propagation time for the maximum water to reach the consequent area relative to the piping breach starts forming; Figure 5.38 and Figure 5.39 illustrate the flood duration time relative to the piping breach starts forming. The spatial mapping of the corresponding figures can be seen in the following pages.

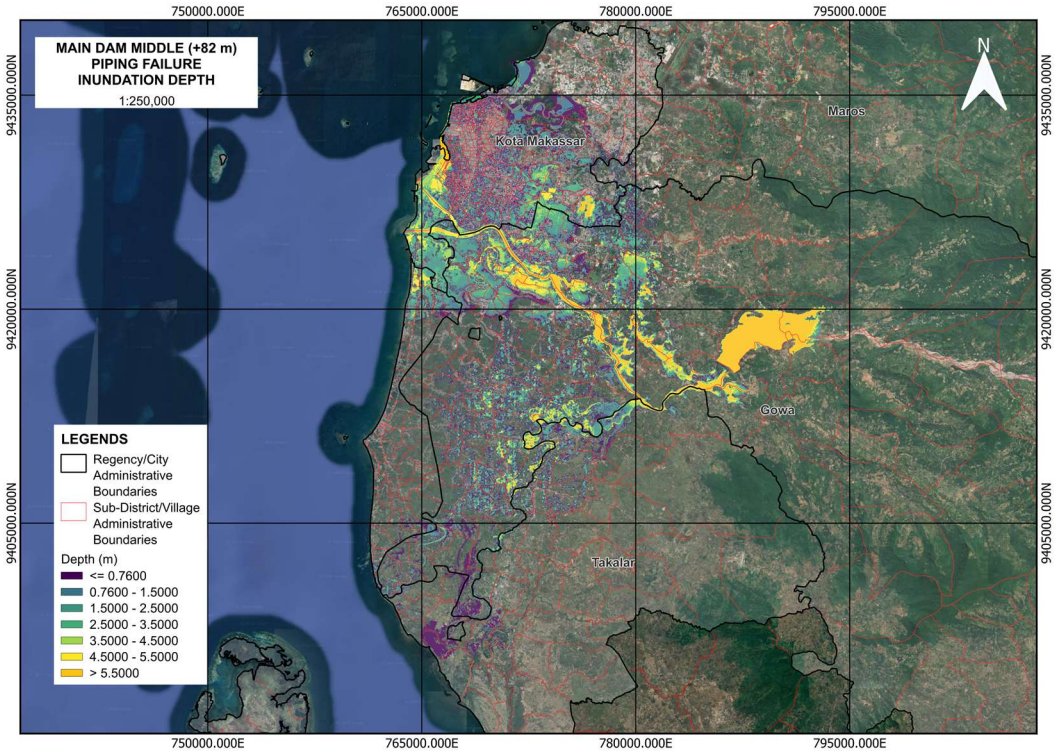

Figure 5. 34 Main Dam Middle Piping Inundation Depth Map

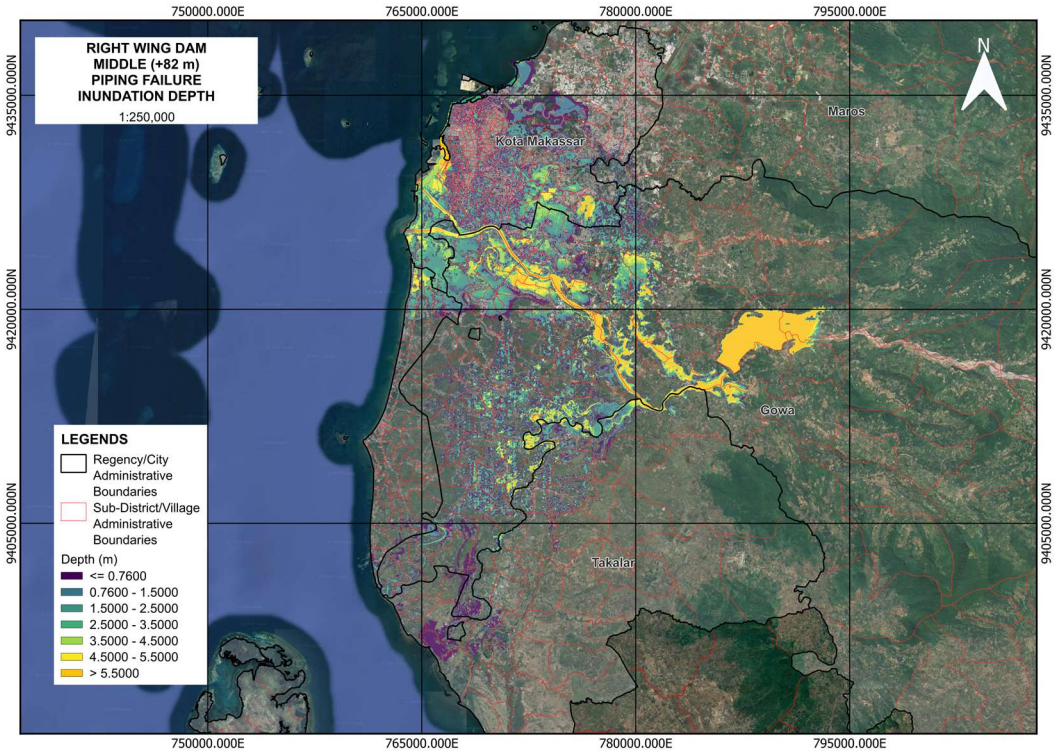

Figure 5. 35 Right Wing Dam Middle Piping Inundation Depth Map

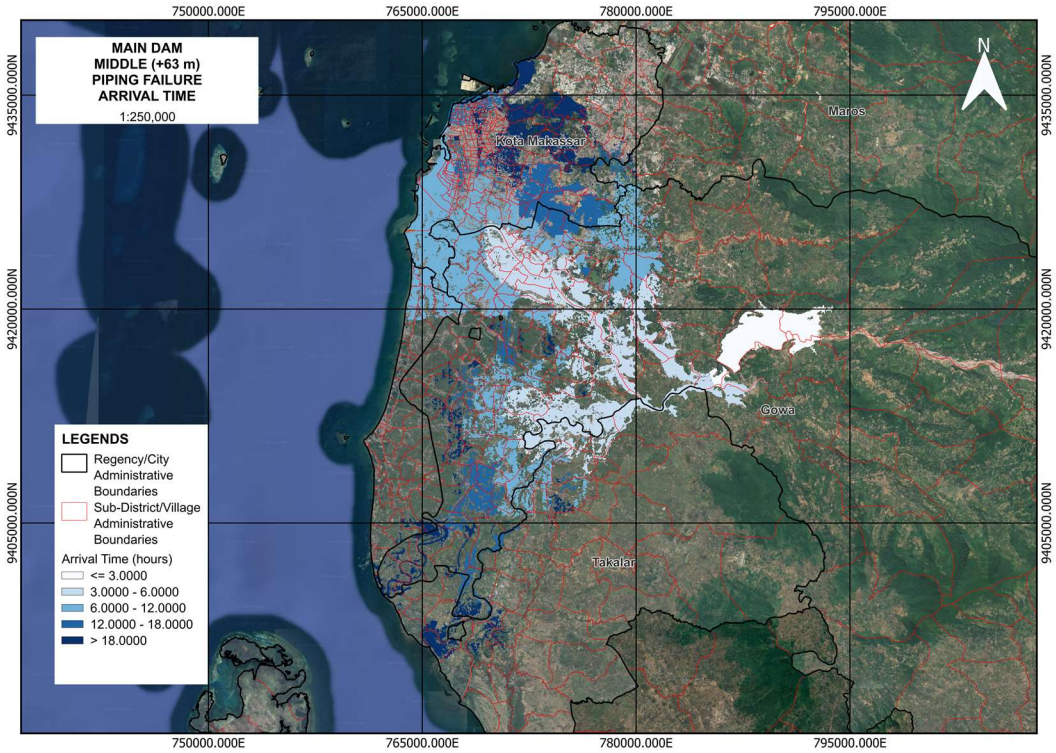

Figure 5. 36 Main Dam Middle Piping Arrival Time Map

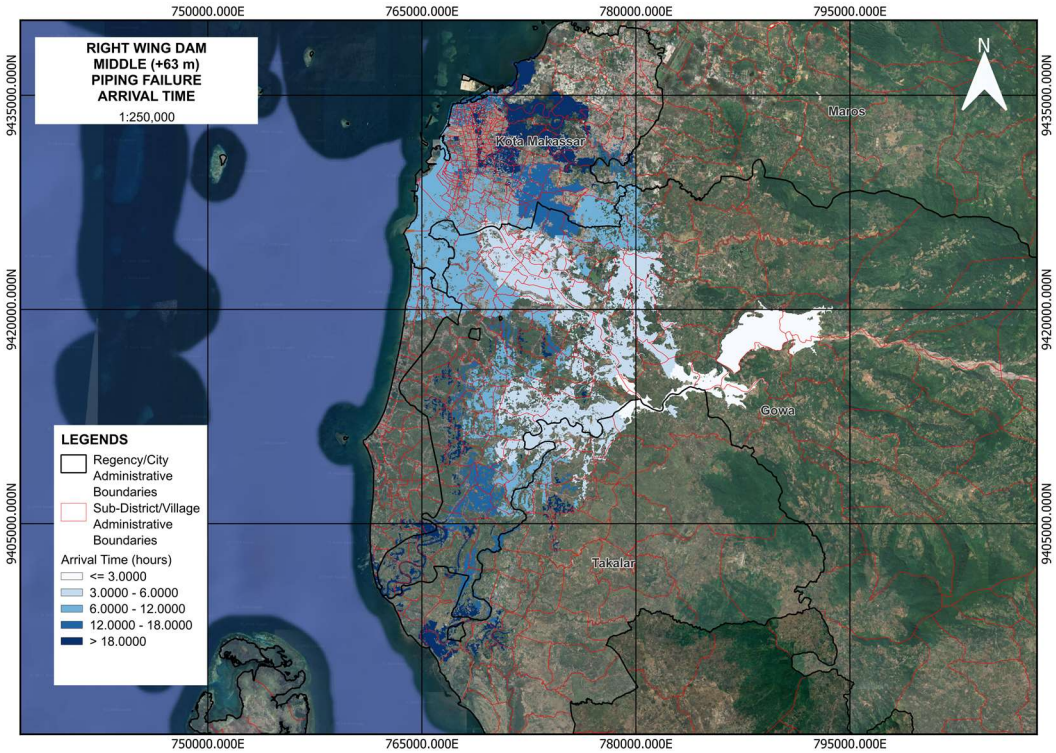

Figure 5. 37 Right Wing Dam Middle Piping Arrival Time Map

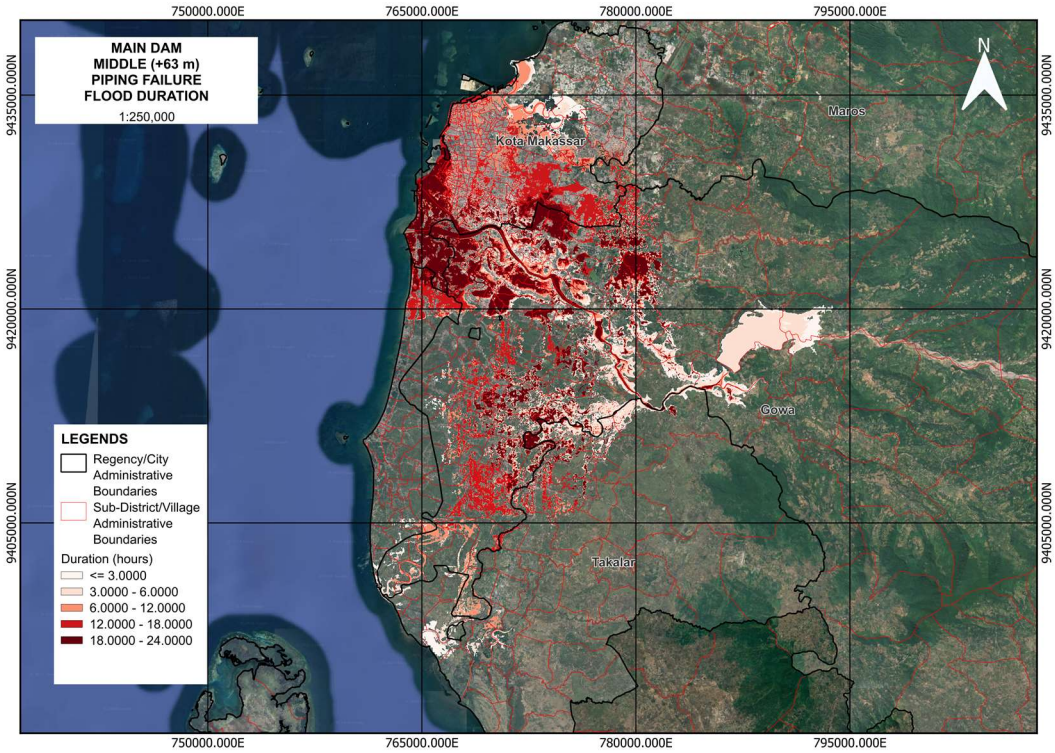

Figure 5. 38 Main Dam Middle Piping Duration Time Map

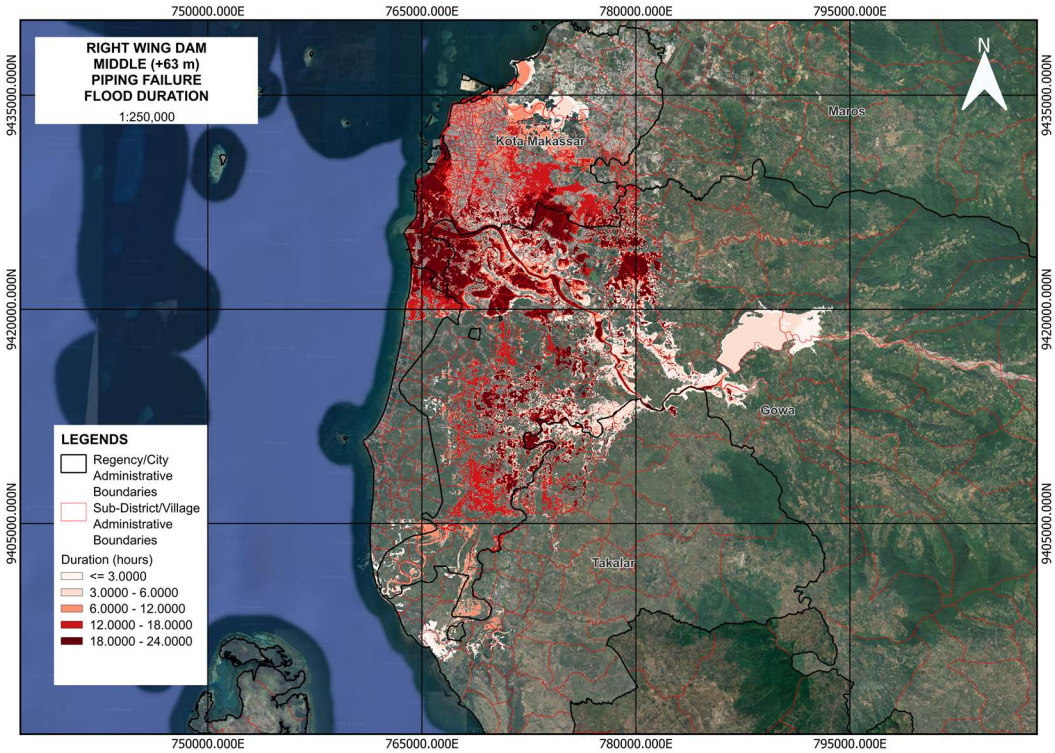

Figure 5. 39 Right Wing Dam Middle Piping Duration Map

Since each scenario produces a different discharge magnitude, the resulting inundation extents downstream also differ, and the figures presented above further highlight this variability by illustrating the middle-piping condition for both the Main Dam and the Right-Wing Dam. This scenario is shown because it consistently produced the most extensive inundation footprint among all simulated breach elevations, making it the best representation of the maximum downstream impact. The comparison of the inundated areas for all scenarios is presented in Table 5.12 as evidence of inundation extent.

Table 5. 12 Inundation Area Comparison

Inundation area of	Main Dam	Right Wing Dam
Bottom Piping (km^2)	231.184	238.266
Middle Piping (km^2)	231.229	238.336
Top Piping (km^2)	230.370	237.608

The results presented in Tables 5.13 and Table 5.14 show the affected villages/sub-districts under the Main Dam (MD) and Right-Wing Dam (RWD) middle piping scenarios based on the average inundation depth greater than 1.5 m. The inundation depth classification refers to the vulnerability class shown previously, showing the >1.5 m as the severe flood category.

Therefore, 100 out of 270 villages on the Main Dam, and 102 out of 272 villages on the Right-Wing Dam, are experiencing an average inundation depth exceeding 1.5 m and are classified as severely affected. The highest average depth of both the Main Dam and the Right-Wing Dam is shown in Desa Bontoramba, Desa Bili-Bili, and Desa Romangloe. In addition, Desa Bontoramba, Desa Bili-Bili, and Desa Romangloe's average depth due to the Main Dam middle piping breach are 5.73 m, 5.37 m, and 5.21 m, respectively. Meanwhile, Desa Bontoramba, Desa Bili-Bili, and Desa Romangloe's average depth due to the Right-Wing Dam middle piping breach is 5.75 m, 5.71 m, and 5.48 m, respectively.

The recapitulation data of the affected village/sub-district based on the average depth of >1.5 m can be seen in Table 5.13 and Table 5.14 on the following page.

Table 5. 13 Main Dam Middle Piping Avg. Depth of >1.5 m Affected Village

No	Village/Sub-district	Regency	Avg. Depth (m)	Covered Percentage
1	Bontoramba	Kab. Gowa	5.73	70.079%
2	Bili-Bili	Kab. Gowa	5.37	42.145%
3	Romangloe	Kab. Gowa	5.21	32.004%
4	Pangkabinanga	Kab. Gowa	4.81	93.273%
5	Mata Allo	Kab. Gowa	4.70	38.756%
6	Kampili	Kab. Gowa	4.43	45.569%
7	Tana Karaeng	Kab. Gowa	4.33	15.397%
8	Tompobalang	Kab. Gowa	4.09	97.088%
9	Borongloe	Kab. Gowa	3.97	48.520%
10	Towata	Kab. Takalar	3.94	17.202%
11	Sokkolia	Kab. Gowa	3.76	50.470%
12	Maccini Sombala	Kota Makassar	3.75	73.718%
13	Mattoangin	Kota Makassar	3.64	84.495%
14	Mangalli	Kab. Gowa	3.59	88.181%
15	Nirannuang	Kab. Gowa	3.59	16.557%
16	Parangbanoa	Kab. Gowa	3.50	51.245%
17	Bontomanai	Kab. Gowa	3.45	61.729%
18	Bontoala	Kab. Gowa	3.32	85.996%
19	Sungguminasa	Kab. Gowa	3.32	77.438%
20	Pandang Pandang	Kab. Gowa	3.30	90.466%
21	Pakatto	Kab. Gowa	3.28	56.218%
22	Taeng	Kab. Gowa	3.28	64.969%
23	Tetebatu	Kab. Gowa	3.27	71.295%
24	Aeng Towa	Kab. Takalar	3.21	86.377%
25	Borongpala'la	Kab. Gowa	3.19	67.056%
26	Kalaserena	Kab. Gowa	3.04	53.089%
27	Benteng Somba Opu	Kab. Gowa	3.01	80.116%
28	Bangkala	Kota Makassar	2.92	75.347%
29	Aeng Batu Batu	Kab. Takalar	2.89	73.546%
30	Lassang Barat	Kab. Takalar	2.87	66.802%
31	Tombolo	Kab. Gowa	2.86	81.299%
32	Bontorannu	Kota Makassar	2.83	96.550%
33	Tanjung Merdeka	Kota Makassar	2.81	87.007%
34	Barombong	Kota Makassar	2.76	82.210%
35	Bontoramba	Kab. Gowa	2.59	40.564%
36	Batua	Kota Makassar	2.59	81.439%
37	Tamangapa	Kota Makassar	2.59	71.972%
38	Pa'bentengang	Kab. Gowa	2.55	59.080%
39	Jene'tallasa	Kab. Gowa	2.54	78.756%
40	Antang	Kota Makassar	2.54	52.204%
41	Panambungan	Kota Makassar	2.45	80.524%
42	Tamarunang	Kab. Gowa	2.44	64.822%
43	Manongkoki	Kab. Takalar	2.40	15.944%

Continuation of Table 5.13 Main Dam Middle Piping Avg. Depth of >1.5 m Affected Village

No	Village/Sub-district	Regency	Avg. Depth (m)	Covered Percentage
44	Limbung	Kab. Gowa	2.39	61.964%
45	Kanjilo	Kab. Gowa	2.38	79.771%
46	Parang Tambung	Kota Makassar	2.26	61.595%
47	Paccinongang	Kab. Gowa	2.25	77.673%
48	Sampulungan	Kab. Takalar	2.25	54.380%
49	Pattallassang	Kab. Gowa	2.23	0.838%
50	Balang Baru	Kota Makassar	2.23	64.424%
51	Tamannyeleng	Kab. Gowa	2.19	77.089%
52	Tamallayang	Kab. Gowa	2.19	53.804%
53	Malewang	Kab. Takalar	2.14	41.764%
54	Kampung Buyang	Kota Makassar	2.13	67.528%
55	Timbuseng	Kab. Gowa	2.12	6.015%
56	Minasa Upa	Kota Makassar	2.11	79.088%
57	Bajeng	Kab. Takalar	2.10	0.665%
58	Salaka	Kab. Takalar	2.10	10.844%
59	Ende	Kota Makassar	2.05	10.872%
60	Bontonompo	Kab. Gowa	2.05	33.889%
61	Lette	Kota Makassar	2.02	68.294%
62	Romang Lompoa	Kab. Gowa	2.01	12.525%
63	Borong	Kota Makassar	1.97	78.588%
64	Sunggumanai	Kab. Gowa	1.93	53.356%
65	Lembang Parang	Kab. Gowa	1.90	65.473%
66	Maloku	Kota Makassar	1.90	25.460%
67	Mattompodale	Kab. Takalar	1.89	47.414%
68	Bulogading	Kota Makassar	1.87	43.545%
69	Karunrung	Kota Makassar	1.86	80.706%
70	Maccinibaji	Kab. Gowa	1.82	58.077%
71	Bitowa	Kota Makassar	1.81	26.167%
72	Pannyangkalang	Kab. Gowa	1.77	45.502%
73	Kassi - Kassi	Kota Makassar	1.77	67.004%
74	Kunjung Mae	Kota Makassar	1.77	62.035%
75	Somba Bella	Kab. Takalar	1.75	8.115%
76	Tubajeng	Kab. Gowa	1.75	39.783%
77	Mangasa	Kota Makassar	1.74	71.675%
78	Panciro	Kab. Gowa	1.74	54.389%
79	Samata	Kab. Gowa	1.73	56.284%
80	Panakkukang	Kab. Gowa	1.70	53.063%
81	Toddotoa	Kab. Gowa	1.69	36.773%
82	Bontolangkasa Utara	Kab. Gowa	1.68	65.838%
83	Mata Allo	Kab. Gowa	1.68	35.775%
84	Bontolebang	Kab. Takalar	1.67	4.380%
85	Pattunuang	Kota Makassar	1.66	21.584%
86	Julukanaya	Kab. Gowa	1.62	24.343%

Continuation of Table 5.13 Main Dam Middle Piping Avg. Depth of >1.5 m Affected Village

No	Village/Sub-district	Regency	Avg. Depth (m)	Covered Percentage
87	Bontolanra	Kab. Takalar	1.62	44.422%
88	Kalebajeng	Kab. Gowa	1.60	47.079%
89	Tamarunang	Kota Makassar	1.59	70.592%
90	Pandang	Kota Makassar	1.58	74.107%
91	Pallangga	Kab. Gowa	1.57	42.891%
92	Karampuang	Kota Makassar	1.57	35.758%
93	Bategulung	Kab. Gowa	1.57	24.895%
94	Barembeng	Kab. Gowa	1.57	24.312%
95	Tindang	Kab. Gowa	1.56	31.454%
96	Tangkebajeng	Kab. Gowa	1.55	37.179%
97	Romangpolong	Kab. Gowa	1.54	24.880%
98	Palleko	Kab. Takalar	1.53	20.208%
99	Batangkaluku	Kab. Gowa	1.51	69.059%
100	Bonto Bontoa	Kab. Gowa	1.51	50.165%

Table 5. 14 Right-Wing Dam Middle Piping Avg. Depth of >1.5 m Affected Village

No	Village/Sub-district	Regency	Avg. Depth (m)	Affected Percentage
1	Bontoramba	Kab. Gowa	5.75	70.569%
2	Bili-Bili	Kab. Gowa	5.71	44.034%
3	Romangloe	Kab. Gowa	5.48	33.523%
4	Mata Allo	Kab. Gowa	5.03	40.752%
5	Pangkabinanga	Kab. Gowa	4.86	93.487%
6	Tana Karaeng	Kab. Gowa	4.63	16.399%
7	Kampili	Kab. Gowa	4.46	48.067%
8	Tompobalang	Kab. Gowa	4.14	97.279%
9	Towata	Kab. Takalar	4.05	18.157%
10	Borongloe	Kab. Gowa	4.01	49.013%
11	Nirannuang	Kab. Gowa	3.86	17.997%
12	Sokkolia	Kab. Gowa	3.86	52.010%
13	Maccini Sombala	Kota Makassar	3.68	73.609%
14	Mangalli	Kab. Gowa	3.63	88.384%
15	Bontomanai	Kab. Gowa	3.61	63.890%
16	Mattoangin	Kota Makassar	3.61	83.725%
17	Parangbanoa	Kab. Gowa	3.55	52.900%
18	Pakatto	Kab. Gowa	3.49	58.349%
19	Borongpala'la	Kab. Gowa	3.45	67.723%
20	Bontoala	Kab. Gowa	3.35	86.325%
21	Sungguminasa	Kab. Gowa	3.34	77.988%
22	Pandang Pandang	Kab. Gowa	3.32	90.852%
23	Tetebatu	Kab. Gowa	3.29	71.999%
24	Taeng	Kab. Gowa	3.29	65.201%
25	Aeng Towa	Kab. Takalar	3.16	86.116%
26	Kalaserena	Kab. Gowa	3.05	53.370%
27	Bangkala	Kota Makassar	3.00	76.234%
28	Benteng Somba Opu	Kab. Gowa	2.97	79.498%

Continuation of Table 5.14 Right-Wing Dam Middle Piping Avg. Depth of >1.5 m Affected Village

No	Village/Sub-district	Regency	Avg. Depth (m)	Affected Percentage
29	Tombolo	Kab. Gowa	2.92	81.701%
30	Lassang barat	Kab. Takalar	2.90	68.005%
31	Aeng Batu Batu	Kab. Takalar	2.85	73.045%
32	Bontorannu	Kota Makassar	2.79	95.947%
33	Tanjung Merdeka	Kota Makassar	2.76	86.521%
34	Tamangapa	Kota Makassar	2.71	75.092%
35	Barombong	Kota Makassar	2.71	81.892%
36	Batua	Kota Makassar	2.67	82.431%
37	Bontoramba	Kab. Gowa	2.63	42.890%
38	Antang	Kota Makassar	2.61	53.174%
39	Pa'bentengang	Kab. Gowa	2.60	60.554%
40	Jene'tallasa	Kab. Gowa	2.56	78.933%
41	Tamarunang	Kab. Gowa	2.49	65.470%
42	Panambungan	Kota Makassar	2.43	79.000%
43	Limbung	Kab. Gowa	2.42	62.382%
44	Manongkoki	Kab. Takalar	2.41	15.974%
45	Kanjilo	Kab. Gowa	2.36	79.709%
46	Paccinongang	Kab. Gowa	2.33	78.201%
47	Timbuseng	Kab. Gowa	2.26	6.541%
48	Parang Tambung	Kota Makassar	2.25	61.389%
49	Balang baru	Kota Makassar	2.22	63.117%
50	Sampulungan	Kab. Takalar	2.21	54.061%
51	Tamallayang	Kab. Gowa	2.21	54.228%
52	Tamannyeleng	Kab. Gowa	2.19	77.100%
53	Minasa Upa	Kota Makassar	2.15	80.441%
54	Malewang	Kab. Takalar	2.14	42.009%
55	Pattallassang	Kab. Gowa	2.12	1.040%
56	Bajeng	Kab. Takalar	2.11	0.665%
57	Kampung Buyang	Kota Makassar	2.11	65.983%
58	Salaka	Kab. Takalar	2.10	10.858%
59	Romang Lompoa	Kab. Gowa	2.06	14.168%
60	Bontonompo	Kab. Gowa	2.06	34.437%
61	Sunggumanai	Kab. Gowa	2.03	56.201%
62	Borong	Kota Makassar	2.02	80.922%
63	Ende	Kota Makassar	2.01	10.758%
64	Lette	Kota Makassar	1.99	66.915%
65	Maloku	Kota Makassar	1.93	24.120%
66	Mattompodale	Kab. Takalar	1.92	48.603%
67	Lembang Parang	Kab. Gowa	1.91	65.282%
68	Karunrung	Kota Makassar	1.90	81.076%
69	Maccinibaji	Kab. Gowa	1.86	59.172%
70	Bitowa	Kota Makassar	1.85	28.256%
71	Bulogading	Kota Makassar	1.84	42.562%
72	Samata	Kab. Gowa	1.82	58.336%
73	Kassi - Kassi	Kota Makassar	1.80	70.081%
74	Pannyangkalang	Kab. Gowa	1.79	46.422%
75	Toddotoa	Kab. Gowa	1.78	38.201%
76	Panciro	Kab. Gowa	1.77	54.264%
77	Tubajeng	Kab. Gowa	1.76	40.209%

Continuation of Table 5.14 Right-Wing Dam Middle Piping Avg. Depth of >1.5 m Affected Village

No	Village/Sub-district	Regency	Avg. Depth (m)	Affected Percentage
78	Kunjung Mae	Kota Makassar	1.76	60.021%
79	Somba Bella	Kab. Takalar	1.75	8.123%
80	Mangasa	Kota Makassar	1.75	72.022%
81	Panakkukang	Kab. Gowa	1.70	53.986%
82	Mata Allo	Kab. Gowa	1.70	36.677%
83	Bontolangkasa Utara	Kab. Gowa	1.69	66.120%
84	Bontolebang	Kab. Takalar	1.65	4.287%
85	Pattunuang	Kota Makassar	1.65	20.847%
86	Pandang	Kota Makassar	1.64	76.038%
87	Julukanaya	Kab. Gowa	1.63	25.693%
88	Romangpolong	Kab. Gowa	1.62	26.068%
89	Kalebajeng	Kab. Gowa	1.62	47.873%
90	Karampuang	Kota Makassar	1.60	36.938%
91	Pallangga	Kab. Gowa	1.60	43.517%
92	Bontolanra	Kab. Takalar	1.58	43.606%
93	Tamarunang	Kota Makassar	1.57	68.220%
94	Bategulung	Kab. Gowa	1.57	25.068%
95	Barembeng	Kab. Gowa	1.56	24.644%
96	Tangkebajeng	Kab. Gowa	1.56	37.679%
97	Tindang	Kab. Gowa	1.55	31.868%
98	Palleko	Kab. Takalar	1.54	21.215%
99	Batangkaluku	Kab. Gowa	1.53	70.793%
100	Julupa'mai	Kab. Gowa	1.52	36.176%
101	Lassang	Kab. Takalar	1.51	52.399%
102	Bonto bontoa	Kab. Gowa	1.51	51.622%

Table 5.15 and Table 5.16 summarize the affected villages/sub-districts under the Main Dam (MD) and Right-Wing Dam (RWD) middle piping scenarios based on the minimum flood arrival time of less than 6 hours. In addition, 6 hours is the maximum summarized flood wave propagation, which was intentionally selected to provide sufficient data extent for future mitigation planning and emergency action plan compilation, particularly in defining evacuation priority zones.

Thus, 56 out of 270 villages on the Main Dam, and 68 out of 272 villages on the Right-Wing Dam identified as having flood arrival times of less than 6 hours under the middle piping scenario. The earliest arrival times are noted in Desa Bili-Bili, Desa Pa'bentengan, and Desa Bontoramba for the Main Dam; and are noted in Desa Bili-Bili, Desa Tana Karaeng, and Desa Lassang for the Right-Wing Dam.

The recapitulation data of the affected village/sub-district based on the minimum arrival time of > 6 h can be seen in Table 5.15 and Table 5.16 on the following page

Table 5. 15 Main Wing Dam Middle Piping Minimum Arrival Time of <6 h Affected Village

No	Village/sub-district	Regency	Avg. Time	Min time
1	Bili-Bili	Kab. Gowa	3h 0m	0h 0m
2	Pa'bentengang	Kab. Gowa	4h 5m	2h 55m
3	Bontoramba	Kab. Gowa	4h 17m	2h 55m
4	Tana Karaeng	Kab. Gowa	3h 1m	2h 57m
5	Mata Allo	Kab. Gowa	3h 36m	2h 58m
6	Lassang	Kab. Takalar	3h 39m	3h 0m
7	Romangloe	Kab. Gowa	3h 16m	3h 1m
8	Towata	Kab. Takalar	3h 25m	3h 3m
9	Julupa'mai	Kab. Gowa	6h 9m	3h 4m
10	Kampung Beru	Kab. Takalar	4h 2m	3h 17m
11	Sokkolia	Kab. Gowa	3h 57m	3h 19m
12	Lassang Barat	Kab. Takalar	4h 56m	3h 21m
13	Nirannuang	Kab. Gowa	3h 38m	3h 23m
14	Pakatto	Kab. Gowa	4h 26m	3h 27m
15	Parang Baddo	Kab. Takalar	4h 3m	3h 35m
16	Borongloe	Kab. Gowa	5h 1m	3h 49m
17	Kampili	Kab. Gowa	4h 55m	3h 56m
18	Timbuseng	Kab. Gowa	4h 34m	4h 4m
19	Parang Luara	Kab. Takalar	7h 24m	4h 5m
20	Bontomanai	Kab. Gowa	5h 39m	4h 13m
21	Paraikatte	Kab. Gowa	7h 56m	4h 16m
22	Maccinibaji	Kab. Gowa	5h 35m	4h 17m
23	Parangbanoa	Kab. Gowa	5h 1m	4h 23m
24	Borongpala'la	Kab. Gowa	6h 15m	4h 36m
25	Tetebatu	Kab. Gowa	5h 22m	4h 42m
26	Batangkaluku	Kab. Gowa	5h 20m	4h 43m
27	Pallangga	Kab. Gowa	6h 53m	4h 47m
28	Pannyangkalang	Kab. Gowa	5h 55m	4h 51m
29	Romang Lompoa	Kab. Gowa	6h 55m	4h 52m
30	Mangasa	Kota Makassar	6h 36m	4h 55m
31	Maradekaya	Kab. Gowa	9h 19m	4h 58m
32	Bontoramba	Kab. Gowa	5h 4m	4h 58m
33	Tamarunang	Kab. Gowa	5h 39m	4h 59m
34	Pangkabinanga	Kab. Gowa	5h 11m	5h 1m
35	Paccinongang	Kab. Gowa	11h 37m	5h 1m
36	Mawang	Kab. Gowa	8h 36m	5h 3m
37	Tompobalang	Kab. Gowa	5h 15m	5h 4m
38	Mangalli	Kab. Gowa	5h 58m	5h 15m
39	Jene'tallasa	Kab. Gowa	6h 12m	5h 16m
40	Toddotoa	Kab. Gowa	9h 22m	5h 17m
41	Bonto bontoa	Kab. Gowa	5h 41m	5h 17m
42	Sungguminasa	Kab. Gowa	5h 44m	5h 23m
43	Bontoala	Kab. Gowa	5h 34m	5h 23m

Continuation of Table 5.15 Main Wing Dam Middle Piping Minimum Arrival Time of <6 h Affected Village

No	Village/sub-district	Regency	Avg. Time	Min time
44	Kalaserena	Kab. Gowa	6h 59m	5h 31m
45	Tamallayang	Kab. Gowa	7h 21m	5h 32m
46	Mattompodale	Kab. Takalar	7h 4m	5h 32m
47	Pandang Pandang	Kab. Gowa	5h 45m	5h 39m
48	Taeng	Kab. Gowa	5h 51m	5h 41m
49	Pa'rappunganta	Kab. Takalar	15h 35m	5h 42m
50	Romangpolong	Kab. Gowa	7h 2m	5h 42m
51	Katangka	Kab. Gowa	6h 12m	5h 42m
52	Kalegowa	Kab. Gowa	5h 48m	5h 46m
53	Tombolo	Kab. Gowa	11h 20m	5h 50m
54	Kalebajeng	Kab. Gowa	7h 55m	5h 56m
55	Parang Tambung	Kota Makassar	8h 1m	5h 58m
56	Karunrung	Kota Makassar	10h 4m	5h 59m

Table 5. 16 Right-Wing Wing Dam Middle Piping Minimum Arrival Time of <6 h Affected Village

No	Village/sub-district	Regency	Avg. Time (h)	Min time
1	Bili-Bili	Kab. Gowa	2h 37m	0h 0m
2	Tana Karaeng	Kab. Gowa	2h 39m	2h 35m
3	Lassang	Kab. Takalar	3h 17m	2h 38m
4	Towata	Kab. Takalar	2h 57m	2h 41m
5	Romangloe	Kab. Gowa	2h 52m	2h 41m
6	Julupa'mai	Kab. Gowa	5h 21m	2h 42m
7	Mata Allo	Kab. Gowa	3h 11m	2h 45m
8	Nirannuang	Kab. Gowa	3h 12m	2h 49m
9	Pa'bentengang	Kab. Gowa	3h 44m	2h 52m
10	Bontoramba	Kab. Gowa	3h 37m	2h 53m
11	Sokkolia	Kab. Gowa	3h 34m	2h 56m
12	Lassang Barat	Kab. Takalar	4h 28m	2h 58m
13	Pakatto	Kab. Gowa	3h 58m	2h 59m
14	Parang Baddo	Kab. Takalar	3h 40m	3h 11m
15	Kampung Beru	Kab. Takalar	3h 38m	3h 13m
16	Parang Luara	Kab. Takalar	7h 18m	3h 38m
17	Kampili	Kab. Gowa	4h 34m	3h 38m
18	Timbuseng	Kab. Gowa	4h 3m	3h 38m
19	Paraikatte	Kab. Gowa	6h 41m	3h 47m
20	Bontomanai	Kab. Gowa	4h 57m	3h 50m
21	Maccinibaji	Kab. Gowa	5h 6m	3h 50m
22	Parangbanoa	Kab. Gowa	4h 39m	4h 1m
23	Borongloe	Kab. Gowa	4h 33m	4h 2m
24	Borongpala'la	Kab. Gowa	5h 41m	4h 4m
25	Batangkaluku	Kab. Gowa	4h 57m	4h 18m

Continuation of Table 5.16 Right-Wing Dam Middle Piping Minimum Arrival Time of <6 h Affected Village

No	Village/sub-district	Regency	Avg. Time (h)	Min time
26	Tetebatu	Kab. Gowa	5h 0m	4h 23m
27	Pannyangkalang	Kab. Gowa	5h 27m	4h 24m
28	Maradekaya	Kab. Gowa	8h 29m	4h 30m
29	Bontoramba	Kab. Gowa	4h 43m	4h 32m
30	Tamarunang	Kab. Gowa	5h 17m	4h 34m
31	Mangasa	Kota Makassar	6h 10m	4h 35m
32	Mawang	Kab. Gowa	7h 13m	4h 35m
33	Pangkabinanga	Kab. Gowa	4h 51m	4h 36m
34	Paccinongang	Kab. Gowa	11h 8m	4h 38m
35	Jene'tallasa	Kab. Gowa	5h 47m	4h 50m
36	Pallangga	Kab. Gowa	6h 23m	4h 51m
37	Tompobalang	Kab. Gowa	4h 53m	4h 51m
38	Bonto Bontoa	Kab. Gowa	5h 16m	4h 52m
39	Mangalli	Kab. Gowa	5h 33m	4h 53m
40	Toddotoa	Kab. Gowa	8h 34m	4h 53m
41	Sungguminasa	Kab. Gowa	5h 20m	4h 56m
42	Bontoala	Kab. Gowa	5h 10m	4h 57m
43	Pa'rappunganta	Kab. Takalar	15h 42m	5h 1m
44	Tamallayang	Kab. Gowa	6h 51m	5h 3m
45	Kalaserena	Kab. Gowa	6h 29m	5h 3m
46	Mattompodale	Kab. Takalar	6h 27m	5h 4m
47	Romangpolong	Kab. Gowa	6h 35m	5h 15m
48	Pandang Pandang	Kab. Gowa	5h 21m	5h 16m
49	Taeng	Kab. Gowa	5h 27m	5h 17m
50	Katangka	Kab. Gowa	5h 47m	5h 18m
51	Kalegowa	Kab. Gowa	5h 24m	5h 23m
52	Tombolo	Kab. Gowa	11h 1m	5h 26m
53	Kalebajeng	Kab. Gowa	7h 16m	5h 27m
54	Parang Tambung	Kota Makassar	7h 27m	5h 33m
55	Romang Lompoa	Kab. Gowa	6h 1m	5h 35m
56	Julukanaya	Kab. Gowa	8h 51m	5h 35m
57	Bontonompo	Kab. Gowa	6h 26m	5h 39m
58	Sunggumanai	Kab. Gowa	6h 15m	5h 42m
59	Tamannyeleng	Kab. Gowa	6h 41m	5h 44m
60	Pattallassang	Kab. Gowa	6h 33m	5h 45m
61	Samata	Kab. Gowa	9h 25m	5h 48m
62	Bonto Duri	Kota Makassar	7h 24m	5h 49m
63	Kanjilo	Kab. Gowa	8h 7m	5h 51m
64	Minasa Upa	Kota Makassar	11h 42m	5h 51m
65	Gunung Sari	Kota Makassar	6h 46m	5h 52m
66	Malewang	Kab. Takalar	8h 10m	5h 54m
67	Mata Allo	Kab. Gowa	8h 16m	5h 54m
68	Karunrung	Kota Makassar	9h 40m	5h 56m

The disaster impact summaries presented in Table 5.17 to Table 5.19 are derived from the InaSAFE analysis based on the middle-piping inundation scenario for both the Main Dam and the Right-Wing Dam. The hazard classification within the InaSAFE assessment was determined using inundation depth thresholds that are represented in Table 3. 7 in advance, where inundation depths are categorized into inundation class 1, inundation class 2, and inundation class 3. Therefore, the tables below provide a compact overview of the estimated impacts on population, buildings, road networks, and land cover using the inundation map generated from the middle-piping scenario and classified according to the national disaster risk reduction standard.

Table 5. 17 Affected Building Number Summary on Middle Piping Failure

Inundation Hazard Classification		**Affected Building Number**	
		Main Dam	**Right Wing Dam**
Class	**(m)**	**-**	**-**
Inundation Class 3	< 0.76	65,300	66,700
Inundation Class 2	0.76 - 1.5	31,900	32,600
Inundation Class 1	> 1.5	44,300	43,800
	Total Exposed	141,500	143,100

Table 5. 18 Exposed Road Length Summary on Middle Piping Failure

Inundation Hazard Classification		**Exposed Road Length**	
		Main Dam	**Right Wing Dam**
Class	**(m)**	**(km)**	**(km)**
Inundation Class 3	< 0.76	1,037	1,062
Inundation Class 2	0.76 - 1.5	416	427
Inundation Class 1	> 1.5	532	528
	Total Exposed	1,985	2,017

Table 5. 19 Affected Farmland Area Summary on Middle Piping Failure

Inundation Hazard Classification		**Affected Farmland Area**	
		Main Dam	**Right Wing Dam**
Class	**(m)**	**(ha)**	**(ha)**
Inundation Class 3	< 0.76	5,000	5,200
Inundation Class 2	0.76 - 1.5	1,700	1,700
Inundation Class 1	> 1.5	2,000	2,100
	Total Exposed	8,700	9,000

The results presented in Table 5.17 compare the affected building numbers under the middle piping failure scenarios of the Main Dam and Right-Wing Dam. The highest number of affected buildings for both dams occurs in inundation class 3, reaching 65,300 buildings for the Main Dam and 66,700 buildings for the Right-Wing Dam. In contrast, inundation class 1 (severe class) records 44,300 buildings for the Main Dam and 43,800 buildings for the Right-Wing Dam. Overall, the total affected buildings under the middle piping scenario amount to 141,500 buildings for the Main Dam and 143,100 buildings for the Right-Wing Dam.

Table 5.18 summarizes the exposed road length under the middle piping failure scenarios of both dams. The greatest affected length is found in inundation class 3, amounting to 1,037 km for the Main Dam and 1,062 km for the Right-Wing Dam. Meanwhile, inundation class 1 (severe class) accounts for 532 km and 528 km for the Main Dam and Right-Wing Dam, respectively. In total, the exposed road length reaches 1,985 km for the Main Dam and 2,017 km for the Right-Wing Dam under the middle piping scenario.

Table 5.19 presents the affected farmland area under the same failure scenarios. The largest impacted area occurs in inundation class 3, with 5,000 ha for the Main Dam and 5,200 ha for the Right-Wing Dam. In inundation class 1 (severe class), the affected farmland reaches 2,000 ha for the Main Dam and 2,100 ha for the Right-Wing Dam. Overall, the total affected farmland area is 8,700 ha for the Main Dam and 9,000 ha for the Right-Wing Dam.

CHAPTER VI
CONCLUSION AND SUGGESTION

6.1 Conclusion

The conclusions are summarized to highlight the main findings of the dam break modelling using HEC-RAS and the impact analysis using InaSAFE, as well as the implications of the modelling approach and data used.

1. The highest peak discharge among the three piping failure scenarios occurs under the top piping (+101 m) for both dams, reaching 26,885.72 m^3/s for the Main Dam and 30,635.40 m^3/s for the Right-Wing Dam.
2. The time required to reach peak discharge (Qp) in the Main Dam is 2 hours 40 minutes for both bottom and middle piping, and 3 hours 10 minutes for top piping. For the Right-Wing Dam, the time to Qp is 2 hours 20 minutes for bottom and middle piping, and 2 hours 40 minutes for top piping.
3. The most extensive inundation among all scenarios occurs under the Right-Wing Dam middle piping (+82 m), covering 238.336 km^2, followed by the Main Dam middle piping (+82 m) with 231.229 km^2.
4. The shortest arrival time of maximum water surface elevation (WSE) occurs at Desa Bili-Bili, Desa Tana Karaeng, Desa Pa'bentengang, Desa Bontoramba, and Desa Mata Allo, all within less than 3 hours after breach initiation. The fastest maximum depth in Kota Makassar is reached within 4–5 hours.
5. The highest average inundation depth, exceeding 5 meters, is observed in Desa Bontoramba, Desa Bili-Bili, and Desa Romangloe under the middle piping scenario for both dams.
6. The greatest overall impact occurs in the Right-Wing Dam scenario, with 143,100 affected buildings, 2,017 km of exposed road networks, and 9,000 ha of affected farmland.

6.2 Suggestion

These suggestions are derived from the experience gained during the modelling process and the findings obtained from the simulation results to support future research and improve dam break modelling and flood risk analysis in a study area.

1. Simulate and perform sensitivity analysis of the breach model within varying breach progression to achieve more realistic hydraulic results.
2. Conduct sensitivity analysis on different 1D numerical equations or 2D solver equation sets.
3. Investigate the HEC-RAS model instability through the Courant number that occurs on a channel. It can be done in the HEC-RAS unsteady spatial plot and unsteady flow time series plot.
4. If the sediment data or the dam is available, reveal the hydrodynamic behaviour of dam failure if sediment is not neglected.
5. Use the highest resolution digital elevation model (DEM) possible to minimize the instability issues and achieve realistic results.
6. Define the coordinate reference system (CRS) correctly. Otherwise, the further GIS-based impact assessment will be more time-consuming.
7. Future InaSAFE dam break impact assessment study using the InaSAFE approach, add more detailed information regarding the exposed road networks, and affected building differs based on the administrative area using aggregation.
8. Future InaSAFE dam break impact assessment study, use an agricultural-focused landcover in the land use impact area assessment.
9. Future InaSAFE dam break impact assessment study, add an estimation of losses and costs that must be incurred to recover the affected areas.

REFERENCES

Amri, M. W. (2021). *Dam Breach Analysis Using HEC-RAS 5.0.7 and QGIS 3.16.7*. Universitas Islam Indonesia.

Bharath, A., Shivapur, A. V., Hiremath, C. G., & Maddamsetty, R. (2021). Dam break analysis using HEC-RAS and HEC-GeoRAS: A case study of Hidkal dam, Karnataka state, India. *Environmental Challenges*, *5*(August), 100401. https://doi.org/10.1016/j.envc.2021.100401

Brunner, G. W. (2014). *Using HEC-RAS for Dam Break Studies - Training Document No.39* (Number August). U.S. Army Corps of Engineers,. https://www.hec.usace.army.mil/publications/TrainingDocuments/TD-39.pdf

Brunner, G. W. (2024). HEC-RAS Hydraulic Reference. In *U.S. Army Corps of Engineers: 6.5* (Number May, pp. 1–477). https://www.hec.usace.army.mil/confluence/rasdocs/ras1dtechref/latest/introduction

Chow, V. Te. (1959). *Open–Channel Hydraulics* (H. E. Davis, Ed.; 1st Ed). McGraw-Hill Book Company, Inc.

Chow, V. Te, Maidment, D. R., & Mays, L. W. (1988). *Applied Hydrology* (1st Ed). McGraw-Hill Book Company, Inc.

FEMA. (2013). *FEMA P-946 - Federal Guidelines for Inundation Mapping of Flood Risks Associated with Dam Incidents and Failures*. https://www.fema.gov/sites/default/files/2020-08/fema_dam-safety_inundation-mapping-flood-risks.pdf

Froehlich, D. C. (1995). Embankment dam breach parameters revisited. *International Water Resources Engineering Conference - Proceedings*, *1*(January 1995), 887–891.

Froehlich, D. C. (2008). Embankment Dam Breach Parameters and Their Uncertainties. *Journal of Hydraulic Engineering*, *134*(12), 1708–1721. https://doi.org/10.1061/(ASCE)0733-9429(2008)134:12(1708)

Froehlich, D. C. (2016). Empirical model of embankment dam breaching. *River Flow 2016*, (June 2016), 1821–1826. https://doi.org/10.1201/9781315644479-285

ICOLD. (2019). *Statistical analysis of dam failures*. (December), 1–65. https://www.icoldchile.cl/boletines/188.pdf

Ikromi, A. I. (2018). *Analisis Hidrodinamik Keruntuhan Bendungan Cipanas*. Universitas Islam Indonesia.

InaSAFE. (2017). *Modul Pelatihan InaSAFE Dam Break* (Number November). InaSAFE.

Khairi, M. A. F., Suprijanto, H., & Hendrawan, A. P. (2022). Analisis Keruntuhan Bendungan Rukoh Kabupaten Pidie Menggunakan Aplikasi HEC-RAS dan Berbasis InaSAFE. *Jurnal Teknologi Dan Rekayasa Sumber Daya Air*, *2*(1), 1–66. https://doi.org/10.21776/ub.jtresda.2022.002.01.05

Novak, P., Moffat, A. I. B., Nalluri, C., & Narayanan., R. (2007). *Hydraulic Structures* (4th Ed). Taylor & Francis Group.

PUPR. (2015). Peraturan Menteri Pekerjaan Umum dan Perumahan Rakyat Republik Indonesia Nomor 27/PRT/M/2015 Tentang Bendungan. In *JDIH*.

Rustan, Irpan Chumaedi, & Handayani, L. (2019). Simulasi Keruntuhan Bendungan Bili-Bili Kabupaten Gowa Provinsi Sulawesi Selatan. *Journal Online of Physics*, *5*(1), 24–28. https://doi.org/10.22437/jop.v5i1.8117

SNI 3432 2020. (2020). *SNI 3432:2020 -Tata cara penetapan banjir desain dan kapasitas pelimpah untuk bendungan*.

Soliman, M., Morsy, M. M., & Radwan, H. G. (2022). Assessment of Implementing Land Use/Land Cover LULC 2020-ESRI Global Maps in 2D Flood Modeling Application. *Water (Switzerland)*, *14*(23). https://doi.org/10.3390/w14233963

Subramanya, K. (2008). *Engineering hydrology* (3rd Ed). Tata McGraw-Hill Publishing Company Limited.

Tessema, B. H., Gebremedhn, A. Y., & Getahun, Y. S. (2024). Dam breach analysis and flood inundation mapping of Dire Dam, using HEC-HMS and HEC-RAS models. *Sustainable Water Resources Management*, *10*(2), 45. https://doi.org/10.1007/s40899-023-01015-w

Triatmodjo, B. (2019). *Hidrologi Terapan*. Beta Offset.

Yilmaz, K., Darama, Y., Melek, A. B., & Unal, C. I. (2022). Flood Hazard Analysis due to Overtopping of Dalaman Akköprü Dam : A Case Study. *14Th International Conference on Hydroscience and Engineering*, (May), 591–602. https://doi.org/10.1007/s11069-023-05891-5

Zhong, Q., Wang, L., Chen, S., Chen, Z., Shan, Y., Zhang, Q., Ren, Q., Mei, S., Jiang, J., Hu, L., & Liu, J. (2021). Breaches of embankment and landslide dams - State of the art review. *Earth-Science Reviews*, *216*(March), 103597. https://doi.org/10.1016/j.earscirev.2021.103597